A new technique for the investigation of cosmic ray showers

H. Coxell

A NEW TECHNIQUE FOR THE INVESTIGATION OF COSMIC RAY SHOWERS

A thesis presented by

H. Coxell

For the Degree of Doctor of Philosophy

at

The University of Durham

January 1961

CONTENTS

PART II

Preface

This thesis describes the general characteristics of the neon flash tube as a detector of ionising particles and the development of the flash tube for use in investigations of extensive air showers of cosmic rays.

The work was carried out at Durham between 1957 and 1960 under the supervision of Dr. A.W. Wolfendale.

Measurements on the neon flash tubes were made using apparatus designed by Dr. S. Krishnaswamy. The design, construction and operation of the extensive air shower array and the analysis of results was the sole responsibility of the author.

The work on the high pressure flash tube has been published by the author and his supervisor (Coxell & Wolfendale, 1960) and further work on the E.A.S. flash tube was presented at the 1959 Moscow Cosmic Ray Conference (Rochester, 1960).

Abstract Ph.D. Thesis H. Coxell

Part I of this thesis contains a discussion of the general principles involved in the neon flash tube technique. An account is given of the development of a high pressure flash tube for use in a high energy cosmic ray spectrograph and the characteristics of this tube are given in detail. The further development of a larger tube with characteristics specially suited for use in studies of extensive air showers of cosmic rays (E.A.S.) is described and Part I concludes with a re-appraisal of the theory of operation of the flash tube.

Part II of the thesis concerns the design, construction and operation of a flash tube array for studies of the directional properties of E.A.S. An investigation of the zenith angle dependence of E.A.S. is described, also a measurement of the particle density spectrum. The performance of the apparatus is critically examined and found to be reliable and accurate. Further applications of the array in E.A.S. are considered and modifications are discussed which would enable an investigation of models of shower development and an examination of the heights of production of mesons in E.A.S.

CHAPTER 1

Introduction

Our present knowledge of cosmic rays is the result of almost 50 years of continuous research. It is now known that the cosmic ray processes occurring in the atmosphere are due to a primary radiation arriving at the top of the atmosphere which consists of approximately 85% protons and 15% α-particles with some heavier nuclei of atomic numbers extending to 26.

The primary particles collide and interact with air nuclei at heights mainly above 16 Km, the interaction length being 70 gm/cm^2 for protons and considerably less for heavier nuclei. As products of the nuclear disintegration there are charged and neutral mesons, hyperons, nucleons and nuclear fragments. These secondary particles undergo further collisions with air nuclei producing more mesons, nucleons etc. Few of these survive to sea level. The nucleons are almost totally absorbed by inelastic collision, the heavy mesons and hyperons decay with numerous schemes

and the charged π-mesons are subjected to the competing processes of decay and interaction. Most of the charged π-mesons of momentum below 20 GeV/c, and a small fraction of those of momentum greater than 20 GeV/c, decay into μ-mesons and these comprise the main part of the charged radiation observed at sea level. The neutral π-mesons have a short mean life of $\sim 10^{-16}$ sec and decay into two photons which can materialise in the presence of nuclei to form electron pairs and eventually an electron-photon cascade. If the energy of the primary is sufficiently high ($\gtrsim 10^{14}$ eV), the cascades so produced may extend as far as sea level where they are observed as the electron component of "extensive air showers". (E.A.S.). This phenomenon is an important topic in its own right and will be considered in detail in Part II of this thesis.

Research in the subject of cosmic rays has been extremely valuable in the discovery of new elementary particles and of new nuclear processes, it has also led to the development and improvement of many experimental techniques, particularly for the observation of ionising particles. Part I of this thesis is an account of the

development of one of the most recent of these, the neon flash tube.

The techniques at present used in studies of the cosmic radiation may be grouped into two broad classes:

a) those whose function is to signify the incidence of a particle and

b) those whose function is to indicate the trajectory of the particle.

An important distinction is that the devices of the former class must be continuously sensitive, whereas those of the latter usually require a "triggering pulse".

In class a) are the well established types of detector such as the gas counters, (the ionisation chamber, proportional counter and Geiger Mueller counter), the scintillator and the Cerenkov counter. The use of each of these is governed only by its own particular advantages and limitations.

The established techniques of class b), designed to furnish details of the particle's trajectory, are more elaborate. The Wilson cloud chamber, the diffusion chamber and the bubble chamber are extremely

valuable instruments capable of highly precise determinations of particle trajectories and, when suitably modified, permit accurate measurements of ionisation, range, scattering and momentum. However, the use of these instruments is restricted: all are highly expensive and require elaborate instrumentation. The diffusion chamber and bubble chamber are inherently limited to machine experiments and the cloud chamber demands continual attention in addition to operational skill.

Fortunately, techniques have been developed recently which offer some degree of compromise between the characteristics of the visual detectors and those of the simpler 'counter' detectors already described. Such devices are the spark counter and the neon flash tube.

Theparallel plate (D.C.) spark counter was introduced by Pidd and Madansky (1948) and was later developed by Keuffel (1948), Robinson (1953), to provide a useful instrument with an efficiency for particle detection of ~98% and a time resolution of ~5 x 10^{-9}sec.

A serious difficulty however was the prevention of discharges not connected with the event under inspection and a solution of this problem was the pulsed spark counter devised by Cranshaw and de Beer (1957). In this method the necessary high voltage was applied as a pulse only when the required particle was known to have traversed the apparatus.

In this form the spark counter was used in several experiments on E.A.S. by the Harwell Group. (Cranshaw, et al 1957,)

Although an attractive proposition on account of its high efficiency and basic simplicity, the spark counter has several disadvantages:

1. The lifetime is short and not well defined.
2. Coincident particles are difficult to distinguish because of preferential sparking along the track of most dense ionisation.
3. The size of the spark counter is limited by its self capacity. Larger capacities result in an increase in the energy going into the

spark, quenching becomes difficult and the dead time is increased.

4. The air spark counter is rendered inoperative if the relative humidity exceeds 60%.

These difficulties are obviated in the neon flash tube counter where the spark is replaced by a glow discharge localised in a glass tube.

The Neon Flash Tube

The neon flash tube was introduced by Conversi (1955) and consists of a glass tube containing neon which is placed between parallel plate electrodes. The application of a high voltage pulse after a particle has passed through the tube will normally cause a visible discharge in the neon. A complete stack of tubes suitably disposed thus forms a very efficient track locator for ionising particles. The technique is simple and reliable, offering a good combination of spatial and time resolution together with the possibility of a large area of collection. The obvious advantages for work in the field of cosmic rays were soon recognised.

The general properties of the flash tube will be fully discussed in Chapter 2 before describing the development of flash tubes for specific applications in cosmic ray experiments in Chapters 3 and 4.

CHAPTER 2

Basic Properties of the Neon Flash Tube

2.1 Introduction

Systematic experimental studies have been carried out over several years by a number of workers (Conversi et al 1955, Barsanti et al 1956, Gardener et al 1957) and the characteristics of the tube are now known in some detail. The behaviour of the tube is dependent on several factors, the gas filling, the parameters of the pulse, and the nature of the glass container. The effect of each of these will be considered in turn: an appreciation of their importance is essential when considering the design of a flash tube for a particular application.

It will be of advantage to describe first the experimental arrangement used to investigate the properties of the tube.

2.2 The Experimental Arrangement

The apparatus used in testing is shown in Fig. 2.1. Layers of tubes are contained between metal electrodes, alternate plates are earthed and the high voltage pulse, of variable size and shape, is applied to the remaining plates when a fourfold coincidence of the G.M. telescope indicates that a particle has passed through the stack.

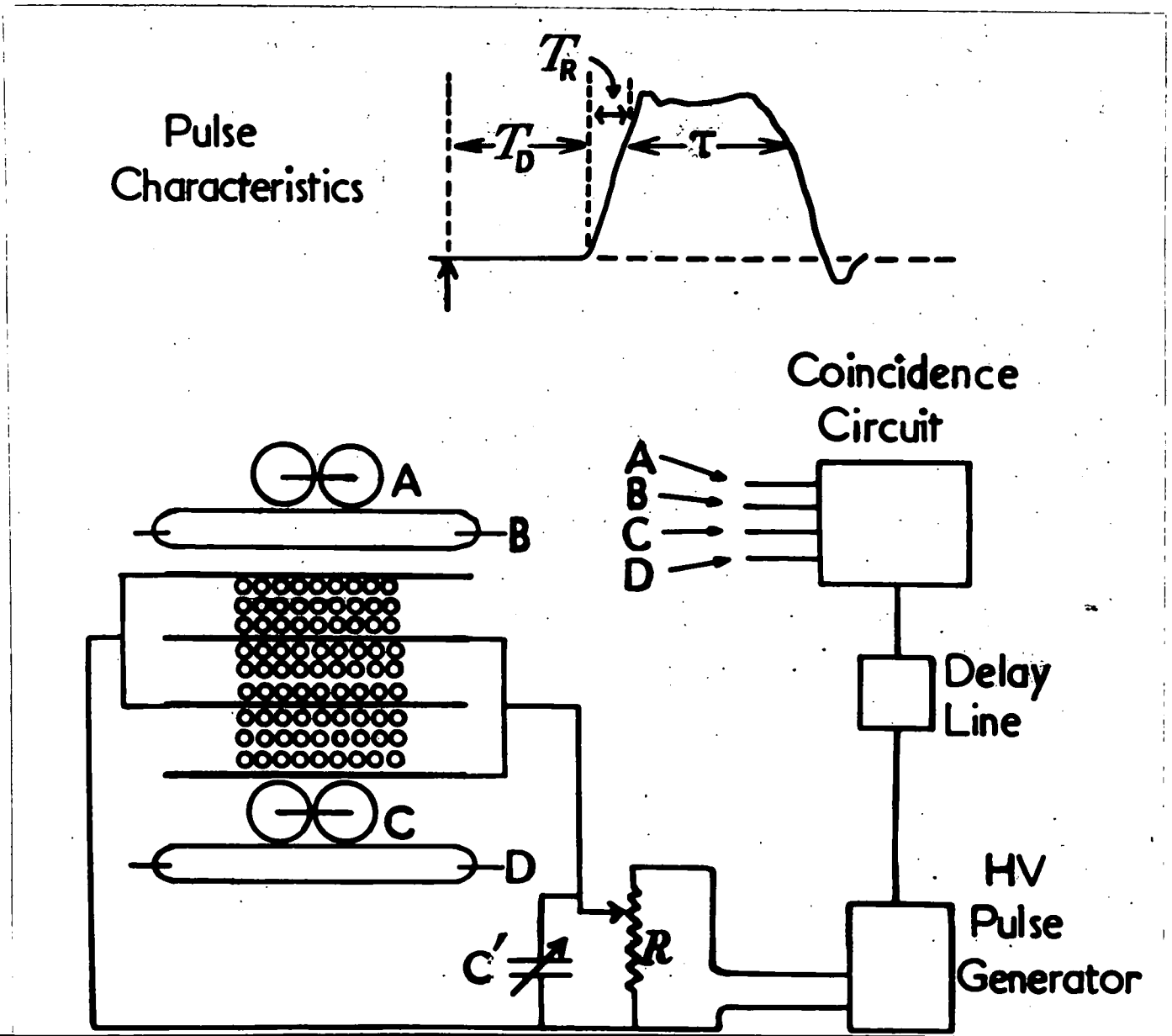
Pulse
Characteristics
T_R
T_D
τ
Coincidence
Circuit
A
B
C
D
Delay
Line
HV
Pulse
Generator
C'
R

Figure 2.1

The characteristic parameters of the pulse are also shown in Fig. 2.1. The pulse is produced by discharging an open delay line through the primary of a pulse transformer by means of a hydrogen Thyratron (Mullard XH8). The circuit is given in Fig. 2.2. The only critical component is the coupling transformer between the small thyratron and the XH8 which must be capable of producing a sharp pulse with a rise time much less than 1μsec. A core of 'Ferrox-cube' (Mullard Ltd.) is satisfactory. The time interval between the passage of the particle and the application of the pulse is controlled by the delay line, which for delays longer than 10μsec is replaced by an electronic delay unit. Variation of the pulse height is obtained by adjusting the tapping on the matching impedance, R. The rise time of the pulse is governed by the capacity of the condenser, c, and different values of pulse width are obtained by varying the number of sections used in the pulse forming network (P.F.N.).

2.3. Efficiency

Probably the most important characteristic of the flash-tube is the probability that it will flash after an ionizing particle has passed through it. Experimentally it is usual to measure the "layer" efficiency, defined as the ratio of the number of (single) flashes observed in a layer to the number of particles having passed through

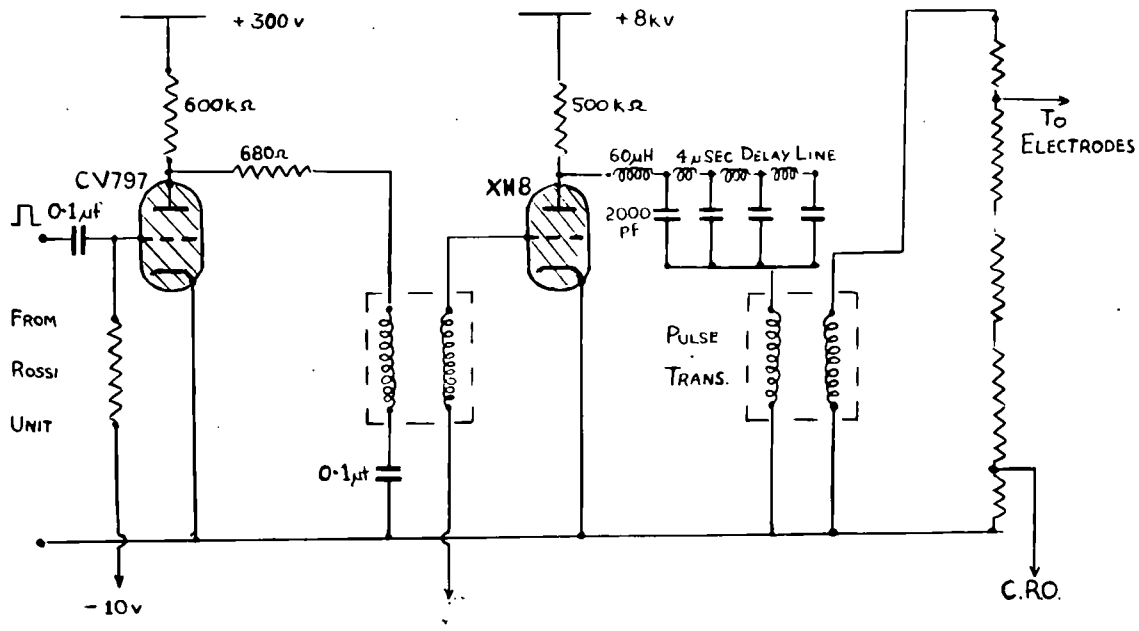

Figure 2.2. The high voltage pulse generator.

that layer. It is reasonable to assume that no flash can occur when a particle passes through the walls of the tube and therefore, for comparison purposes, the layer efficiency is converted to "internal" efficiency by multiplying by a constant factor, R, which is the ratio of the separation of the centres of adjacent tubes to the internal diameter of the tube.

2.4 The Gas Filling

Neon is an obvious choice for use in the flash tube because of its comparatively easy breakdown characteristics and because the red glow discharge is easily seen and photographed.

2.4.1. Purity of the Neon

Several grades of neon are available commercially. Of these, two types have been tested in the flash tube - 'Spectroscopic' and 'Commercial'. The compositions of each are given in Table I. In general it is found that Commercial neon gives characteristics which are comparable with, and in some respects superior to, those of Spectroscopic neon. This is fortunate since the use of Spectroscopic neon for a large array of tubes would normally be prohibited simply by the expense involved.

2.4.2. Addition of Argon

The presence of small quantities of argon in the neon has a profound effect on the discharge characteristics. This is attributed to the "Penning" effect which involves ionization of argon atoms by metastable states of neon having energy greater than the ionization potential of argon. The reaction is :-

$$Ne^* + A \longrightarrow Ne + A^+ + e^-$$

where Ne^* represents a metastable neon atom.
The effect is twofold, firstly a large increase in the initial ionization, secondly an increase of the ionization coefficient of the gas. Both should contribute to increasing the efficiency of the tube and this is in fact observed, as shown by the results of Barsanti et al given in Fig. 2.3. However, the marked increase in efficiency is obtained only at low field values and at these fields the light output is too small for useful operation. The addition of argon is therefore of little practical value.

2.4.3. Impurities

In the process of filling the tubes the introduction of a certain amount of air is unavoidable. The chief effect of residual air is a reduction in the maximum efficiency of the tube - due to loss of initial electrons by attachment to oxygen molecules. The actual percentage

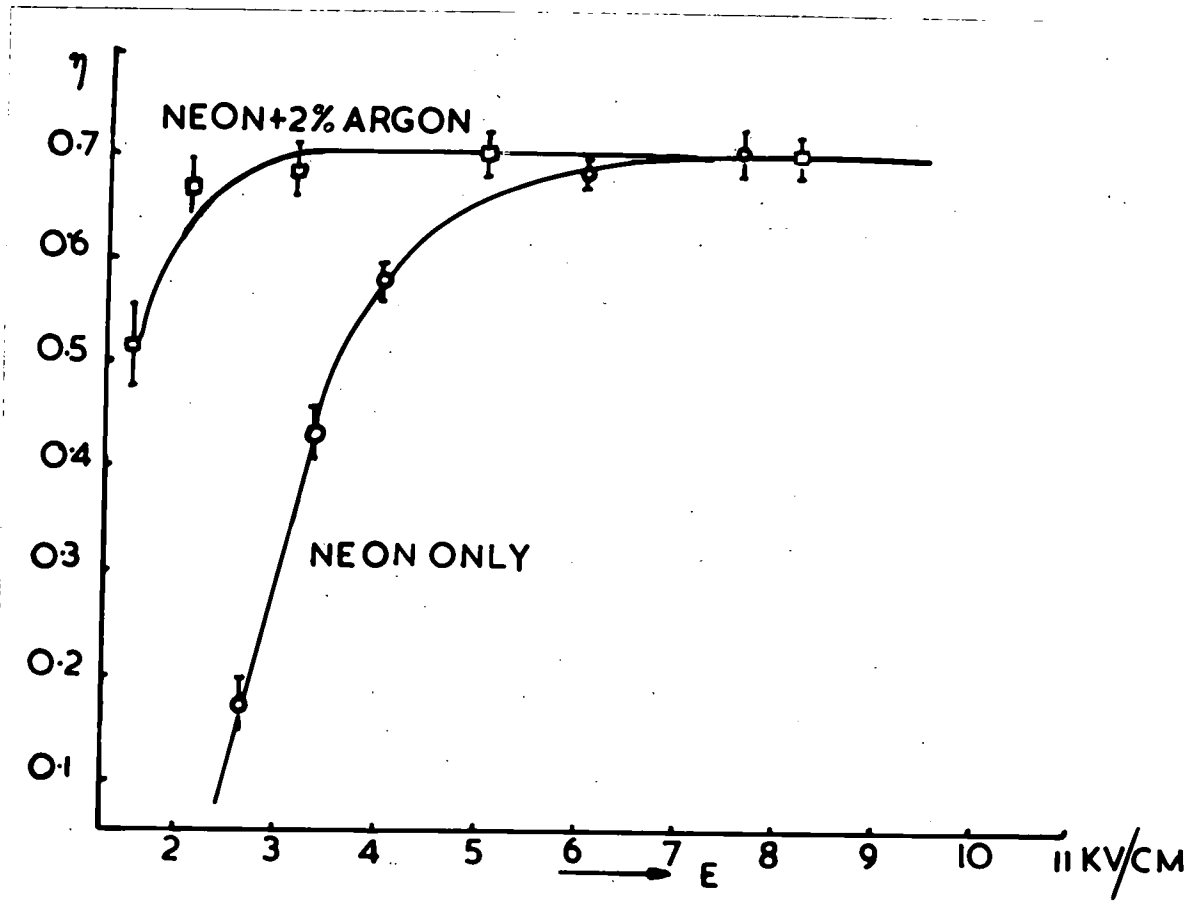

Figure 2.3. The variation of (layer) efficiency with field. (Barsanti et al, 1956)

TABLE I

Composition of neon (B.O.C.)

(vpm = volumes per million)

Gas	Commercial neon	Spectroscopic neon
Ne	98% ± 0.2%	99.9%
He	2% ± 0.2%	<1 vpm
O_2	10 vpm	~1 vpm
N_2	100-200 vpm	1 vpm
A	~0.5 vpm	-

of (residual) air which can be tolerated depends on the final pressure of the gas and on the time delay to be used. Evacuation of the tube to a residual pressure of 5×10^{-5} mm Hg of air is sufficient for all cases and for many applications a figure of 10^{-3} mm Hg is adequate. The tube itself must always be well outgassed by an extended period of evacuation but baking is unnecessary.

2.4.4. Pressure of Neon

The maximum efficiency of the flash-tube increases directly with pressure of neon as shown in Fig. 2.4. This is to be expected because of i) an increase in initial ionization and ii) a reduction in the diffusion of the initial ions before the pulse is applied. The efficiency of flashing depends of course on the probability of an electron being present in the gas when the pulse is applied.

2.5. Parameters of the Pulse

The critical parameters of the high voltage pulse, as shown in Fig. 2.1, are the height, the rise time and the pulse width.

2.5.1. Pulse Height

The variation of efficiency with pulse height is as shown in Fig. 2.3. As operating point a value of field well on the plateau is chosen. This ensures both maximum

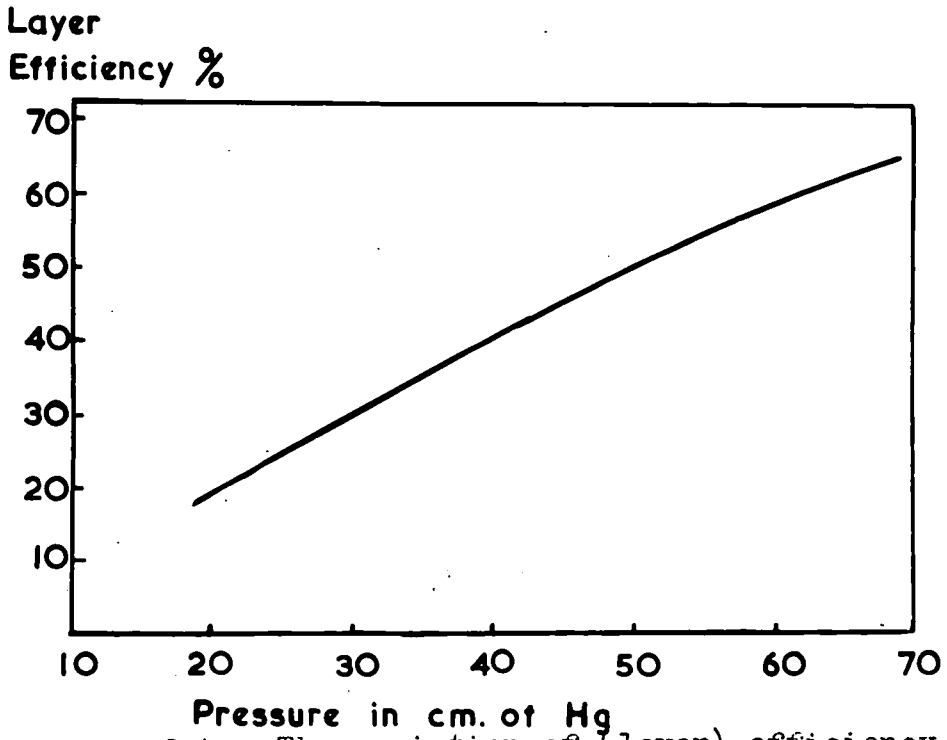

Figure 2.4. The variation of (layer) efficiency with pressure of neon.
(Gardener et al, 1957)

efficiency and adequate light output which, incidentally, is found to increase directly as the field above the minimum value for flashing. A practical limit is set to the maximum field which can be employed by the onset of brush discharge from the electrodes. Any further attempt to increase the field results in sparking and a consequent reduction in efficiency.

2.5.2. Rise Time of the Pulse

It is important to know the effect of variation of the rise time of the pulse on tube efficiency because in practice the value used may be dictated by the capacity of the tube assembly. A slowly rising pulse will tend to clear electrons to the walls of the tube before imparting to them sufficient energy to initiate a discharge. The efficiency of the tube therefore falls with increase in rise time of the pulse as shown in Fig. 2.5. An approximate quantitative treatment of the variation has been given by Gardener et al. An important point is that the attachment coefficient of oxygen for electrons has a resonance at 2 eV and this probably accounts for the greater reduction in efficiency observed in the case of tubes containing larger amounts of residual air.

2.5.3. Pulse Width

The results of Barsanti et al on spectroscopic neon show no change in efficiency with pulse widths greater than

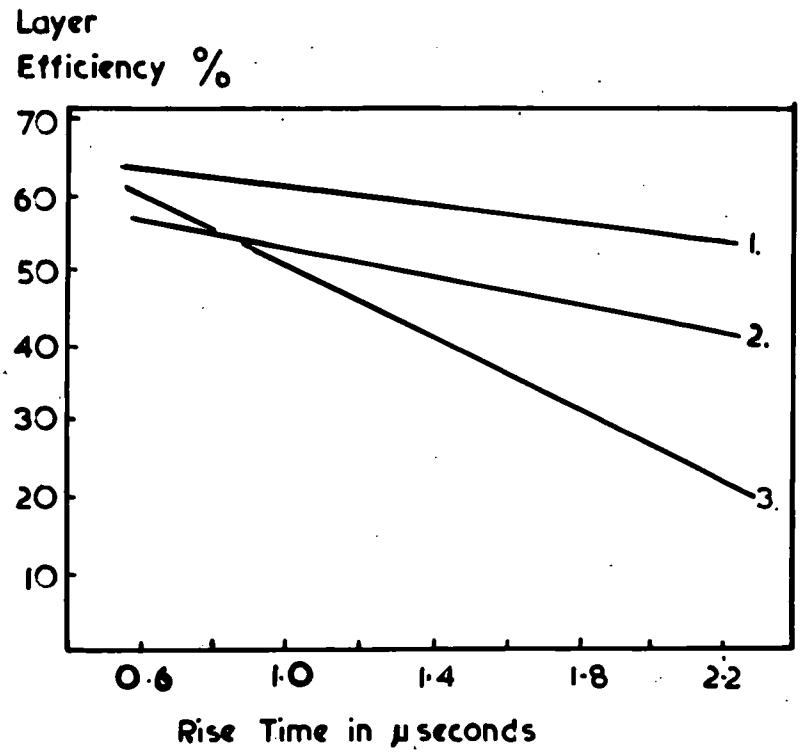

Figure 2.5. The variation of (layer efficiency with rise time, residual air as parameter.
(Gordener et ae.)

Curve 1, 66cm Ne + 6.10^{-5} mm Air
2, 65cm Ne + 1.3×10^{-3} mm Air
3, 67cm Ne + 1mm Air

3μsec but below this figure the efficiency is dependent on pulse width. The starting field for plateau efficiency is also found to depend on pulse width, if below 3μsec, becoming higher as the pulse width is reduced. This effect is not easily explained and will be considered later. With commercial neon no change in efficiency is produced by increasing the pulse width beyond 2μsec.

2.6. Time Delay

The time elapsing between the passage of a particle and the application of the pulse is termed the 'time delay'. It is necessary to know how the efficiency of the tube varies with time delay for two reasons:

1. In practice the minimum time delay attainable will be set by the apparatus. It is therefore essential to know the efficiency which can be expected at that value.
2. The variation of efficiency with time delay gives a direct measurement of the sensitive time of the tube and this determines the time resolution which can be attained.

The reduction in efficiency with increase in time delay, as shown in Fig. 2.6, is due to the removal of initial electrons from the tube by several mechanisms:-

1. recombination
2. capture and attachment to form negative ions
3. diffusion to the walls.

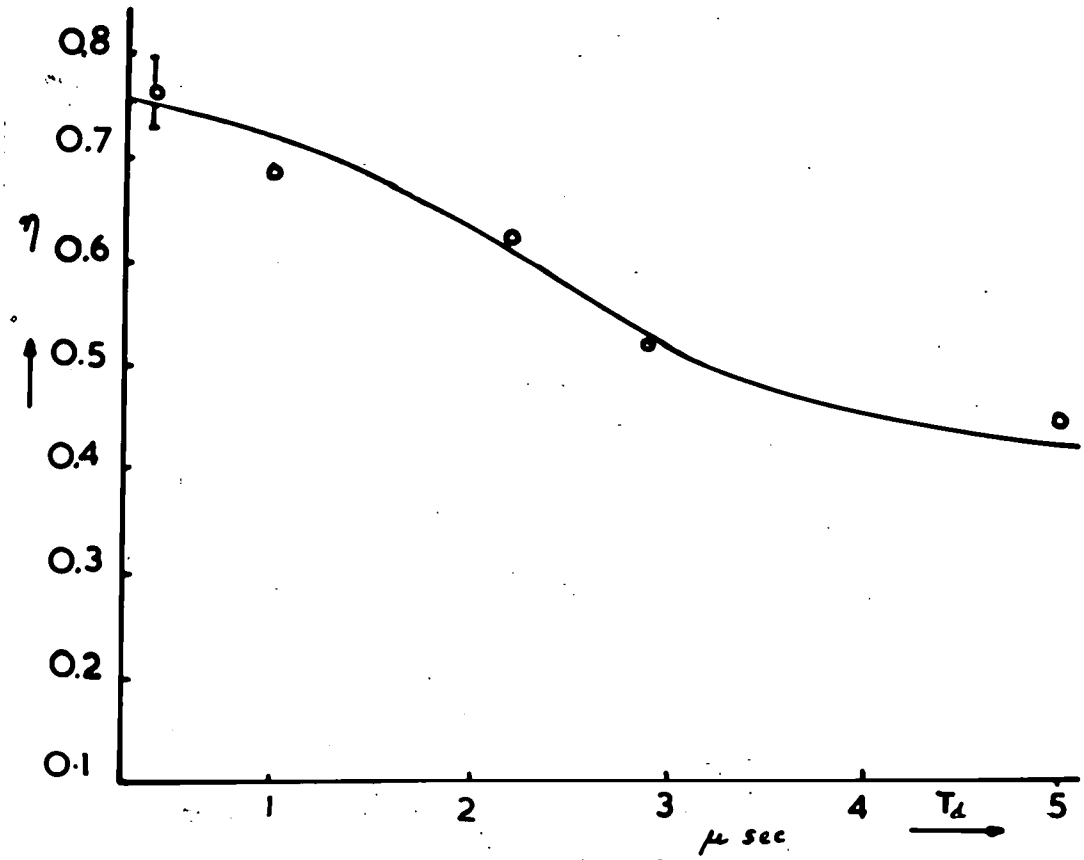

Figure 2.6. The variation of (layer) efficiency with time delay.
(Barsanti et al, 1956)

The relative contribution of each must be considered.

2.6.1. Recombination

The rate of recombination is given by

$$\frac{dN}{dt} = \alpha_r n_+ n_-$$

α_r, the coefficient of volumnar recombination is 2×10^{-7} cm^3/ion/sec for neon and n_+, n_- will be ~20 ions/cm^3 at a pressure of 65 cm. Thus the rate of recombination will be $\sim 10^{-4}$ ions/sec which for our purposes is negligible.

Preferential recombination is more important but as the free electrons produced have appreciable energies and soon escape from the neighbourhood of the positive ions, this effect, too, should be small.

2.6.2. Electron Attachment

Certain electronegative gases have high probabilities for electron attachment and the presence of a small amount of one of these, oxygen, is unavoidable in the flash-tube because of the residual air content. Oxygen has an electron attachment coefficient which varies with energy, at thermal energies it is 2.5×10^{-4} ions/cm falling to a minimum at 1.3 eV and then rising to a second maximum of 3.5×10^{-4} ions/cm at 2 eV. A simple calculation shows that with a residual air pressure of 1 mm almost 10% of the original electrons will be attached after 10μsec.

This explains the more rapid fall of efficiency with time delay observed in the case of tubes containing larger percentages of air.

2.6.3. Diffusion of Electrons to the Walls

Electrons produced in the tube by an ionizing particle diffuse rapidly to the walls of the tube where some become attached before the pulse is applied. It is very unlikely that these will participate in the avalanche since even if they are detached by the pulse, the short range attractive force exerted by the wall will cause the electrons to move tangentially and not across into the tube. Experimental results support this view therefore it can be assumed that the probability that a tube will flash depends on the number of electrons remaining in the gas. Thus the variation of efficiency with time delay should be fully accounted for in terms of diffusion theory. This will be considered in detail when discussing the theory of operation of the tube.

2.7. The Glass Container

The important relation between the efficiency of the flash tube and the properties of the glass envelope were not at first realised. The factors which must be considered are the dimensions of the tube and the composition of the glass.

2.7.1. Tube Dimensions

From purely geometrical considerations, the spatial resolution attainable with the flash tube is controlled by the dimensions of the glass container. For high resolution a small diameter is obviously required, and for high layer efficiency, a minimum wall thickness. Unfortunately the issue is complicated by the mechanism of the discharge and it has not been found possible to produce an efficient flash tube of internal diameter less than 3 mm. This is due to the limited initial ionization and to the restricted path length available for starting the discharge. In practice the required degree of resolution is obtained by using several layers of larger diameter tubes suitably staggered.

The second, and more unexpected, limitation is due to anomalous relation between tube efficiency and the thickness of the glass wall (Fig. 2.7). For tubes of internal diameter 0.6 cm, optimum efficiency is obtained using walls 1 mm thick. This effect poses a further problem and will be considered later.

2.7.2. The Chemical Composition of the Glass

The composition of the glass is also important. Pyrex was found unsuitable after the early experiments because of its tendency to cause spurious flashes even at quite low

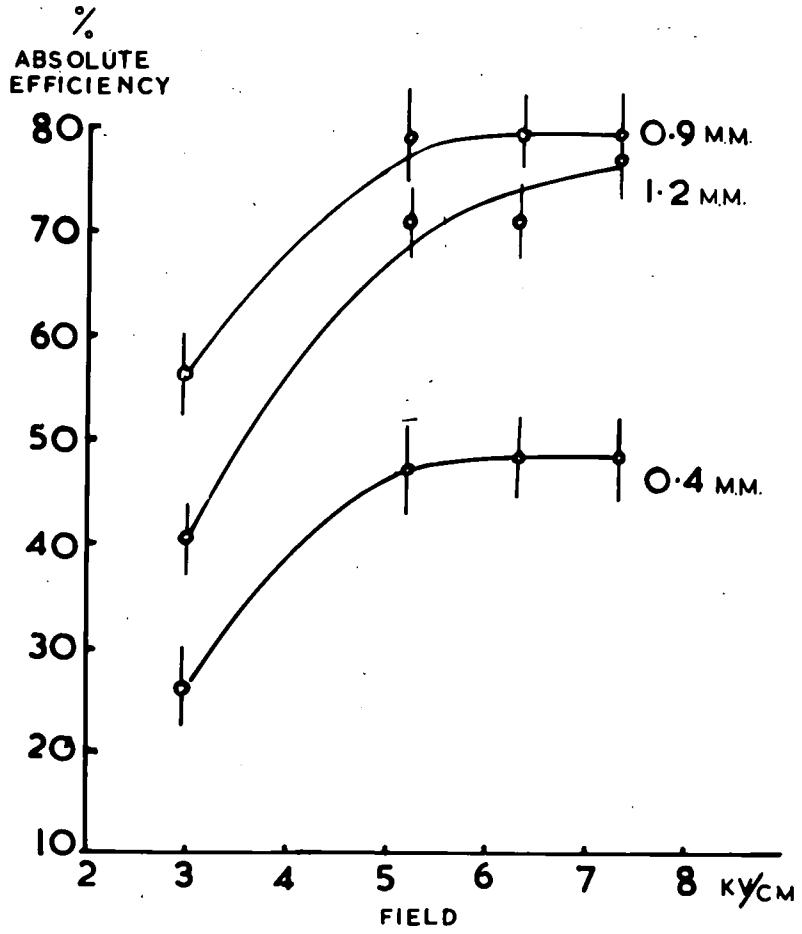

Figure 2.7. The variation of efficiency with glass thickness.

values of field. This however is probably due to the method of its manufacture. Pyrex tubing is made in a continuous process in which the glass is drawn over a steel mandrel. This is liable to result in many surface defects compared with the "drawn" soda glass tube which has in effect a "fire polished" surface. Surface imperfections, of course, are important in causing "field emission" - the irregularities producing intense local fields. Soda glass has further advantages in its electrical properties: the photoelectric current yield (proportional to the density of sodium atoms) is at least six times that of Pyrex and similarly, secondary electron production is higher.* The volume and surface resistivities are in fact lower than those of Pyrex but it is difficult to assess the effect of these on the efficiency of the tube. The outside surface conductivity of the glass will certainly tend to quench the field inside the tube but as the time constant involved is much longer than the duration of the pulse, the effect should be negligible.

The requirements of the container may be summarised as soda glass tubes of wall thickness 1 mm and diameter preferably not less than 0.6 cm.

(*Rohatgi, 1957; Gill and Von Engel, 1949.)

2.8. Conclusions

As a detector of ionizing particles the neon flash tube proves to be a robust and inexpensive device of relatively simple construction, well suited to mass production methods. Correctly operated it is capable of a satisfactory performance under most conditions.

CHAPTER 3

The High Pressure Neon Flash Tube

3.1. Introduction

Development of the neon flash tube was undertaken to provide a particle locator which would fulfil the particular requirements of a cosmic ray spectrograph. These may be stated as:

1. High efficiency for flashing after traversal by an ionising particle
2. Short sensitive time
3. Low rate of spurious flashing
4. High spatial resolution
5. Stability of operation
6. Long lifetime.

The question of the spatial resolution obtainable with the flash tube has already been considered. For the reasons discussed it was decided to use soda glass tubes of internal diameter of 5.5 mm and to employ several layers of tubes to achieve the required accuracy of track location. Further parameters affecting the behaviour of the tube were systematically investigated as will be described:-

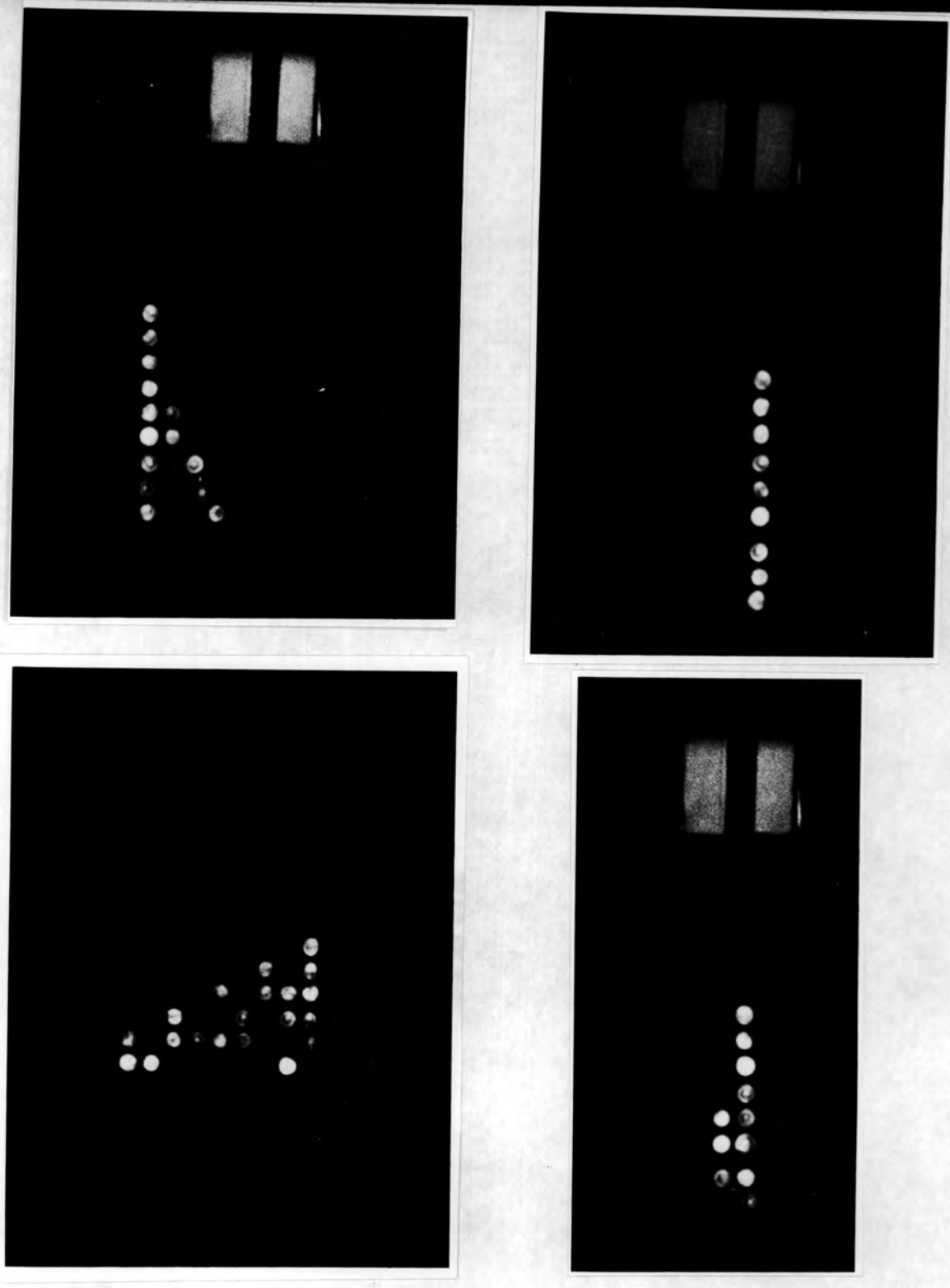

Plates II. Photographs of the high pressure flash tubes.

3.2. The Pressure of Neon

For time delays exceeding 5μsec the efficiency of tubes filled at a pressure of 0.8π falls off rapidly. However the results shown in Fig. 2.4 implied that the high efficiency could probably be restored by increasing the gas pressure. Pressure greater than one atmosphere were obtained by partially immersing the tubes in liquid nitrogen whilst maintaining the pressure in the system just below atmospheric during the sealing off process. Measurements were made at a variety of pressures and results showing the dependance of plateau efficiency on time delay in the range 0.8 to 3.0π are given in Fig. 3.1. It is obviously an advantage to use pressures greater than two atmospheres if time delays in the region of 5μsec are to be encountered. A consequence of increased pressure is, however, a correspondingly longer sensitive time. Thus in operation, flashes will appear due not only to the triggering particle but also to earlier, unwanted particles. Obviously the number of such flashes should be kept to a minimum and a compromise pressure must be adopted for which the layer efficiency is reasonably high and the rate of unwanted flashes sufficiently low. Considering expected time delays of up to 10μsec this optimum pressure is approximately 2.3π for tubes of internal diameter 6.0 mm. The study of the characteristics of tubes filled at this pressure will now be described.

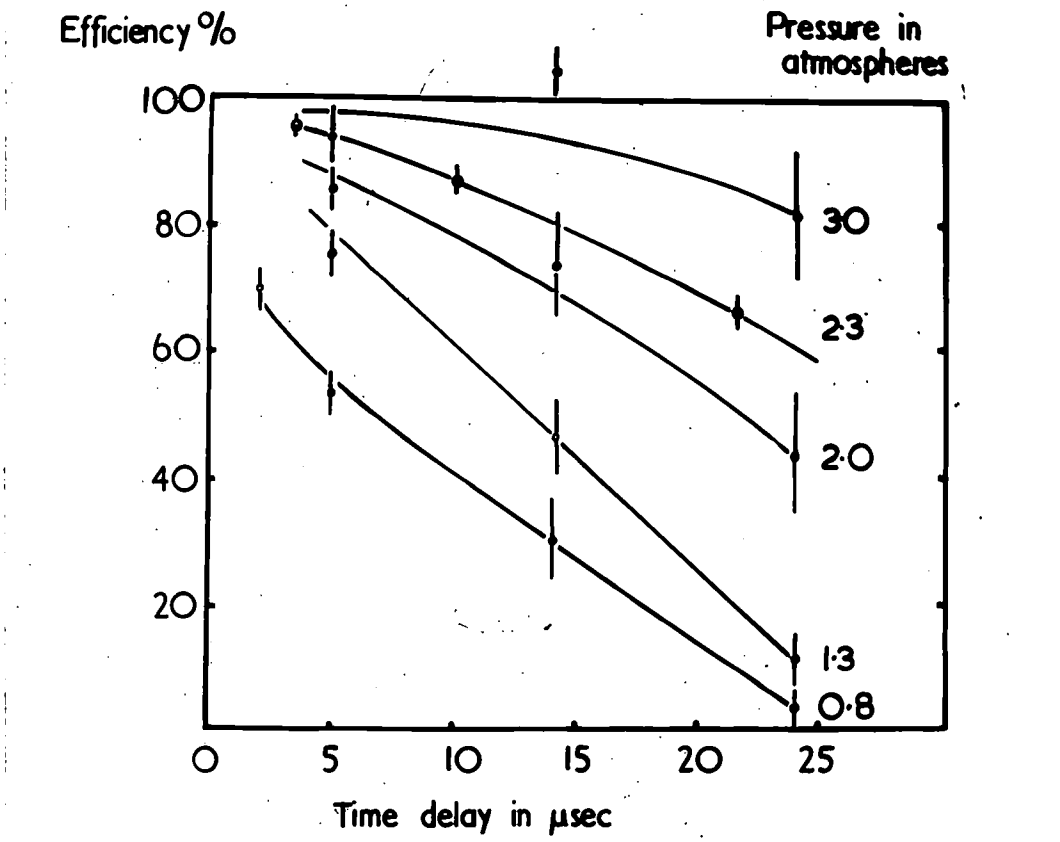

Fig. 3.1. The efficiency, time delay characteristics of flash tubes with gas pressure as parameter. E_{max} = 6.3 Kv/cm, T_R = 0.5 μsec and τ = 3.0 μsec

3.3. Experimental Arrangement

The apparatus was of the pattern previously described. The stack consisted of 81 tubes in 9 layers with electrodes every third layer; this arrangement providing the minimum amount of electrical leakage between the plates.

To prevent photons spreading from a flashed tube to cause photo-flashing in adjacent tubes not traversed by particles, the outside of each tube was painted black. In previous experiments a black paper wrapper had been employed but the painting method was considered easier. Flashes were recorded on Ilford H.P.S. film, the camera having an F 3.5 lens.

The layer efficiency was evaluated according to the definition in Chapter 2. An issue of some importance is the accuracy of these experimental values. The statistical uncertainty in the measured layer efficiency η_L was derived from the experimental data using the relationship:-

$$\sigma_L = \frac{\eta_L \sqrt{1 - \eta_L}}{\sqrt{n}}$$

where n is the observed number of flashes. For the value of n (~100) used in most of the experiments the relation is accurate for efficiencies to within a few per cent of the maximum value. The internal efficiency is therefore:

$$\eta = R\left[\eta_L \pm \frac{\eta_L \sqrt{1 - \eta_L}}{\sqrt{n}}\right]$$

R in this case being 1.472.

The derivation and limits of accuracy of this relation are given in appendix I.

3.4. The Variation of Efficiency with Parameters of the Pulse

The variation of efficiency with field is shown in Fig. 3.2. Apart from the peak height, the main parameters of the pulse are rise time, T_R, and width, τ, The dependance of efficiency on rise time is shown in Fig. 3.3 and the effect of extreme values of T_R on the efficiency-field characteristic are shown in Fig. 3.4. In practice the rise time will rarely exceed 0.5μsec. Throughout the experiments a pulse width of 3.5μsec was used.

3.5. Purity of the Gas

Impurities in the gas are usually detrimental and arise from two sources - those present in the gas sample and those due to insufficient evacuation before filling. In Commercial neon the constituent showing by far the biggest variation in quantity from one cylinder to another is nitrogen. Tests were therefore made on tubes containing spectroscopic neon together with various, known concentrations of nitrogen up to 1,000 vpm. (All filled at 0.8 atmospheres total pressure). The results, given in Table II, show no apparent reduction in efficiency even at the

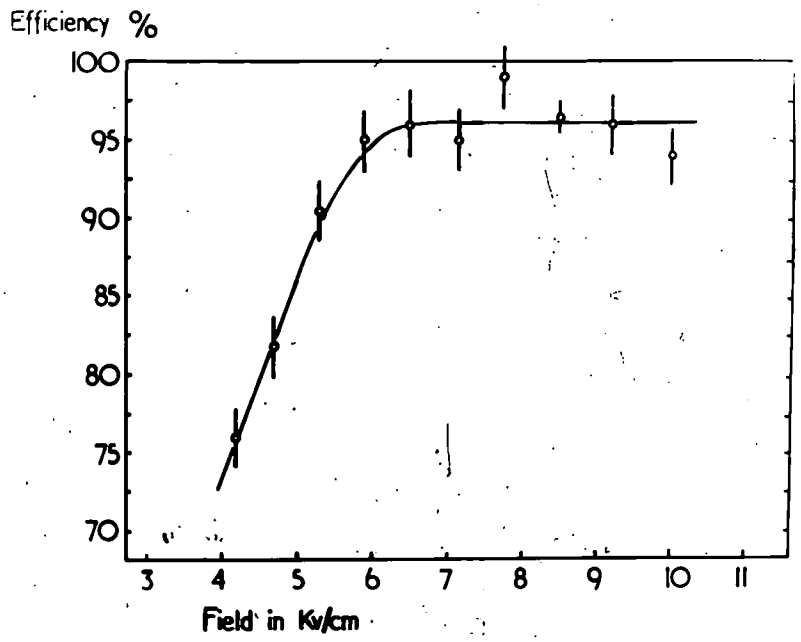

Figure 3.2. The efficiency, field strength characteristics Neon pressure 2.3 atmospheres. T_R = 0.5 μsec τ = 3.5 μsec and T_D = 3.4 μsec.

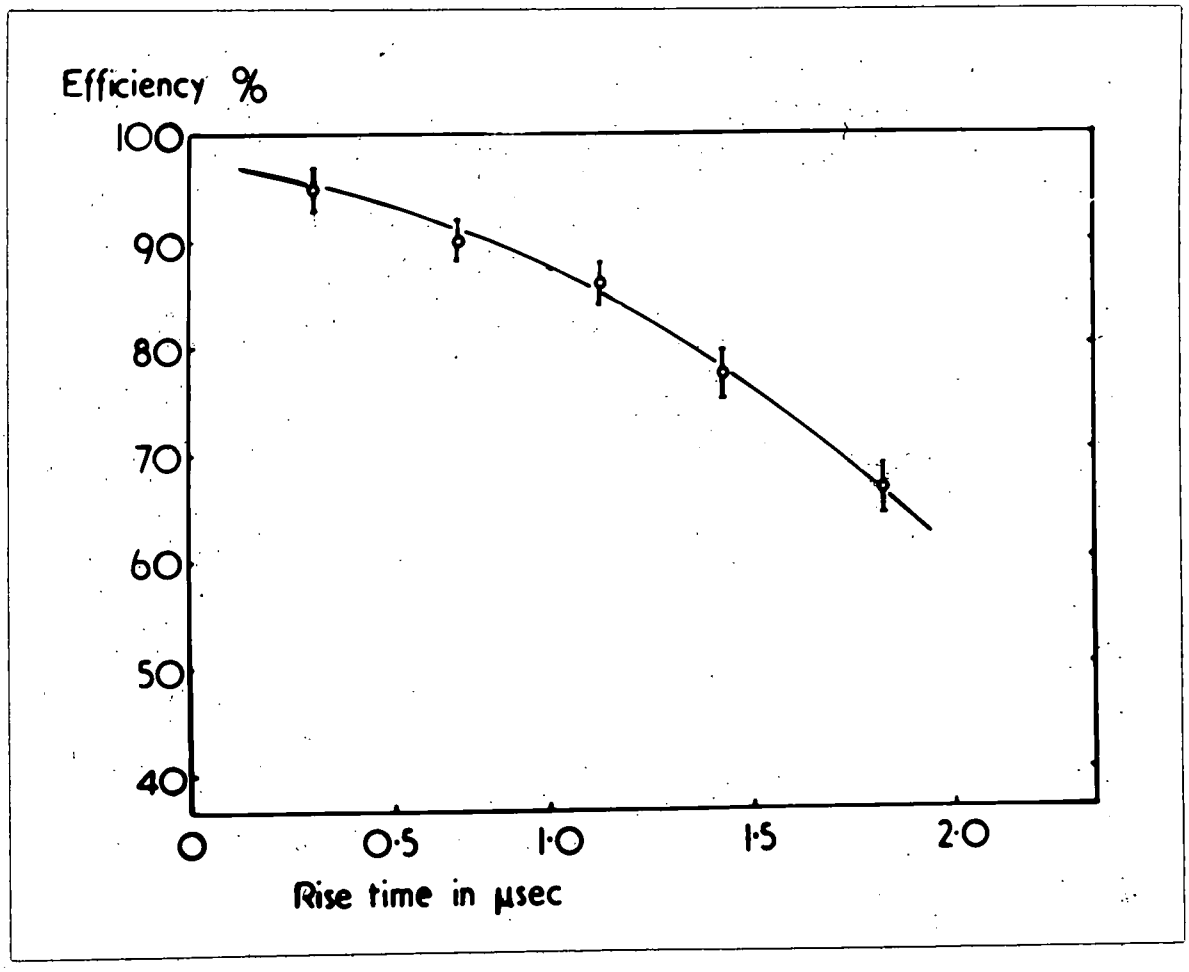

Fig. 3.3. The variation of plateau efficiency with rise time. Neon pressure 2.3 atmospheres; E_{max} = 7.0 Kv/cm, T_p = 4.0 μsec and τ = 3.5 μsec

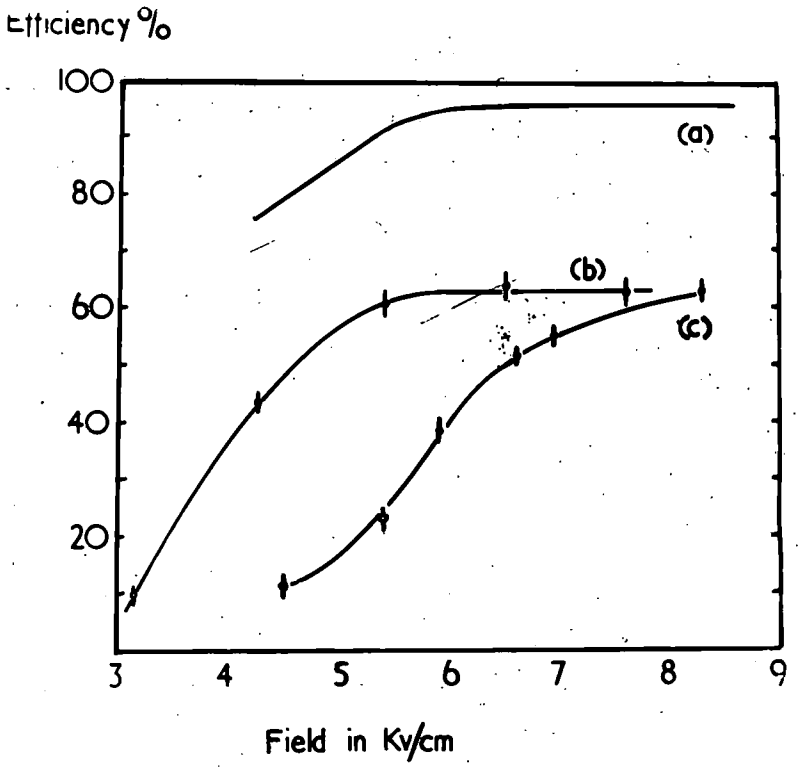

Figure 3.4. The dependence of efficiency on field strength at long time delay and extended rise time.

a) T_R = 0·5 μsec τ = 3·5 μsec T_0 = 3·4 μsec

b) T_R = 0·5 μsec τ = 3·5 μsec T_0 = 26 μsec

c) T_R = 2·0 μsec τ = 3·5 μsec T_0 = 4·0 μsec

TABLE II

The variation of efficiency with pressure of nitrogen impurity

Nitrogen content: vpm	250	500	750	1000
Internal efficiency	85 - 90%	80 - 85%	80 - 85%	94 - 100%

The neon in the tubes was of spectroscopic quality at a pressure of 0.8 atmospheres.

The pulse characteristics were E_{max} = 6.5 Kv/cm, T_R = 0.6 μsec, T_D = 4.0 μsec and τ = 3.5 μsec.

highest concentration of nitrogen. A considerable change in colour, however, was noted, the characteristic red glow becoming progressively blue with added nitrogen, but no change in the intensity of the photographic image was observed. (This effect, incidentally, provides a useful method of estimating the actual nitrogen content of neon samples).

Oxygen is certainly detrimental because of the high probability of electron attachment as already mentioned. Since the oxygen content of commercial neon can be as high as 10^{-3}% there is little to be gained by evacuating the tubes down to a pressure below 10^{-3} mm Hg of residual air and the tubes used in the present investigation were in fact evacuated to this limit.

Some degassing of the glass was effected by continued pumping over several hours.

3.6. The Sensitive Time of the Tube

The variation of efficiency with time delay is shown in Fig. 3.5. At long delay the curve flattens off to the background rate, which will be discussed in the next section. After subtracting this background, the sensitive time is given by:

$$T_S = \int_{-\tau}^{\infty} \eta(t)\, dt$$

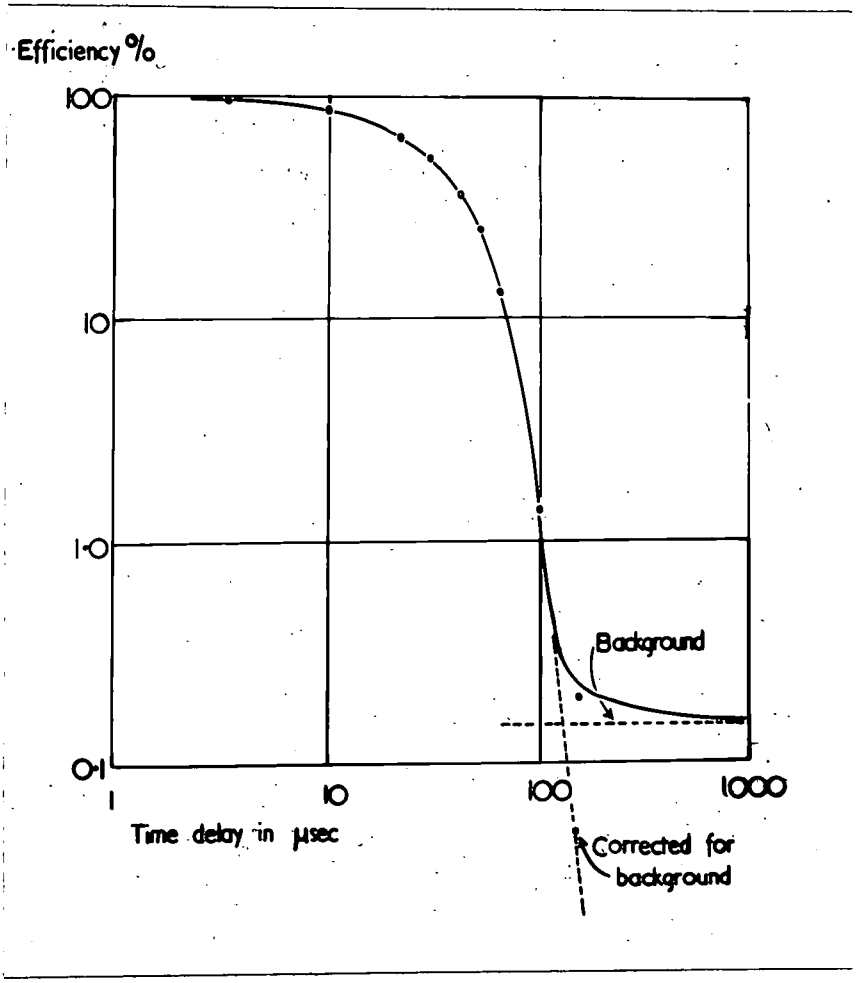

Fig. 3.5. The variation of plateau efficiency with time delay. The variation is also shown after correction for background.

E_{max} = 8.5 Kv/cm, T_{β} = 0.5 μsec and τ = 3.5 μsec

The lower limit, $-\tau$, is necessary to allow for flashes produced by particles traversing a tube during the time, τ, for which the pulse is applied. The observed value of T_s, 39 μsec, is sufficiently short for most cosmic ray experiments but in certain work with particularly high particle rates it could be excessive. Methods of reducing the sensitive time were therefore investigated.

3.7. The Application of a Clearing Field

Theoretically it should be possible to apply a static clearing field which would sweep unwanted electrons to the walls of the tube in the time between events. An inspection of the known values of electron mobility indicates that a field of about 100 v/cm should reduce the sensitive time to some 5μsec. Experimentally, however, fields as high as 2Kv/cm were required to produce any significant variation in sensitive time. A possible explanation is that the static field was partially "backed off" by movement of charges round the inside of the walls, together with a weak discharge in the gas. At a field of 2Kv/cm this discharge, which was easily visible, was sufficient to render the tubes inoperative because of the increased rate of spurious flashing. The use of a clearing field to reduce the sensitive time was therefore considered impracticable.

A change in pulse characteristics, such as an extension of the rise time, can be used to reduce the sensitive time but this also reduces the maximum efficiency.

3.8. The Dead-Time of the Tube

In most particle detectors a certain dead-time follows each detected particle during which subsequent particles will not be recorded. When a neon tube has flashed there is a finite probability that the tube will flash again if a subsequent pulse is applied. This so called "after-flashing" is caused by ions remaining in the tube from the previous discharge and falls fairly rapidly from unity after a characteristic "dead-time".

In cosmic ray experiments the particle rate is seldom high enough for the limitation set by the dead time to be important and in practice the after flashing can be a useful characteristic for two reasons:

1. It enables a much more intense photographic record to be made, if required, by applying a succession of pulses which causes repeated flashing.
2. Repeated flashing imparts a memory to the system so that some selection of events can be made and the camera shutter only opened when a selected event occurs.

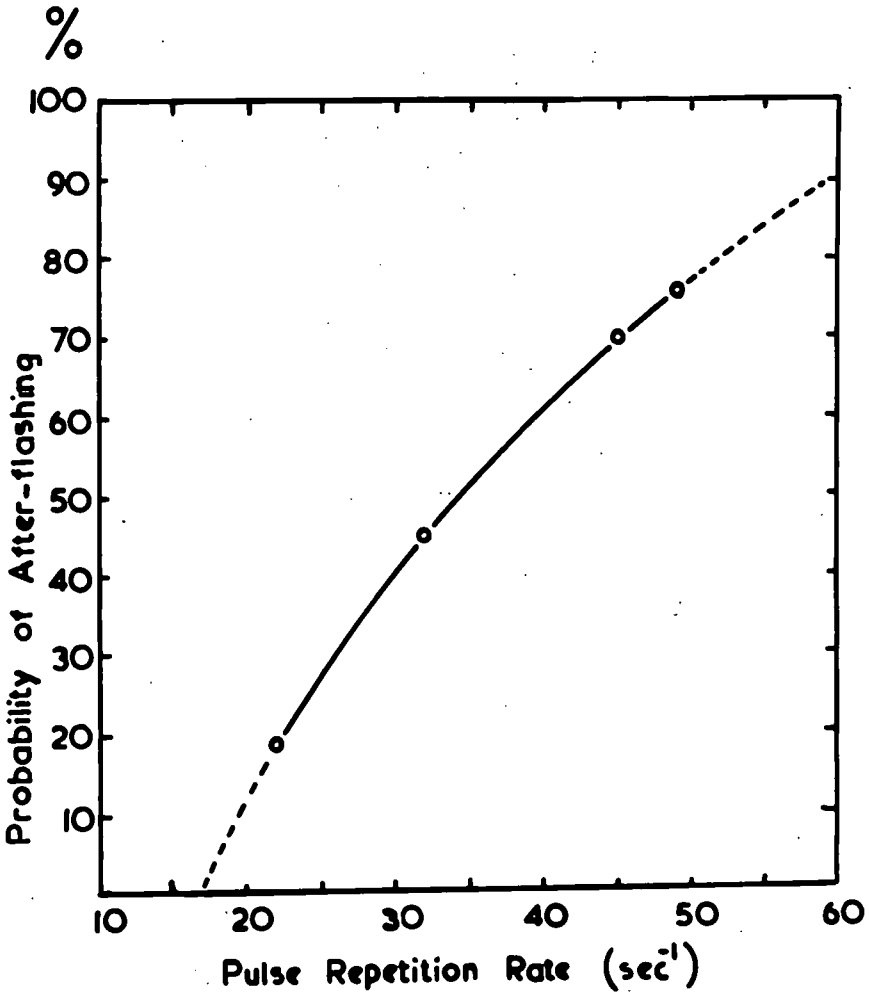

Figure 3.6. The probability of repeated after-flashing of a tube as a function of the repetition rate of the applied pulse. E_{max} = 7.0 Kv/cm, T_D = 3.4 μsec, T_R = 0.5 μsec and τ = 3.5 μsec.

An experimental study was made of the pulse repetition rate required to ensure repeated flashing. Pulses were applied at a variable rate for 2 seconds after each triggering pulse and the probability of after-flashing determined visually. The criterion was a minimum of 4 consecutive after-flashes but in most cases after-flashing continued for the full period of 2 seconds. The results are given in Fig. 3.6. It is seen that a repetition rate of 60 pulses/sec is required for efficient after-flashing.

The repetition rate for a 50% probability of after-flashing is 36/sec - corresponding to a repetition period of 28 m.sec. Thus the probability of a flash being followed by another will fall to 50% for a time interval rather greater than 28 m.sec and the dead time of the detector is therefore of this order.

3.9. Spurious Flashes

An experiment was performed to find the probability of a tube flashing under a random pulse - that is a pulse not directly associated with an incident particle. The G.M. counter triggering was dispensed with and the tube was subjected to pulses at a rate of about 70/min. Flashes were recorded photographically keeping the camera shutter open for extended periods. For a pulse

with E_{max} = 8Kv/cm, T_R = 0.6μsec and τ = 3.5μsec, the spurious rate, p, was found to be 1.12 x 10^{-4} per pulse per tube. The background rate plotted in Fig. 3.5 is accordingly $\frac{pn}{R}$ where n is the number of tubes in a layer and R is the geometrical factor 1.472.

The flashing probability due solely to cosmic rays passing through the tube at times before the instant of application of the pulse is given by $P_e = NT_S$ where N is the rate of cosmic rays passing through a single tube and T_S is the sensitive time. Substituting the appropriate values, suitably corrected for the effect of showers and knock-on electrons, P_e = 2.64 x 10^{-5}. The ratio of observed to expected is thus 4.2 : 1.

There are two probable sources of the extra flashes. The first is field emission from the glass, which is found to be prominent with Pyrex tubes at high fields, (10-12Kv/cm) but this is unlikely in the present case since the operating fields were low - and the flashes were randomly distributed.

The second likely source of spurious flashes is radioactive contamination of the glass and the surroundings. Flashes due to radioactivity will arise from photoelectrons, liberated by γ-rays, giving rise to widely differing degrees of ionisation in the gas. Consequently an appreciable variation of spurious flashing

with field is expected since, at higher fields, smaller numbers of electrons are required to initiate a discharge. This effect was examined by varying the size of the applied pulse. The results, given in Fig. 3.7, show that the probability of spurious flashing varies approximately as the square of the field. Also shown in Fig. 3.7 is the result of a similar experiment in which the rate of spurious flashing was enhanced by the proximity of a radioactive source. The form of the variation is very similar to that observed with no source and appears to confirm that most of the spurious flashes are of radioactive origin. Further evidence in favour of this hypothesis is the fact that the ratio of genuine to total flashes (1:4) is of the same order as the ratio of cosmic ray to total counts in a typical copper-in-glass Geiger counter. In the latter case it is generally considered that radioactive impurities are responsible for the non-cosmic ray counts.

The conclusions drawn from this study of spurious flashes were that their origin is reasonbly well known and, for most applications, their presence is no serious disadvantage.

3.10. Stability of Operation

External conditions which might affect the stability of operation are ambient temperature and humidity. Since

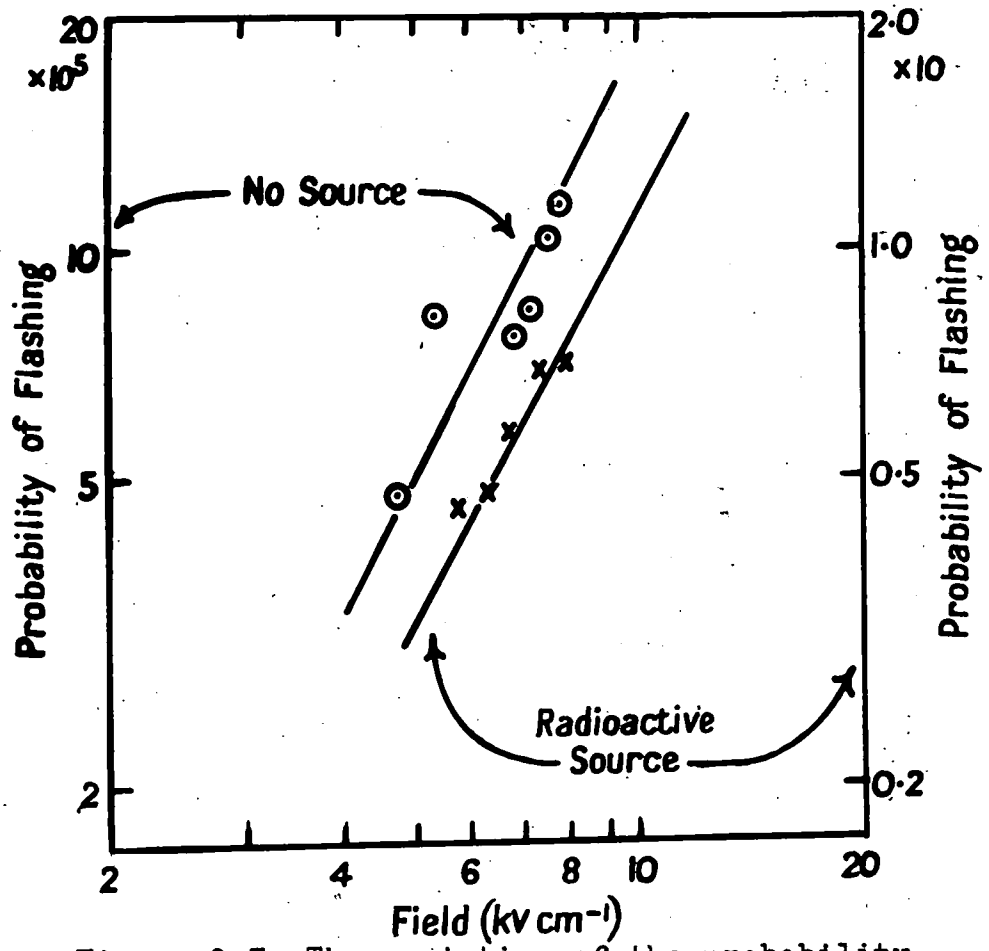

Figure 3.7. The variation of the probability of spurious flashing with applied field. The two sets of points refer respectively to normal flashing and to flashing under the influence of a radioactive source. The tubes and pulse characteristics are as for figure 3.2.

the electron agitation energy is related to the ambient temperature, any change in temperature might affect the plateau efficiency. The diffusion coefficient of the electrons is also temperature dependent, but a theoretical analysis shows both effects to be very small in the temperature range encountered. However, detailed measurements were made at a variety of temperatures and these showed that there was in fact no significant change over the temperature range used, 14 - 40°C.

High humidity can cause electrical leakage between the plates with a consequent reduction of field and therefore of intensity of flashing. Normal values of humidity (~65% R.H.) are quite satisfactory. Where this is expected to be exceeded an effective remedy is to encase the assembly of tubes and electrodes in paraffin wax. This, incidentally, gives extremely stable working characteristics.

3.11. Lifetime

An important characteristic of any detector is its expectation of life. If the flash-tube contained only a pure gas an infinite life might be expected. However impurities are present in the original gas filling and others may be introduced from the glass walls by ionic impact. Since the characteristics of a discharge are

affected by even minute quantities of impurities it cannot be stated a priori that the lifetime will be long and an experimental check must be made.

A set of tubes of previously measured efficiency was subjected to pulses at a rate of approximately 1 per second for 13 days. A nearby radioactive source was used to ensure a flash in each tube for almost every pulse which resulted in a total number of over 10^6 flashes for each tube. The efficiencies were re-measured at the end of the experiment with the result given in Table III. There was no significant change in efficiency at normal time delays but at 40μsec delay there appeared to have been an appreciable reduction. This reduction could have been due to a change in the internal surface conditions following the repeated ionic bombardment or, more likely, to changes in the composition of the gas due to electrophoretic action.

The change in characteristic is not important in practice.

3.12. The accuracy of spatial resolution

In many applications high spatial resolution is required. This is best attained by using several layers of tubes staggered so as to give roughly constant resolution over the angle of acceptance of inci-

TABLE III

Lifetime test

	a)	b)
Efficiency at start	97.5 ± 3.4%	47.0 ± 2.8%
Efficiency after 10^6 flashes	94.5 ± 3.4%	35.5 ± 2.9%

The pulse characteristics were E_{max} = 10 Kv/cm

T_R = 0.6 μsec τ = 3.5 μsec.

a) T_D = 4 μsec b) T_D = 40 μsec.

The tubes contained commercial neon at a pressure of 2.3 atmospheres.

dent particles. The situation for tubes of rather low internal efficiency (~72%) has been described by Ashton et al (1958), where it is shown that the standard deviation of the positional uncertainty from a stack consisting of five layers of tubes, of identical diameter to those used in the present study, is 0.6 mm. For the high pressure tubes described here the uncertainty is appreciably lower and a geometrical analysis indicated a value of 0.46 mm for five layers of tubes staggered in the optimum manner. The distribution in deviations between the known and predicted track position, found by geometrical analysis, is roughly Gaussian. In practice a longer "tail" is expected due essentially to spurious events, i.e. the flashing of tubes not traversed by the triggering particle. The contribution from the phenomena described in 3.9 is very small and most of the effect arises from knock-on electrons. These occur when the triggering particle passes through the gap between the sensitive volumes of two tubes and a knock-on electron produces a flash in one of them. An estimate of the magnitude of this effect can be made. The probability of two adjacent tubes flashing in one layer was found experimentally to be 3.75%. The probability of a knock-on event of the type described above will be higher, of the order of 5%, and the result in these cases is an error of location in that layer of almost one tube

radius. However, in some cases the knock-on events can be recognised on account of misalignment with the flashes in other layers and the effect is reduced. It is concluded that the error in the mean position resulting from unrecognised knock-on events is about 1 mm and occurs with a frequency of about 3%. This frequency is only the same as that expected on the Gaussian distribution and the effect is thus barely significant.

3.13. Conclusions

The investigations described show that the 2.3π flash tube is an efficient particle detector characterised by low frequency of spurious flashes, long lifetime and stability of operation.

The tube was subsequently produced in large numbers and installed in the Durham Cosmic Ray Spectrograph where it is used for the precise location of μ-meson trajectories. Similar tubes have been used at the Pic du Midi for the location of incident proton trajectories in studies of high energy nuclear interactions in a magnet cloud chamber.

3.14. Discussion

From the results described it would appear that it is possible to design a flash tube suitable for specific applications. The design is carried out in two stages:

firstly, subject to the conditions already mentioned, a tube diameter is chosen which will give the required spatial resolution without requiring an excessive number of layers. Secondly a gas pressure is chosen to give a) a high enough plateau efficiency at the prescribed time delay and b) a low enough rate of spurious flashes.

To facilitate the choice of optimum pressure the possibility of establishing a universal relation between efficiency and some function of time delay and pressure was considered. The single parameter T_D/P was found suitable and the variation of η with T_D/P is shown in Fig. 3.8. In addition to measurements made in the present work, those of Gardener et al at a pressure of 46.1 cm Hg of neon are included to cover a range of pressure from 0.6 to 3.0 atmospheres.

The pressure required to obtain a particular efficiency at a certain time delay can thus be determined from the curve of Fig. 3.8 and the frequency of spurious flashes can be found by multiplying the area under the curve by a factor of four - to allow for the cosmic ray rate and the contribution from background radioactivity.

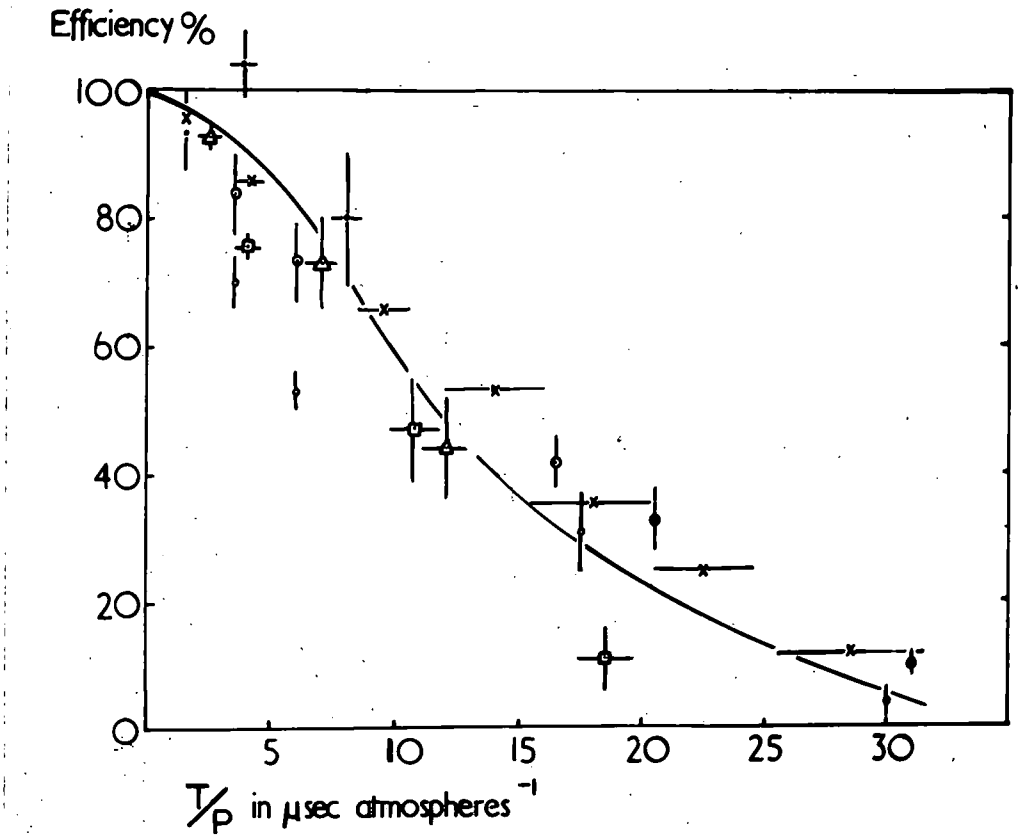

Fig. 3.8. The variation of efficiency with the ratio of time delay to pressure. The curve is an approximate best-fit to the experimental points.

CHAPTER 4

The Development of a Flash Tube for Use in Studies of Extensive Air Showers.

4.1. Introduction

The flash tube is eminently suited to experiments in extensive air showers because of the facility with which large areas of detectors can be produced and the simplicity and ease of their operation. Therefore the possibility of developing a flash tube for applications in E.A.S. was considered.

In most experiments the requirements of spatial and of time resolution should not be as critical as those demanded in the previous application. A longer sensitive time could be in fact a decided advantage in view of the time delays which might be introduced by the necessarily wide distribution of apparatus. The tube and its associated equipment should be readily adaptable for production in large numbers. Essentially the requirements of the tube are:

1. High plateau efficiency
2. High efficiency at reasonably long time delays
3. Neon pressures less than one atmosphere for ease of filling.

4.2. Tube Size

Experiments on tubes of small diameters had shown that the maximum efficiency falls as tube diameter is reduced. It was logical, therefore, to presume that the use of larger diameter tubes would result in higher efficiencies. In E.A.S. work, extremely high spatial resolution is seldom required, therefore the use of a larger diameter tube presents no disadvantage. Accordingly, trial tubes were produced having internal diameters of 0.8 cm, 1.0 cm and 1.5 cm. These were filled at 35 cm Hg (Ne C) and when tested gave the results shown in Table IV. The very high efficiency attained with the 1.5 cm tube was encouraging and development was started using tubes of this diameter. Soda glass was used throughout, a tube length of 24 cm being chosen simply for convenience in testing and filling.

4.3. Gas filling

In addition to the 'Spectroscopic' and 'Commercial' neon already mentioned, a third variety is available which contains a nominal 80% Ne and 20% He with up to 2% Nitrogen and small amounts of other impurities. This had been found unsuitable in small diameter tubes but an investigation was carried out to find if it could be used in the larger tubes. (This was not a purely academic

TABLE IV

The variation of efficiency with tube diameter

Tube internal diameter	0.8 cm	1.0 cm	1.5 cm
Layer Efficiency	63.3%	70.5%	81%

The tubes contained Commercial neon at a pressure of 35 cm Hg.

The characteristics of the pulse were :

E_{max} = 8 Kv/cm T_R = 0.6 μ sec. T_D = 3.0 μ sec.

τ = 3.5 μ sec.

exercise. It was estimated that some 180 litre-atmospheres of neon would be required for an E.A.S. array, therefore a considerable economy could be effected by using this less expensive grade.) Tubes were filled at pressures of 35 cm, 45 cm, 65 cm and 1.9π and tested. The characteristic blue colour of the nitrogen discharge was much in evidence and field strengths exceeding 20Kv/cm were found necessary. The results are given in Table V. The trend of lower efficiency with increase in pressure was unexpected, and is not easily explained. The fact emerges that this variety of neon is not suitable for the production of tubes of high efficiency.

4.4. Pressure of Neon

Tubes filled at various pressures of neon were prepared to ascertain the effect of pressure on the efficiency of the tube. Tests in this case were carried out in a 'wax' stack - that is with tubes and electrodes encased in paraffin wax. This results in an improved field distribution inside the tube together with more stable operating conditions. The characteristics obtained are shown in Figs. 4.1 and 4.2. Change of pressure is seen to have a more marked affect on the variation of efficiency with time delay. (The effect of applying a

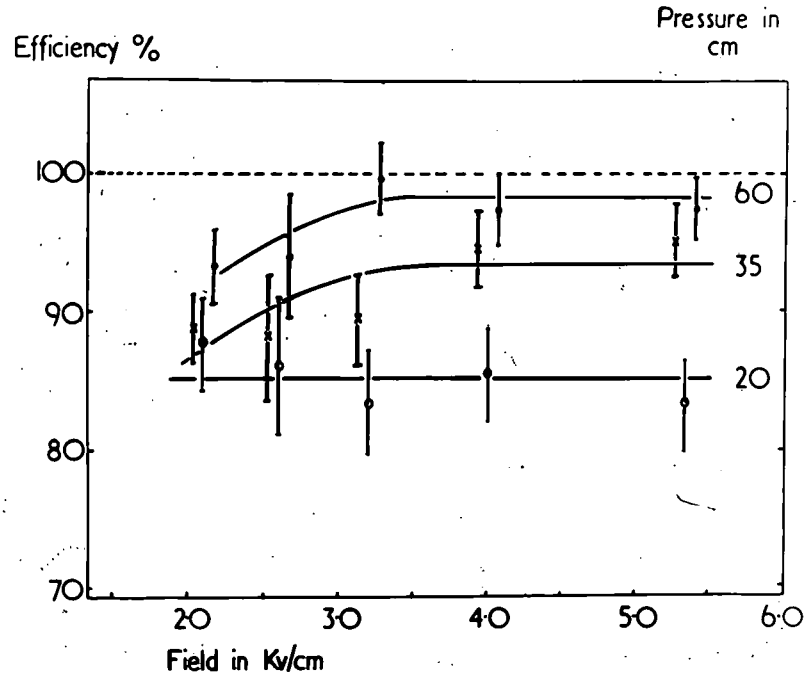

Figure 4.1. The efficiency, field characteristics for 1.5 cm diameter tubes with gas pressure as parameter. T_D = 3.2 μsec, T_R = 0.5 μsec and τ = 4 μsec.

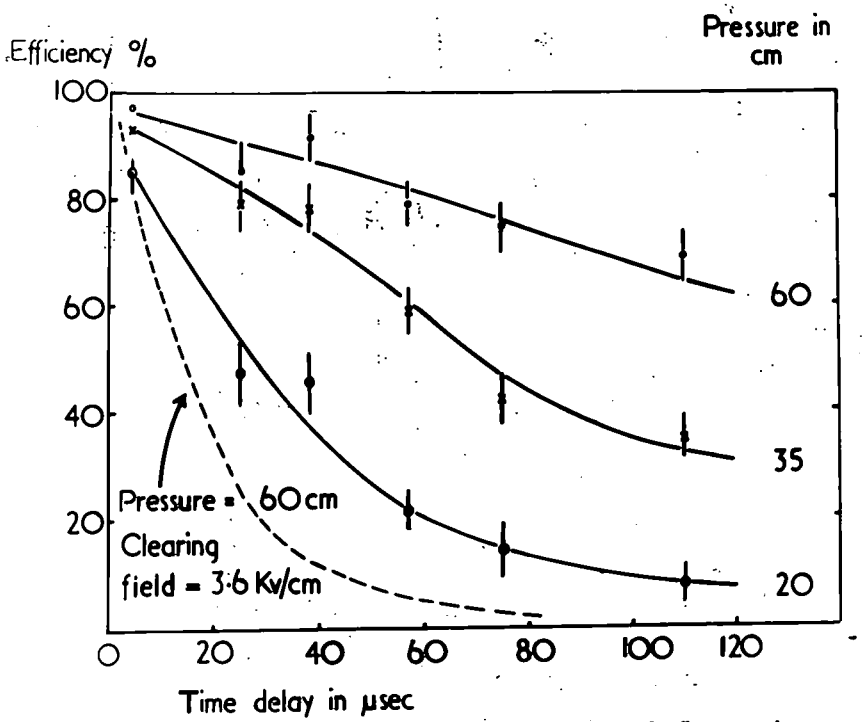

Figure 4.2. The efficiency, time delay characteristics for 1.5 cm diameter tubes with gas pressure as parameter. E_{max} = 3.7 Kv/cm, T_R = 0.5 μsec and τ = 4 μsec.

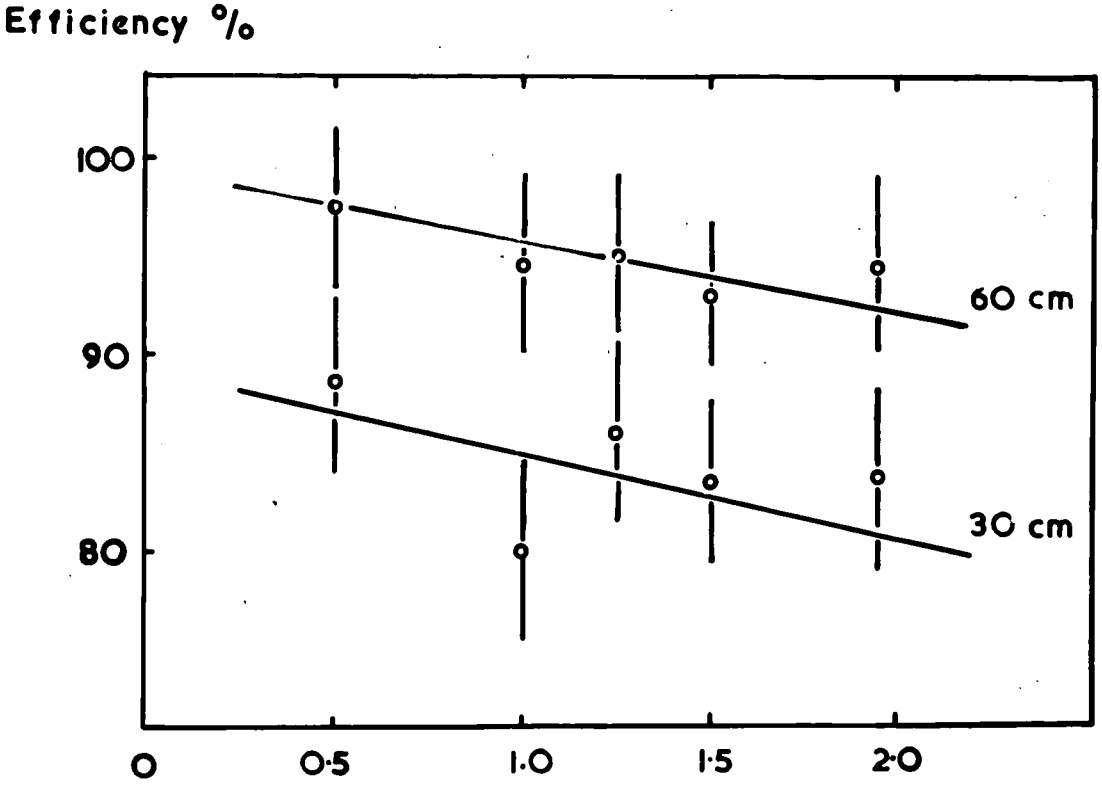

Figure 4.3. The variation of efficiency with rise time for 1.5 cm diameter tubes. Gas pressure as parameter.

E_{max} = 3.0 Kv/cm, T_D = 3.2 μsec and τ = 4 μsec.

TABLE V

The variation of efficiency with pressure for tubes containing mixture of 80% Ne and 20% He

Pressure in cm Hg	35	45	65	180
Layer Efficiency	61%	42.6%	14.2%	10.4%

The characteristics of the pulse were :

E_{max} = 26.7 Kv/cm T_D = 2.25 μsec.

T_R = 0.4 μsec τ = 2.6 μsec.

a clearing field, also shown in Fig. 4.2, will be discussed later). The variation in efficiency with rise time of the pulse is shown in Fig. 4.3. It is evident that this parameter is less critical in the case of large diameter tubes.

4.5. Residual Air

It was suspected that the initial conditions for evacuation would not be particularly stringent in the case of large diameter tubes. To find the limits permissible tests were carried out on tubes filled with 65 cm of neon plus varying amounts of air. Prior evacuation was to 3×10^{-4} mm Hg in all cases. The results in Fig. 4.4, show the effect is greatest at longer time delays, the change in plateau efficiency being small.

An interesting effect was observed with a trial set of tubes which were attached to the manifold for evacuation and filling by means of rubber tubing. This procedure could be useful since it obviates the laborious "sealing on" process which normally consumes a large amount of time in addition to demanding a proficient glass working technique. The characteristics of the tubes filled in this manner were comparable with tubes containing $\sim 10^{-2}$ mm air but the rate of spurious flashing was considerably higher and precluded further use of the method.

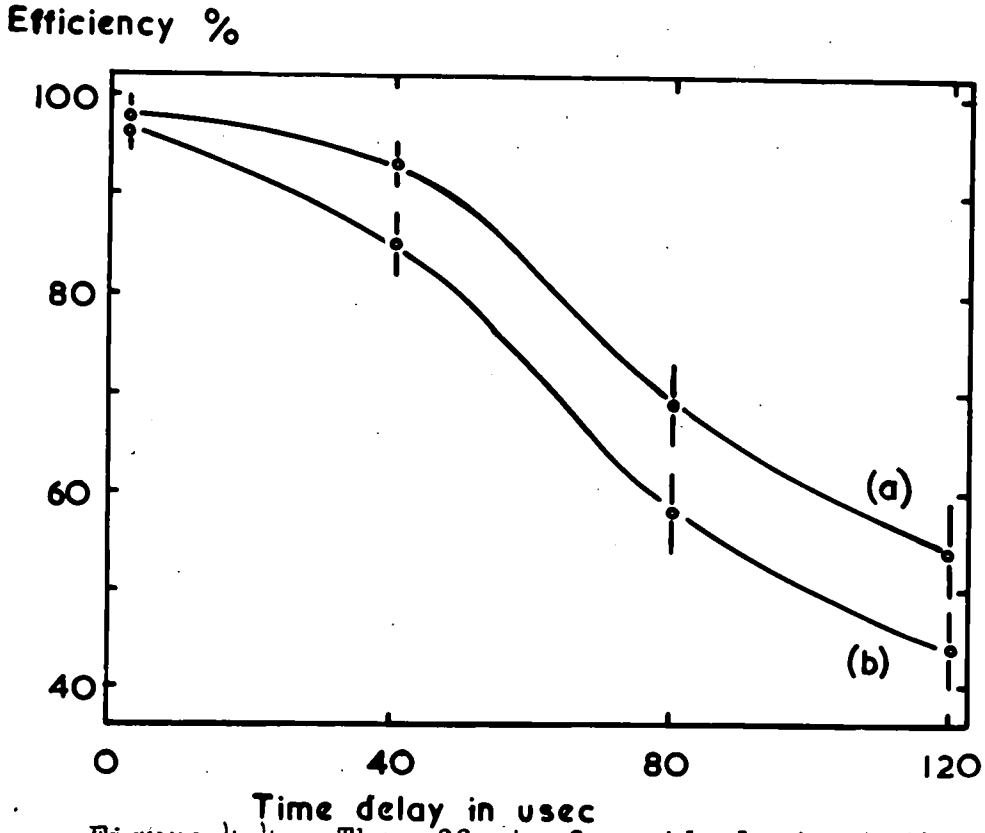

Figure 4.4. The effect of residual air on the variation of efficiency with time delay for 1.5 cm diameter tubes.
E_{max} = 3.5 Kv/cm, T_R = 0.5 μsec and τ = 4 μsec.

Curve (a) 65cm Ne + 10^{-4} mm Air
(b) 65cm Ne + 1 mm Air

It would appear that the important issue in prior evacuation is degassing the tube - this being accomplished quite effectively by continued pumping at pressures $\sim 10^{-4}$ mm Hg. Residual amounts of air up to 1 mm Hg are tolerable at a pressure of 65 cm of neon.

4.6. The Application of Clearing Fields

For some applications, the sensitive time of the large tubes ($\sim 100\mu$sec) could be excessive and it was necessary to consider how this could be reduced when so required. Investigations made using the wax stack showed that, in the case of the large tubes, a clearing field could be successfully applied. The effect becomes more pronounced at longer time delay thus permitting easier inspection, therefore a value of 28μsec was chosen and the tube efficiency measured at various values of clearing field. The results are shown in Fig. 4.5. The modification of the time delay characteristic obtained by applying the maximum clearing field of 3.6 Kv/cm is shown in Fig. 4.2. In the case of the '60 cm' tube the sensitive time is reduced by a factor of 4.

Theoretically the effect of the clearing field should be different when its polarity is reversed - a larger reduction in efficiency being expected when the clearing field is applied in the same direction as the pulse.

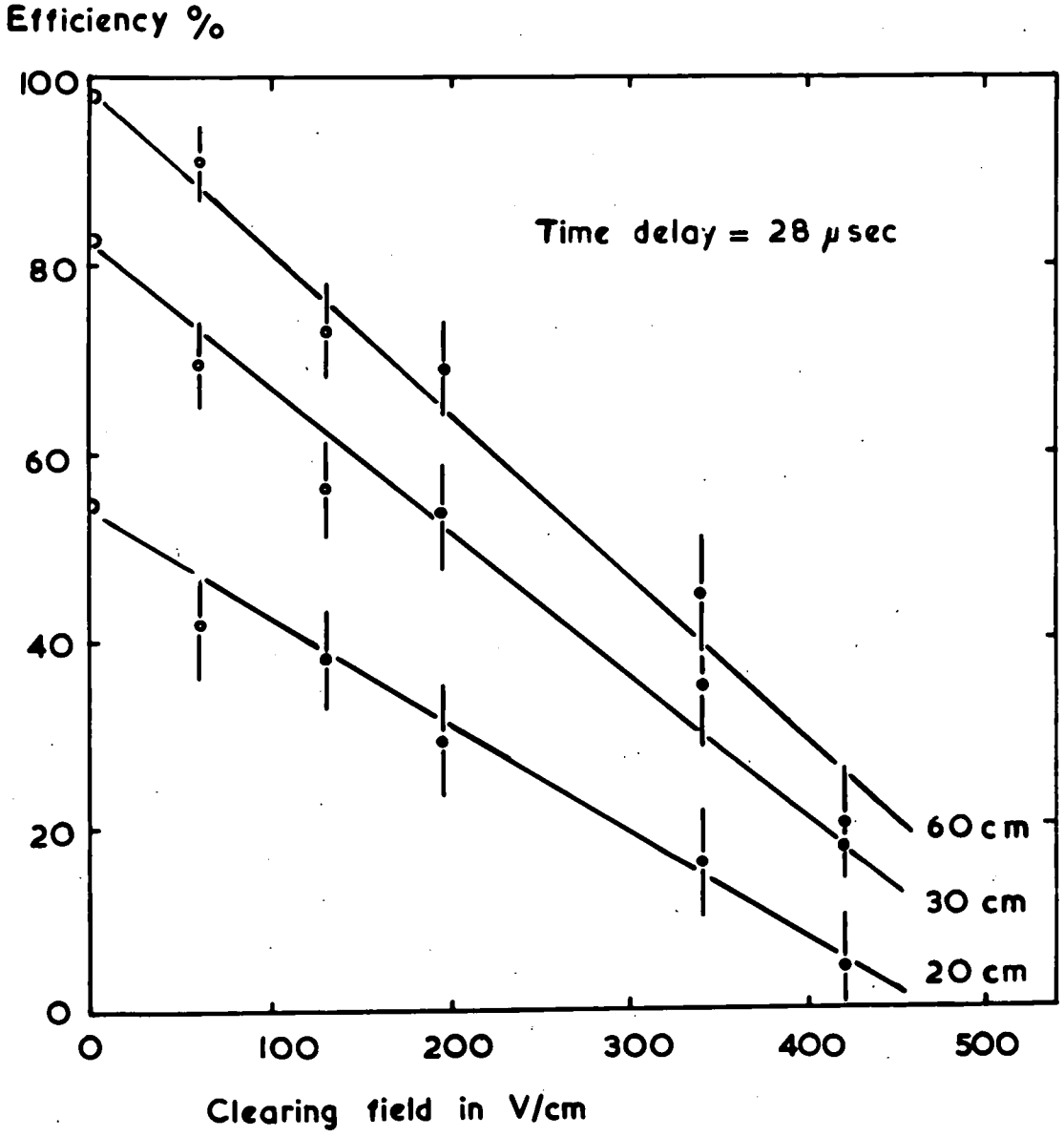

Figure 4.5. The effect of a clearing field on the efficiency at a time delay of 28 μsec.
E_{max} = 3.5 Kv/cm, T_R = 0.5 μsec and τ = 4 μsec.

This effect was investigated using a clearing field of 455 volts, again at a time delay of 28μsec. A slight change of efficiency in the expected direction was observed but as this was within the limits of accuracy of the measurement, the result may not be classed as conclusive. However, it may be taken as evidence that electrons, when swept to the walls of the tube, do in fact "stick" and are not detached by the pulse.

4.7. Rate of Spurious Flashing

Spurious flashing is caused by the presence of ionisation from sources other than the triggering particle.

Detailed measurements of the probability of spurious flashing were made by the open shutter method as previously described. The results are given in Table VI. It is interesting to note that the variation of spurious rate with field follows a similar type of curve to the efficiency-field characteristic, reaching a plateau at 2Kv/cm. At fields higher than 8Kv/cm the spurious rate for the '20 cm' tubes shows a sudden and rapid increase. It is presumed that this is due to field emission from the glass. It is noticed first in the case of the low pressure tubes because of the comparative ease of starting the discharge. The theory is supported by results obtained when a clearing field (270v/cm) was applied:

TABLE VI

Spurious Flashing

The rates are per tube per 1000 pulses

a) Normal

Pressure \ Field	2.1	2.8	3.5	4.2	4.9	5.6	Kv/cm
60 cm	0.18	0.54	0.37	0.6	0.6	0.6	
35 cm	0.0	0.18	0.0	0.18	0.2	0.8	
20 cm	0.18	0.18	0.18	0.2	1.2	4.0	

b) With a clearing field of 270 v/cm applied

Pressure \ Field	2.1	2.8	3.5	4.2	4.9	5.6	Kv/cm
60 cm	0	0	0	0.36	0.9	0.36	
35 cm	0	0	0.1	0.0	0.0	0.36	
20 cm	0	0.2	0.4	0.4	2.7	5.4	

The characteristics of the pulse were :

τ = 3.5 μsec T_R = 0.5 μsec.

the spurious rate of the plateau was appropriately reduced but the onset of the anomalous rate occurred at the precise value of field observed with no clearing field present. Furthermore, the spurious rate was found to vary directly as the electrode length only at fields below the anomalous region.

As previously described, the "expected" spurious rate may be calculated from the known C.R. flux and the sensitive time of the tube and compared with the observed value. For the 60 cm tube the ratio is 4.4 : 1 which is of the order expected.

4.8. Light Emission from the Flash Tube

The possibility of imparting a memory to a flash tube system by means of a multiple flashing procedure has already been mentioned. This could be of particular value in certain experiments on E.A.S. An obvious method of selecting events is to view the tubes with a photo-multiplier system. Fundamental studies of the dependance of the light output of the flash tube on factors such as pressure and the parameters of the pulse were therefore undertaken. These also provided interesting data for the theory of the flash tube.

An advantage of the large diameter tube is that it permits an investigation of the light output from a single flash tube - the operation of which can be fully controlled. As the most intense lines of the neon discharge are at 6402 Å, 5882 Å and 5852 Å, a red sensitive photomultiplier (P.M.) is necessary. The E.M.I. 6095 type 4 (Bi-Ag-Cs) was found suitable. A variable aperture and filters were used to confine the working region to the linear portion of the P.M. response curve.

The variation of light output with field was investigated using tubes at various pressures and the results are given in Fig. 4.6. The output pulse of the P.M. was of almost constant width, therefore its height was taken as a measure of the light output. The effect of variations in T_R, the rise time of the H.V. pulse, was also investigated with the results given in Fig. 4.7. It is of interest to note that the peak of the light output pulse was progressively retarded as the rise time of the H.V. flashing pulse was increased. The indication is that flashing occurs at a constant threshold value of field.

A typical light output pulse is shown in Fig. 4.8. The peak is normally reached less than 1μsec after the application of the H.V. pulse and the duration of the

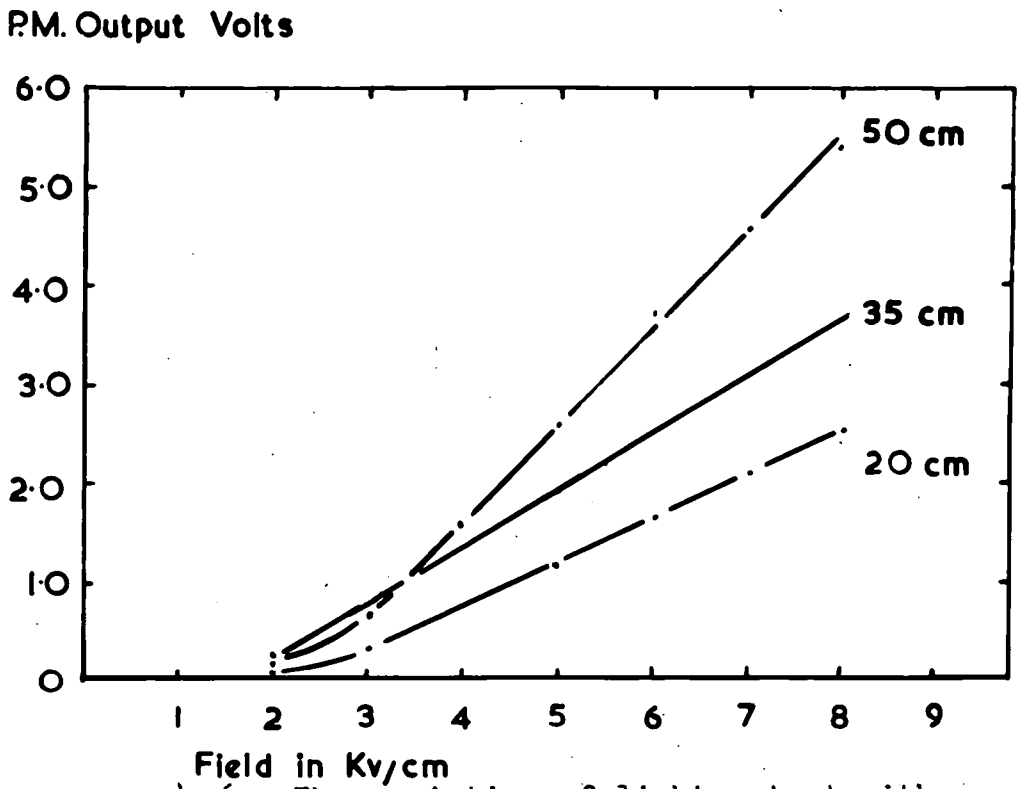

Figure 4.6. The variation of light output with field strength. Gas pressure as parameter.

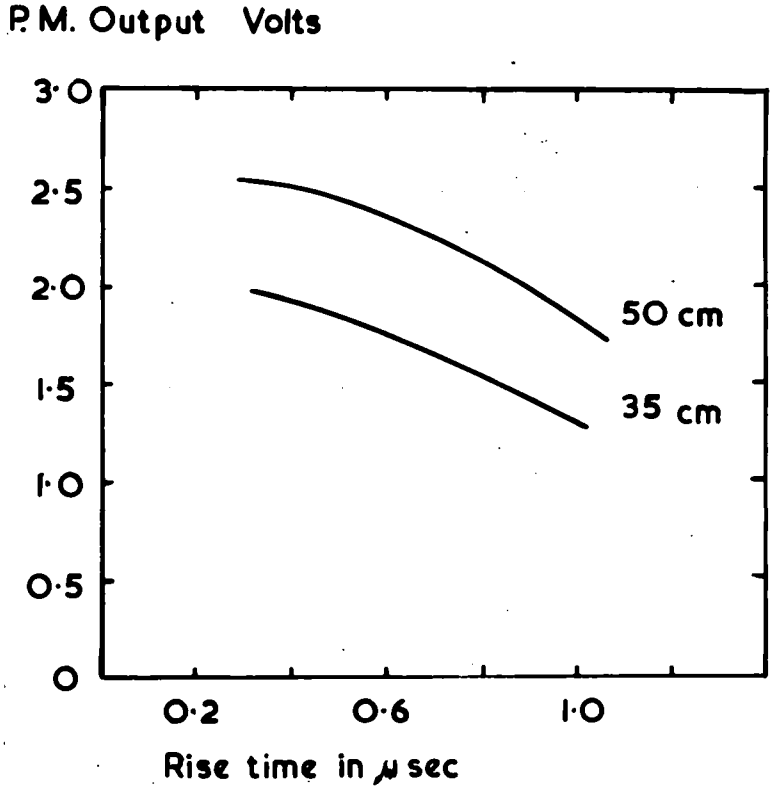

Figure 4.7. The variation of light output with rise time of pulse, at gas pressures of 60 and 35 cm. Hg. of Ne.

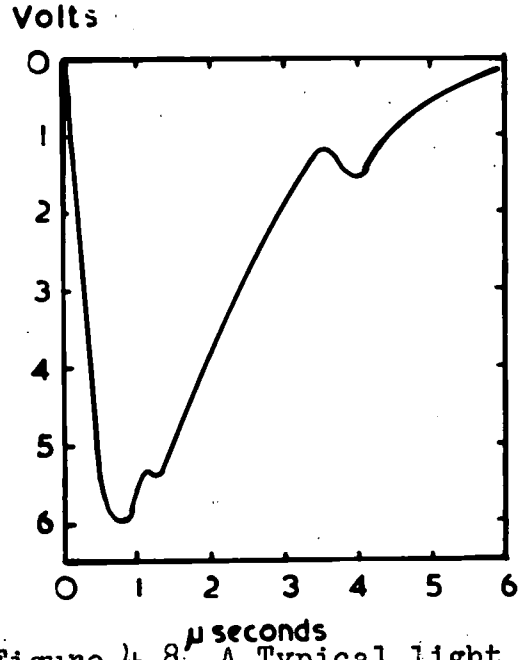

Figure 4.8. A Typical light output pulse.

light output is not affected by changing the width of the H.V. pulse, if this is longer than 1μsec. It is presumed that the tail of the light output pulse is due to radiation from metastable states of the neon atom.

It may be concluded that the light output of the flash tube is governed by the applied field and the neon pressure. The width of the applied H.V. pulse is not critical provided it exceeds 1μsec. Some theoretical implications of these studies will be considered in the next chapter.

4.9. Conclusions

From the results presented it is apparent that a flash tube can be produced which is versatile and well-suited for applications in E.A.S. work.

Commercial neon may be used at pressures less than one atmosphere. Layer efficiencies exceeding 80% are obtained at moderate field strengths and can be retained at time delays approaching 20μsec. The sensitive time of the tube is continuously variable over the range 40 to 120μsec and the rate of spurious flashing is less than 0.4%. The light output can be controlled and is ample for use with a photomultiplier, it may in fact be sufficient to permit the use of a simple photoelectric cell technique.

Using the data obtained, a flash tube was designed for application in an air shower experiment to study the directional properties of the various components and the particle density distributions. This will be described in Part II of this thesis.

To complete the study of the neon flash tube, Chapter 5 will comprise an approach to the theoretical aspects of its operation.

CHAPTER 5

The Theory of Operation of the Neon Flash Tube

5.1. Introduction

A sound theoretical explanation of the behaviour of the flash tube is obviously desirable ; if this is established the operation of the tube becomes completely predictable. Although in principle the mode of operation of the flash tube is simple, no fully satisfactory theory has yet been advanced. However, the basis of a rigorous approach to the problem is provided by the recent work of Lloyd (1960) on the application of exact diffusion theory to the flash tube. The essential features of this work will be outlined before going on to consider the actual mechanism of the discharge. For analysis therefore, the operation of the tube will be divided into two distinct parts:-

1. The initial production of ions and the effect of their subsequent diffusion on the probability of starting a discharge.
2. The mechanism of the discharge.

5.2. Initial Ionisation

An ionising particle passing through the gas in the tube leaves a trail of positive ions, electrons and excited neon atoms. In our considerations the positive

ions may be neglected: their low mobility precludes any movement during the pulse and their numbers are too few to cause distortion of the field. The excited atoms play more part. They may radiate resonance or non-resonance photons or be metastable. Resonance photons will progress slowly through the gas undergoing continual absorption and re-emission and will be in effect "locked up" during the critical period when the pulse is applied. Non-resonance photons go immediately to the wall and may there produce photoelectrons. These could be important but because of their proximity to the wall it is very likely they will collide again and stick before the pulse is applied. The Neon metastables should also be considered since the gas contains some 10^{-4}% of argon which could result in the introduction of free electrons by the Penning effect. The free electrons produced by both the initial particle and the metastables, diffuse rapidly and those reaching the wall may be considered as lost. The initiation of the discharge therefore depends solely on the electrons remaining in the gas and the probability of the tube flashing can thus be determined by evaluating their number.

5.3.1. Electron diffusion

The diffusion equation is obtained from Fick's law and the equation of continuity. If the concentration of

the diffusing substance is denoted by n then

$$\frac{\delta n}{dt} = \nabla \cdot (D\nabla n)$$

The diffusion coefficient D may depend on the concentration or position of the point in question but if, as in our case, D can be taken as constant the equation reduces to

$$\frac{\delta n}{dt} = D\,\nabla^2 n$$

Transforming to cylindrical polars : r, θ, z,

$$\frac{\delta n}{dt} = D\left[\frac{\delta^2 n}{dr^2} + \frac{1}{r}\frac{\delta n}{dt} + \frac{1}{r^2}\frac{\delta^2 n}{d\theta^2} + \frac{\delta^2 n}{dz^2}\right]$$

The equation is non-homogeneous and can readily be solved by separation of the variables. However in our case it is particularly advantageous to establish the appropriate Greens function. The solution of this gives the concentration at any point $(r,\theta, z,)$ at time t due to a unit instantaneous point source at (r', θ', z') when t = o. Multiplication by the volume element $rd\theta$, dr, dz thus gives the probability that an electron freed at $(r', \theta', z',)$ will be found in this element at time t:-

$$\rho(r', \theta', z';t) = \frac{2}{\pi a^2 l}\sum_{m-1}^{\infty}\exp\frac{-Dm^2\pi^2}{l^2}t \sin\frac{m\pi z}{l}\sin\frac{m\pi z'}{l}$$

$$X \sum_{\infty}^{\infty}\cos n(\theta-\theta') \sum_{-\alpha}^{}\exp\left\{-D\alpha^2 t\right\}\frac{Jn(\alpha r)Jn(\alpha r')}{\left[J'n(\alpha a)\right]^2}rd\theta dr dz$$

where α,a are the positive roots of Jn (αa) = o.

The probability of the electron remaining in the gas is found by integrating over the volume of the tube. Considering only events well removed from the ends of the tube the expression can be summed over z then, noting that only n=o yields a non-zero average over θ, the probability of the electron remaining in the gas becomes:

$$\rho(r',t) = 2 \sum_{\beta} \exp\left(\frac{-\beta^2 Dt}{a^2}\right) \frac{Jo\left(\frac{\beta r'}{a}\right)}{\beta J_1(\beta)}$$

where $\beta = \alpha a$ and take the values 2.4048, 5.5201, 8.6537 etc. (Jahnke and Emde, 1945).

5.3.2. Electron Liberation

To account for the initial liberation of electrons additional rectangular cartesian coordinates are required whose axes are perpendicular to the tube axis and whose origin is at the tube centre. Assuming the primary particle passes along the line x = constant and the probability of it producing a free electron in dy is $Q_1 dy$, then the number of electrons surviving to time t will follow a Poisson distribution with mean

$$N_x = \int Q_1 \rho(r';t)\, dy = 2Q_1 \sum_{\beta} \exp\left(\frac{-\beta^2 Dt}{a^2}\right) \frac{\int Jo\left(\frac{\beta r'}{a}\right) dy}{\beta J_1(\beta)}.$$

The functions $2\int \frac{Jo\,\beta\left(\frac{r'}{a}\right)}{a\,\beta J_1(\beta)} dy$

necessary for computations of N_x are given in Fig. 5.1 for the first few values of β.

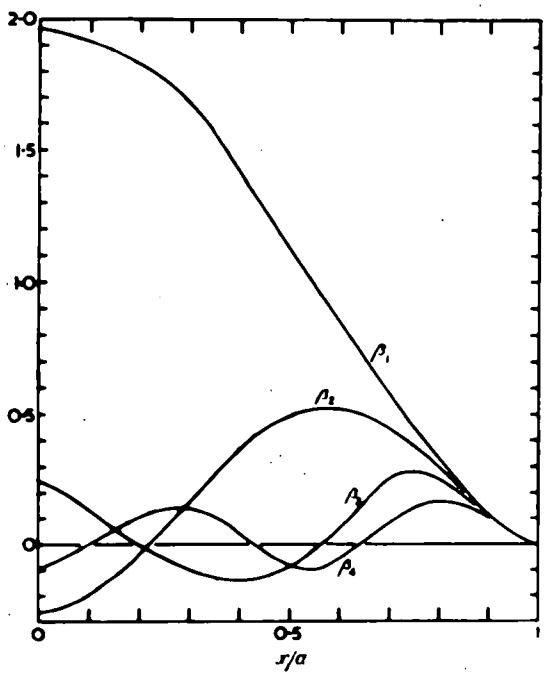

Figure 6.1. The first four functions $2\int J_0(\beta r'/a)dy/a\beta J_1(\beta)$, which are defined and used in § 6.2.2

5.3.3. Efficiency

At the start of the pulse there are N_x free electrons in the gas produced by the particle traversing the tube along a particular value of x. The shape of the electron density function soon becomes independent of the place of origin of the electrons therefore the probability of an avalanche being caused may be considered independent of the place of origin of the initiatory electron.

Let the probability of an avalanche occurring when $N_x = 1$ be f_1, then the probability that a flash will be caused by the electrons present at the start of the pulse will be

$$\sum_{n=o}^{\infty} \left[1 - (1-f)^n\right] \frac{N_x^n}{\lfloor n} \exp - N_x$$

$$= 1 - \exp(-f_1 N_x)$$

This then is the efficiency for that particular value of x.

i.e. $\eta_x = 1 - \exp(-f_1 N_x)$

and the overall efficiency for a tube of radius a is thus

$$\eta = \frac{1}{a} \int_o^a \eta_x \, dx.$$

5.3.4. Results

The value of η can be obtained as a function of various parameters by numerical integration of the expression given above. Computed values of η as a

function of $\frac{Dt}{a^2}$ are given in Fig. 5.2 with af_1Q_1 as parameter. It must be mentioned that these results are approximate only, since for small values of $\frac{Dt}{a^2}$ the electrons are in fact still distributed along the path of the particle. For time delays such that $\frac{Dt}{a^2}$ exceeds 0.2 the first term of the β series may be used alone and therefore the efficiency depends only on $af_1Q_1 \exp\left(-\beta_1^2\frac{Dt}{a^2}\right)$. This is shown in Fig. 5.3. If a is constant and f_1Q_1 almost so, it is evident that the efficiency depends only on Dt, that is on $\frac{t}{p}$. This is the theoretical foundation for the empirical curve (Fig. 3.8) giving the efficiency as a fn. of $\frac{T_D}{p}$. To enable comparison with experimental results a normalising point is necessary. Fig. 5.4 shows a family of theoretical curves with the separate time scales so adjusted that all curves pass through the same point at an efficiency of 5%. The experimental points, a precise set obtained with the 2.3π tubes, (Fig. 3.2) have been similarly treated and agreement with the curve for $af_1Q_1 = 6$ is good. Results for the large diameter tubes also agree well for delays of up to 150μsec. Beyond this it is possible that f_1Q_1 may vary appreciably with time.

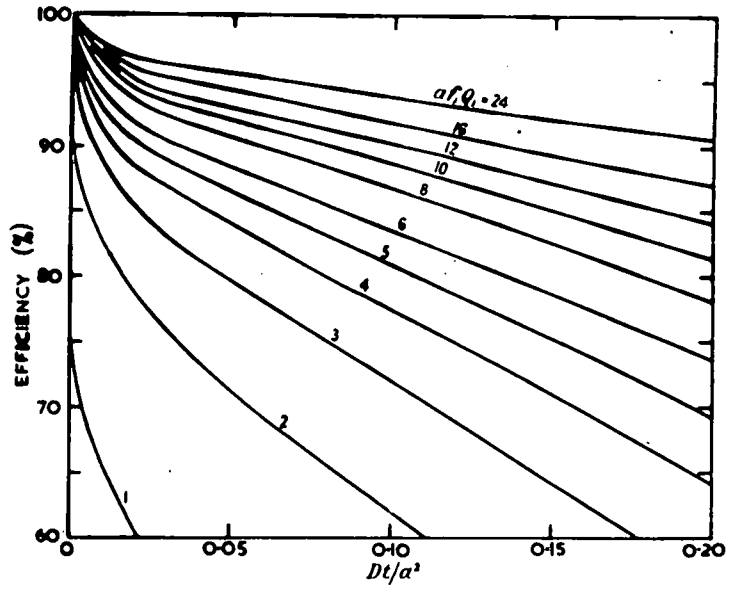

Figure 5.2 Variation of computed efficiency with time delay, for small time delay, as a function of f_1, the 'electron efficiency'. D is the diffusion coefficient of thermal electrons in neon and a is the tube internal radius.

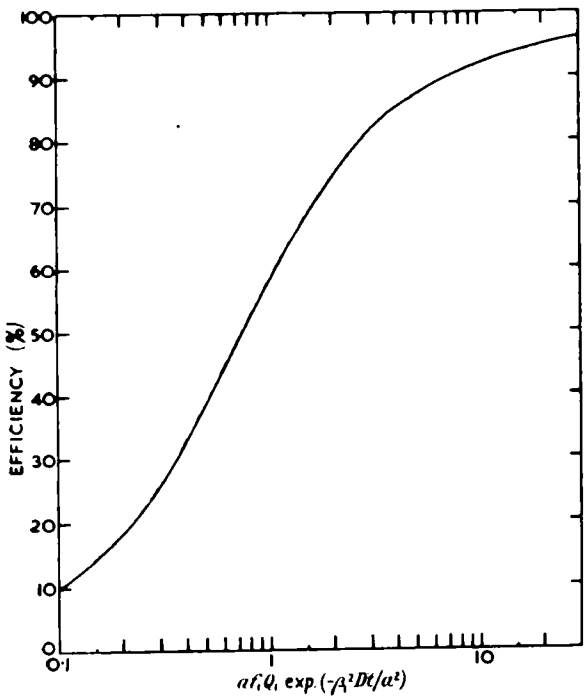

Figure 5.3 Variation of computed efficiency with $af_1Q_1 \exp(-\beta_1^2 Dt/a^2)$. This curve may be used when $Dt/a^2 > 0{\cdot}2$. $\beta_1^2 = 5{\cdot}783$.

From the close agreement between experimental results and theoretical curves it may be concluded that electron diffusion is in fact the process controlling the variation of efficiency with time delay. The value of D, the diffusion coefficient, can be found from the relation

$$D \simeq \left(\frac{a^2}{\beta_1 t_{5\%}}\right) \ln (20\, a f_1 Q_1)$$

and has been evaluated by Lloyd using results given in Chapter 3 and some due to Gardener et al (1957). The variation of D with p is shown in Fig. 5.5. No experimental values of D for thermal electrons are available for comparison but it may be surmised that the value lies between 600 and 2200 $cm^2/sec/atmos.$ from consideration of the equation (from kinetic theory)

$$D_e = \frac{\bar{v}\lambda_e}{3}$$

since $\frac{1}{\lambda_e}$ is known to lie between 2 and 7 cm^2/cm^3 at 1 mm Hg (Von Engel, 1959).

A further important conclusion to be drawn from the comparison of theory and experiment is that $f_1 \sim 1$, being typically 0.4 for p = 2.3 atmos. and near unity for p = 0.6 atmos., for tubes of radius 0.3 cm. A value of f_1 greater than unity would indicate a fundamental error in the basic theory: no such value has been found.

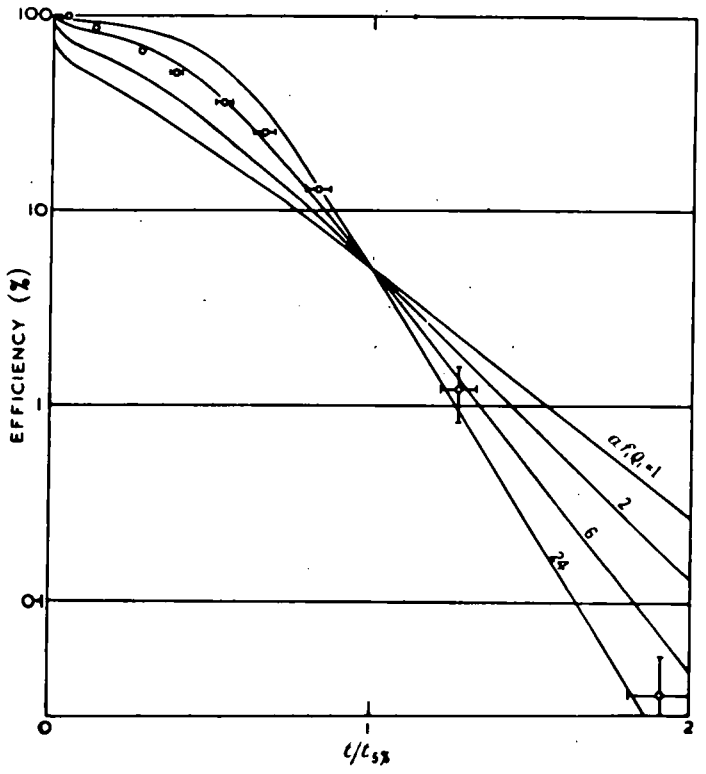

Figure 5·4

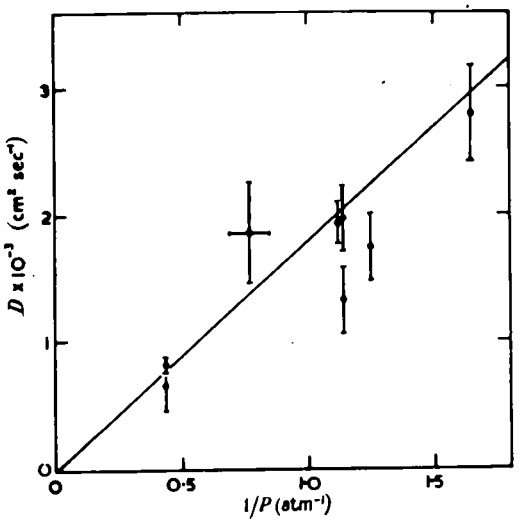

Figure 5·5 Values of D, the diffusion coefficient of thermal electrons, estimated as in figure 4, for various pressures p.

5.4. The Mechanism of the Discharge

Although the basic theory of the gas discharge was established for low pressures with uniform fields and metal electrodes, the fundamental equation of Townsend

$$i = io \frac{e^{\alpha d}}{1 - \gamma(e^{\alpha d} - 1)}$$

remains applicable to all cases of breakdown. The symbols in the equation have their usual notation: i represents the total current, due to an initial ionising current io, flowing between plates a distance d apart when a uniform field is applied. α is the primary (or Townsend) ionisation coefficient and γ is the secondary ionisation coefficient.

The correct interpretation of Townsend's "sparking" condition, $\gamma e^{\alpha d} = 1$, (when i tends towards ∞) is that one initiatory electron is able to produce a self sustained discharge and this defines the sparking threshold. The condition is seen to depend on the product of two quantities expressing primary and secondary processes. Since the nature of the primary gas multiplication process is well established, the critical factor is that of the secondary mechanism.

Two basic secondary processes are known: one involves cathode phenomena and leads to a Townsend-type mechanism, the other, occurring in the gas, leads to streamer mech-

anism. The fundamental difference is that the streamer theory requires photoionisation in the gas together with extensive field distortion - conditions normally encountered at high pressures and fairly large electrode separations. The exact values of p and d, however, for the transition from Townsend to streamer mechanism are not known. In a homogeneous gas, photoionisation is rare below the threshold for the self sustained discharge but gas mixtures can be particularly effective.

Photographs have been obtained of the actual discharge occurring in a flash tube and are shown in plates V(i) to (iii). Many characteristics of the streamer formation are exhibited but it should be noted that the comparatively narrow spark track does not necessarily indicate streamer mechanism since the lateral diffusion of the avalanche is naturally reduced at higher pressures. However the necessary conditions are present: the gas is certainly a mixture - at a pressure which might render photoionisation possible, and it is known that in discharges started by more than one electron, space charge accumulation due to neighbouring avalanches can cause effective distortion of the field. The streamer mechanism must therefore be considered.

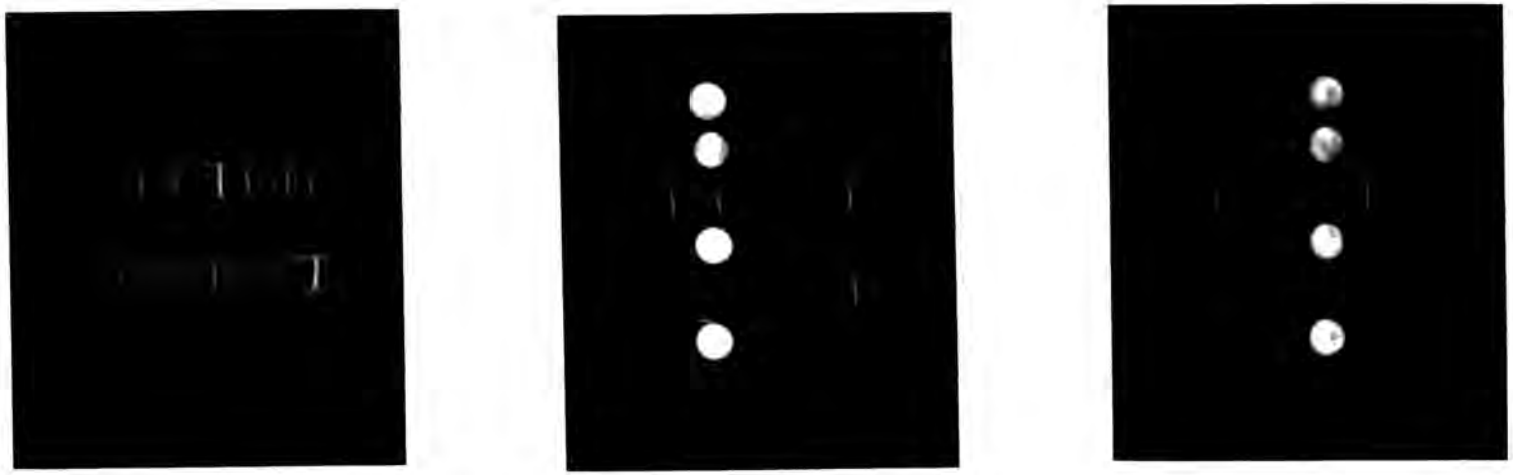

Figure 5.7. Photographs of the discharge occurring along the length of two 1.5 cm diameter flash tubes. The circular flashes signify the trajectory of the triggering particle, which was located using similar tubes at right angles to the two tubes under inspection.

5.4.1. Streamer Theory

The streamer and kanal theories of breakdown were developed independently by Meek (1940) and Raether (1940) mainly to account for the unexpectedly rapid breakdown observed in gases at high pressures. Both theories depend on secondary electrons being generated in the gas by photoionisation due to photons produced in the primary electron avalanche. This is rapid only when the original field is highly distorted by positive space charge at the head of the main avalanche and Meek's criterion is attained when the space charge field becomes equal to the applied field. The breakdown threshold, E_S, is then given in the equation:

$$\alpha d + \log \frac{\alpha}{p} = 13.7 + \log \frac{E_S}{p} - \tfrac{1}{2} \log (pd) + \log d.$$

Where α and d have their normal significance, p is the gas pressure and the numerical factor is a constant depending on the gas in question. (13.7 in the case of neon)

It has been pointed out (Zeleny, 1942) that in Meek's postulate the space field does not act in the direction proposed, therefore the equation is really empirical, however it does enable a quantitative approach to the problem. In the case of the high pressure tubes p is known to be 2.3 x 760 mm Hg, d may be taken as 0.48 cm. (the mean diameter of the tube) and α obtained from the values given by Druyvestyn and Penning (1940) for a

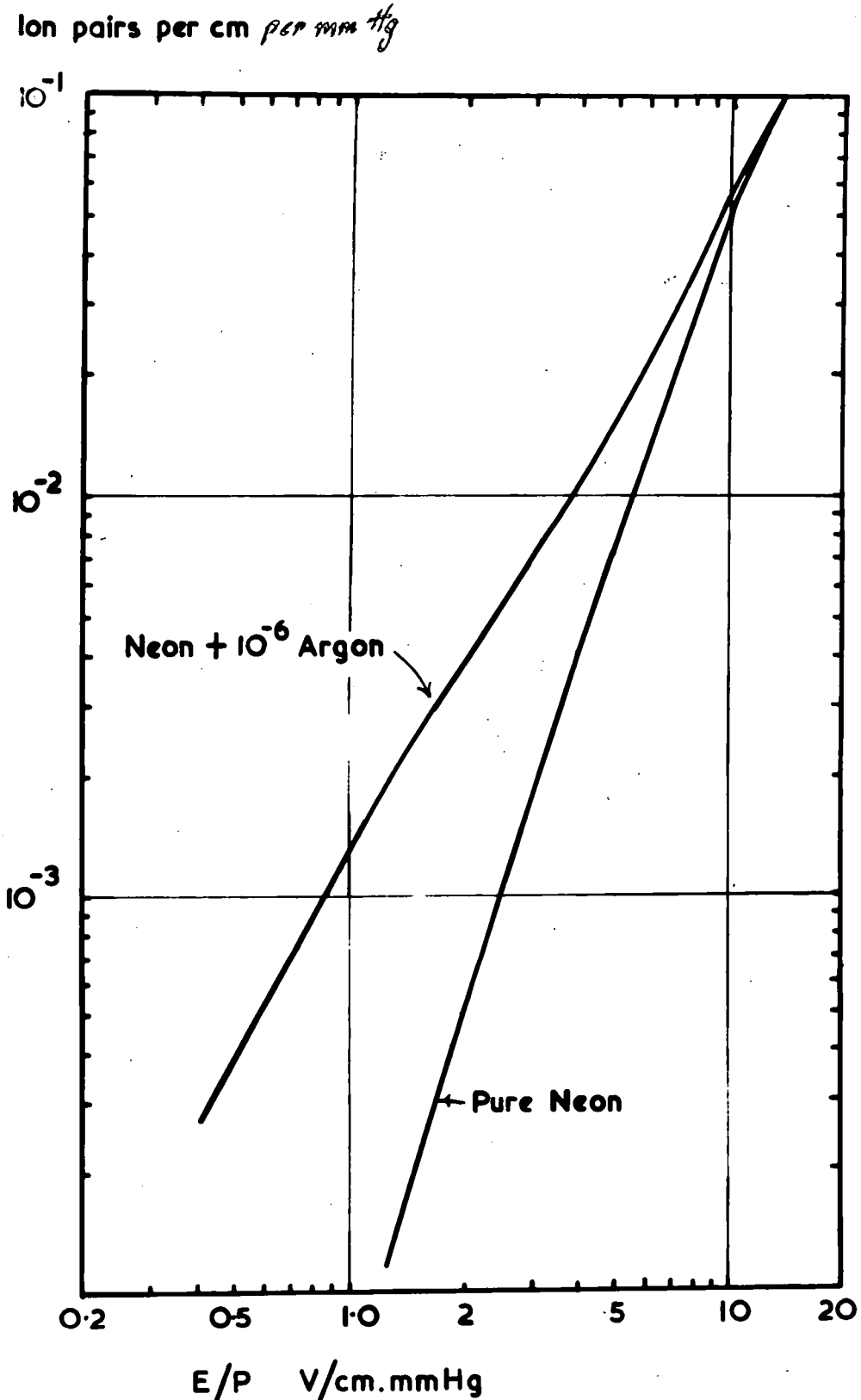

Figure 5.6. The ionisation coefficient as a function of the reduced field E/P.
(From Druyvestyn and Penning, 1940)

mixture of neon with 10^{-4}% argon. (Fig. 5.6). On solving the Meek equation using the appropriate values of p, d and α, a threshold field of 11 Kv/cm is predicted.

The observed value of threshold field is obtained from Fig. 32. In evaluating the field acting in the gas account must be taken of the dielectric effect of the glass tube. This is considered in Appendix II, the result for the case of the 0.6 cm diameter tube is that the internal field is 64.5% of the field applied. The observed threshold field must therefore be taken as approximately 4 Kv/cm - much less than the value predicted by Meek's equation.

Raether's theory is based on the achievement of a "critical" amplification and his sparking condition is defined as

$$e^{\alpha d} = N = \text{constant}$$

with observed values of αd lying between 18 and 20. Assuming the lower figure, $\alpha d = 18$, and substituting appropriate values of α and d, a threshold field of 11 Kv/cm is again obtained.

It is obvious that the streamer mechanism does not provide a quantitative theory of the flash tube.

5.4.2. Townsend Type Mechanism.

The secondary mechanism proposed by Townsend depends

on additional electrons being liberated at the cathode. In the case of a system such as the flash tube, with external electrodes, any proposed secondary mechanism acting on the cathode must be replaced by one acting on the glass walls of the tube. As possible agents for the γ mechanism there are:

1. positive ions - as originally proposed by Townsend.
2. excited and metastable atoms.
3. fast neutral atoms.
4. photons.

Consideration of transit times renders the first three processes most unlikely. The maximum mobilities of ions and atoms are of the order of 10^5 cm/sec and the pulse is applied and withdrawn within 5×10^{-6} sec. Photomultiplier studies also indicate that the onset of the discharge occurs within one μsec of the start of the pulse. Recourse must therefore be made to photons.

Convincing evidence for the production of photo-electrons by 16 eV neon quanta on glass is given by Harries and von Engel (1954). The studies were of high frequency breakdown therefore the results quoted for values of breakdown fields are not directly applicable to the present case. However, an essential observation was made in that processes acting on the glass walls of

the container are important even at reasonably high pressures.

An acceptable value for the coefficient γ for photon action on glass is 0.01. Applying this in the Townsend sparking criterion.

$$\gamma\, e^{\alpha d} = 1$$

gives

$$\alpha d = 4.6$$

Substituting the values of d = 0.48 cm, p = 2.3 x 760 mm Hg

$$\frac{\alpha}{p} = 5.45 \times 10^{-3}$$

on consulting the curve of Fig. 5.6, the equivalent threshold field emerges as 4.4 Kv/cm. This value is in reasonably good agreement with the observed figure of ~4 Kv/cm.

If the Townsend theory applies to high pressure tubes it should certainly apply to tubes at lower pressures. In the case of tubes at 60 cm Hg, a sparking threshold of 4.8 Kv/cm is predicted and the observed value, reported by Gardener et al (1957), is 5 Kv/cm. The agreement is close enough to suggest that the dominant mechanism is in fact Townsend-Type acting on the glass.

A convincing experimental check can easily be carried out. The photoelectric emission from borosilicate glasses such as Pyrex is known to be less than that from

soda glass by a factor of the order of 6. If, therefore, the secondary mechanism is Townsend type on the glass, tubes made from Pyrex should be less efficient. Accordingly tubes were prepared from Pyrex glass and filled at 2.3π neon under similar conditions to the tubes already described. At high pressures no trouble with spurious flashing was found and the tubes were thoroughly tested. The maximum layer efficiency obtained was 18%, less than one third of the efficiency obtained using soda glass. The evidence, therefore, may be taken as conclusive.

5.5. Discussion

Further problems which should be considered in relation to the mechanism of the flash tube are:

1. The effect of the rising edge of the pulse
2. The anomalous values of efficiency observed with thin glass tubes.
3. The effects of d.c. clearing fields.

In the previous considerations the effect of the finite rise time of the pulse has been ignored. A simple calculation reveals that the multiplication expected when an electron is accelerated across the tube by the rising field of the pulse is so small as to be negligible. It would thus appear that all the initial electrons should be swept to the walls of the tube long before the field has attained a value high enough to

cause a discharge. Experimental observations suggest that this is not the case.

A tentative theory is that the initial electrons inside the tube are in fact screened from the rising edge of the pulse by an accumulation of ions on the inside surface of the tube. This condition is not uncommon in work with highly insulating substances such as glass. It is therefore proposed that no significant field is established inside the tube until the surface ion distribution has been effectively cleared. By the time this has been achieved the pulse has reached almost peak height with the initial electrons still in favourable positions to start the discharge.

The number of ions distributed on the inside surface will depend on the leakage resistance of the glass wall and therefore on its thickness. Thin glass tubes should have smaller charge accumulations and so offer less screening to the rising pulse. The clearing effect in this case should be greater, hence thin glass tubes should exhibit a lower efficiency - as is observed.

The theory is offered some support by the effects observed in experiments with clearing fields. The values of clearing field found necessary to produce a change in the efficiency of the flash tube, even at reasonably long time delays, are much higher than would be expected from

considerations of the known values of electron mobility. The effect can be accounted for quite simply by an accumulation of charges on the inside surface of the tube. The application of a d.c. field results in a conduction current being established which partially backs off the field applied.

Unfortunately, the data available on the electrical properties of glass are inadequate for the formulation of a quantitative theory. However, from measurements of the displacement current through a tube when flashed, the number of electrons taking part in the discharge can be estimated at $\sim 10^{12}$. After allowing for extensive recombination processes, this figure should still furnish a sufficient number of residual ions to permit the effect prescribed.

An alternative process suggested by Lloyd is that electrons drifting to the wall create excited states of neon atoms which radiate non-resonance photons to the wall. Some of the photoelectrons there produced are in a favourable position to be accelerated by the pulse which has by then attained its maximum height. The theory is in reasonable agreement with some observations but it offers no solution to such problems as the variation of efficiency with glass thickness or the action of clearing fields.

5.6. Conclusions

The experimental features most amenable to theoretical treatment are the variation of efficiency with time delay and the threshold field for flashing. It has been shown that these features are well described by simple diffusion of the initial electrons and a Townsend-type discharge. There remain further problems of operation for which only a qualitative explanation can be offered.

CHAPTER 6

The Extensive Air Shower

6.1 Introduction.

Before proceeding to discuss the application of the flash tube to studies of this branch of cosmic ray physics, a brief review will be made of some of the more important aspects involved.

The simultaneous arrival at sea level of the large numbers of particles comprising extensive air showers (E.A.S.) is a consequence of the entry into the earth's atmosphere of primary cosmic rays of great energy, certainly more than 10^{14} eV and possibly as high as 10^{19} eV. Investigations of the primary cosmic radiation at these extremely high energies are important for two main reasons:

1. The shape of the energy spectrum and the spatial distribution of the incoming particles are dependent on the origin of the particles, the mechanism of their acceleration and the structure of the galaxy. The apparent extent of the spectrum to at least 10^{18} eV without any abrupt change of slope puts severe strain on any theory postulating the source of C.R. as being in our galaxy. The question of anisotropy at the

highest energies is therefore important since it is very difficult to explain how particles may be accelerated to energies of 10^{18} - 10^{19} eV and still kept isotropic if they are confined to our own galaxy. If the findings of no change in the slope of the spectrum and no anisotropy are confirmed an extra-galactic source of H.E. cosmic rays would seem inevitable.

Experimental observations are therefore important with regard to both astrophysical theories and origin theories of cosmic rays.

2. Experimental investigations of the interaction properties of nucleons and other elementary particles at the highest energies are of fundamental importance in modern studies of nuclear physics. The energy range of the cosmic ray primaries is many orders of magnitude greater than that available from laboratory accelerators and a new range of phenomenon might be expected.

The intensity of the primaries in this energy region is however so small as to render their direct observation impossible. (For example the intensity of primaries with energies above 10^{16} eV is $\sim 5.10^{-8}$ m^{-2} sec^{-1} $sterad^{-1}$ i.e. about one per square metre per month). The shower products, on

the other hand, can be detected at sea level at quite useful rates (1/ hr) and thus provide the only usable source of information on the highest energy primaries and their interactions. A difficulty is that the approach is necessarily indirect and must depend largely on the model assumed to represent the development of the shower.

6.2. Historical Ideas.

The original view of the E.A.S. was that of a giant photon-electron cascade produced in the atmosphere by an ultra high energy electron or photon. Theories for the development of the cascade, based on the purely electromagnetic processes of pair production and bremsstrahlung, were advanced by Heisenberg, Moliere, and others. More detailed investigations, however, showed that the properties of the shower, particularly the presence of penetrating particles, were not well represented by these theories. Finally the experiments of Critchfield (1950) demonstrated that the number of electrons present in the primary radiation was less than 0.5% of the total flux and the flux of high energy primary photons was very low. The theory was then revised to include initiation of the shower by a nuclear primary and a subsequent nuclear cascade. The electron-photon component was accounted for as the decay process of π^{o} mesons pro-

duced in the nuclear interactions. The general picture of the shower is thus as shown in Fig. 6.1.

Before describing details of the most recent shower models it will be of help to consider some general features of observed showers such as the lateral structure and the longitudinal development of the shower, together with some characteristics of the nuclear interactions.

6.3. The Lateral Structure of E.A.S.

Elaborate detecting arrays have been used to investigate the lateral distributions at ground level of particles in the electron component, the μ-meson component and the nuclear active component of E.A.S.

6.3.1. The Electron-Photon Component.

The lateral structure of the electron-photon cascade is determined almost entirely by the Coulomb scattering of the electrons. An exact theoretical expression for the electron density as a function of distance from the shower axis has been evaluated by Nishimura and Kamata (1951) who give for the density at a distance r the relation

$$\Delta_r = N f(r)_s$$

where N is the total number of particles and $f(r)_s$ is the 'structure function', which is independent of N but varies with the parameter S characterising the stage of

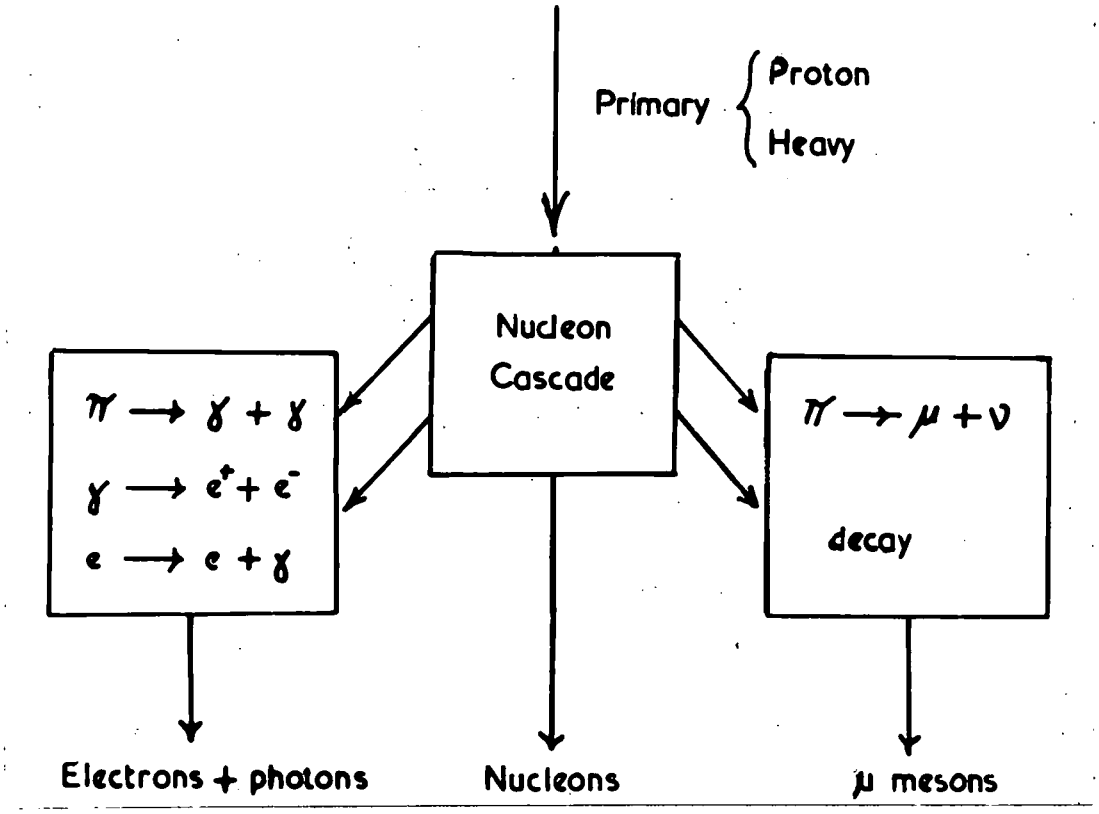

Fig. 6.1. Schematic diagram showing the development of the components of an extensive air shower.

longitudinal development, or 'age', of the shower. The general form of $f(r)_s$ is somewhat complicated but approximate and empirical relations are available which apply in various regions of the shower. Probably the most useful of these is that due to Rossi (1957)

$$f(r) = \frac{\exp\left(-\frac{r}{r_o}\right)}{2\pi\, r_o\, r}$$

in which r_o is a "characteristic radius" depending on the scattering experienced by electrons at the level of observation.

Experimentally the average lateral distribution of showers is found to agree with the Nishimura-Kamata function for S = 1.25 at all shower sizes but large fluctuations occur in individual showers giving values of S between 0.6 and 1.4. The existence of these fluctuations is an important and characteristic feature of E.A.S. Their origin may be ascribed to one or more of the following:

1. Fluctuations in the atmospheric depth of the first interaction resulting in the shower.
2. Fluctuations in the inelasticity of the nuclear interactions resulting in the shower.
3. The production of some showers by heavy primaries.

6.3.2. The μ-meson Component.

The lateral distribution of the μ-meson component is found experimentally to have a radial dependence which is, on average, very nearly proportional to $\frac{1}{r}$. It must be presumed that a significant part of the lateral spread is due to angular divergence of the parent π-mesons at production. If the spread were due entirely to Coulomb scattering then an asymetric lateral distribution would be expected due to the effect of the earth's field and this is not observed.

6.3.3. The Nuclear Active Component.

Detailed studies of the shower core reveal a radial dependence $\alpha \frac{1}{r^n}$ with $n = 0.6$ for 5 cm $< r <$ 30 cm

and $n = 1.0$ for 30 cm $< r <$ 3 cm

Accordingly the radius of the core may be taken as ~30 cm. This fact is extremely significant. The transmission of most of the energy in the nuclear active cascade with scarcely any lateral diffusion of the core, implies an intense angular collimation of the secondary products of the initiating nuclear interaction.

6.4. The Longitudinal Development of E.A.S.

Unfortunately, no method of observing the longitudinal development of a single shower has yet been devised. It can, however, be inferred from measurements

of the shower size spectrum and the dependence of shower rate on altitude:-

The rate at which showers of size N_s (particles) are observed at sea level is given by the integral size spectrum

$$F(>N_s) \quad \alpha \, N_s^{-\gamma} \qquad \ldots\ldots\ldots\ldots\text{(i)}$$

A shower of size N_s at sea level has size N at depth $\underline{t}$ given by

$$N = K N_s \, e^{-\frac{t}{\lambda}} \qquad \ldots\ldots\ldots\ldots\text{(ii)}$$

where λ is the shower attenuation length. Since we are referring to the same showers, the rate of occurrence of showers of size N at depth $\underline{t}$ must also be proportional to

$$(N_s)^{-\gamma} = \left[\frac{1}{K} N \, e^{\mp \frac{t}{\lambda}}\right]^{-\gamma}$$

$$= \left[\frac{N}{K}\right]^{-\gamma} e^{-\frac{\gamma}{\lambda} \cdot t} \qquad \ldots\ldots\ldots\ldots\text{(iii)}$$

Thus, if showers of a fixed size are observed and the variation of rate with depth is measured, an exponential absorption $e^{-\frac{t}{\Lambda}}$ is found where $\Lambda = \frac{\lambda}{\gamma}$

Substituting the experimentally observed values of $\gamma = 1.5$, $\Lambda = 130$ gm/cm^2, the value of λ, the shower attenuation length, is obtained as ~200 gm/cm^2. This value is found to be remarkably constant over all shower sizes. Considering an electron-photon cascade, exact calculations can be carried out for the development since the cross-sections involved are well known both theoretically and experimentally. The devel-

opment is characterised by the age parameter S which varies from zero, through unity at maximum development, to ~2 when only one particle remains. Growth ceases, of course, when the energy of the electrons falls below the critical energy (84 MeV in air) and the number of electrons is then attenuated exponentially with depth

$$N \propto e^{-\frac{t}{\lambda}}$$ (see Fig. 6.2).

The electrons present at this final stage are wholly secondary to photons and in fact represent the ionisation accompanying the exponential absorption of the photons. The attenuation length λ is a function of S, increasing as S increases, and therefore tends to a limiting value of 60 gm/cm^2 corresponding to the minimum attenuation of low energy photons.

This is far removed from the experimentally derived value of 200 gm/cm^2 and emphasises the important modifying effect of the nucleon cascade.

6.5. Characteristics of the Nuclear Interactions.

Certain characteristics of the nuclear interactions occurring at high and ultra high energies can be inferred from observations of shower structure at ground level. The more salient features which emerge are:

1. The effective interaction cross-section remains close to geometrical up to the highest energies known.

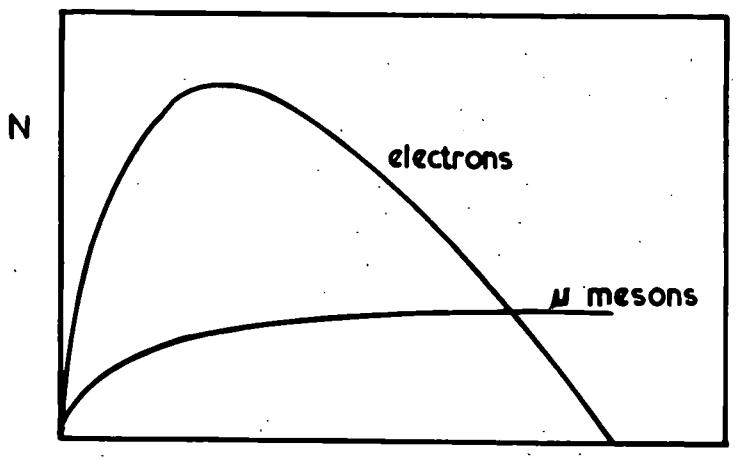

Figure 6.2. The altitude variation of the electron and μ-meson components of an extensive air shower. (After Nishimura and Kamata, 1951).

2. Most of the primary energy (in the laboratory system) is concentrated on one, or at most few, nucleons.
3. The angular distribution of the secondary particles in the C.M. system is strikingly anisotropic in the forward and backward directions.

6.6. Recent Shower Models.

The purpose of any shower model is to account for the observed features of shower structure and development and to permit the relation of observations at sea level to the primary cosmic ray spectrum. The essential features of three of the most recently advanced models will be described.

6.6.1. The Nuclear Active Cascade Model. (Rossi, Olbert et al.)

Two basic assumptions are made in this model:

1. The interaction length of a nuclear active particle corresponds to the geometrical nuclear cross section (~ 70 gm/cm^2).
2. At each interaction only one particle is emitted with sufficient energy in the laboratory frame to maintain the cascade.

(The second assumption is strongly supported by the extremely small lateral extent of the core observed experimentally).

The energy lost by the nuclear active cascade with an inelasticity α goes mainly into electron-photon cascades. These are absorbed much more rapidly than the nuclear active cascade therefore an equilibrium is soon established in the course of shower development and the number of electrons then falls off with depth at the same rate as the energy of the nuclear active cascade is attenuated. If I is the energy in the nuclear active cascade,

$$\frac{dI}{I} = - \alpha \frac{dx}{\lambda_{int}}$$

thus λ, the number attenuation length of the shower, is

$$\lambda = \frac{\lambda_{int}}{\alpha}$$

Inserting the observed value of λ as 200 gm/cm^2 the inelasticity is given by

$$\alpha = \frac{70}{200} = \sim 0.4$$

Detailed calculations based on this model have been made by Olbert who obtains the relationship between the shower size N and the energy E_o of the incident primary:

$$N = 1.7 \cdot 10^5 \left(\frac{E_o}{10^{15}} \right)^{1.14}$$

It should be noted that Olberts' model assumes that the majority of particles created in collision are π mesons. This is probably correct at low energies but there are indications that it may be wrong at energies $> 10^{14}$ eV.

For example the γ ray spectrum measured at 10 Km altitude by the Bristol emulsion group could be taken to imply that the fraction of primary energy appearing as π^{o}s may diminish as the energy of the interaction increases. However this trend is not supported by evaluations of the π-production spectrum from observations of the μ meson spectrum at sea level and the problem must be regarded as open.

The second two models to be outlined are particularly concerned with interpretation of the fluctuation problem mentioned in § 6.3.1.

6.6.2. Fluctuation Model A. (Miyake)

If the electron-photon cascade dies out after maximum development, whilst the number of μ-mesons remains constant, there will exist a correlation between the relative numbers of μ mesons and electrons and the age of the shower. The development of a shower can be shown schematically in terms of $N\mu$ and N_{total} with limits imposed by the atmospheric depth traversed by the shower. The ratio $\frac{N\mu}{N}$ observed at sea level can therefore be related to the height at which the cascade originated. If further assumptions are made that:

1. After the maximum, the shower curve has an exponential decrease of constant attenuation length λ.

2. The distance from the starting point to the shower maximum is expressed by B $\log_e E_o$ + c where E_o is the primary energy.
3. N_μ is essentially constant after the shower maximum and is proportional to the primary energy.
4. N at the shower maximum is proportional to the primary energy.

then characteristics such as the primary interaction length λ_i, the shower attenuation length λ, and the constant B can be deduced from plots of the experimentally observed frequency distributions of N for fixed N_μ and of N_μ for fixed N.

The model has been applied with reasonable success by Oda.

The interesting contention of this model is that the observed fluctuations in shower development can be completely explained in terms of fluctuations in the atmospheric depth of the first interaction.

6.6.3. Fluctuation Model B. (Cranshaw, Hillas)

In the model prepared by Cranshaw and Hillas (and in the similar model due to Zatcepin) it is suggested that a shower consists of a chain of perhaps five or more nuclear interactions between the top of the atmosphere and sea level, from each of which is launched a

relatively short range electron-photon cascade. To a first approximation any overlapping of these cascades is ignored and it is supposed that the cascade observed at sea level comes mainly from the previous nuclear interaction.

Fluctuations must now be considered at every stage in the nuclear active cascade. When this is done, and experimentally observed values of Λ, γ and λ_{int} are inserted, it is found that the observed variations of Λ with shower size can be explained with interactions of constant inelasticity 0.5 without introducing energy dependent parameters. A further, interesting result is that the apparent constancy of measured values of λ and S reflects not a feature of the longitudinal development of the shower but simply a bias in the technique of measurement.

It must be remarked that this model is liable to underestimate the energy of the initiating primary because particles at levels other than the observational level are ignored.

6.7. Discussion.

The extensive air shower is a complex phenomenon as yet by no means fully understood. Although a large amount of experimental data has been accrued it is apparent that the measurements are still not precise

enough for more than a general picture to be drawn. Results obtained by different workers are often not concordant, particularly in respect of values of Λ and γ. Also, if the shower model of Cranshaw is correct, it can no longer be assumed that the shower size at sea level is a unique function of the primary energy.

It is evident that the nucleon-nucleon collision theory of low energies can not be extrapolated to include the high energy interactions in E.A.S. No comprehensive theory is in fact available for the basic nuclear interactions involved in the formation of the extensive air shower.

The emphasis in experimental observation is already turning to the μ-meson component since the lateral distribution of the mesons reflects the history of the shower whereas the lateral distribution of the electrons depends only on the characteristics of the air near the point of observation. An investigation of the angular distribution of the μ mesons in E.A.S. may be the most direct approach to the urgent problem of deciding which, if any, is the true shower model and an experiment along these lines will be described in Chapter 7.

Returning to the role of flash-tubes in E.A.S; two principle applications of a flash tube array can be envisaged.

1. Investigation of the directional properties of showers and the angular distributions of the various components.
2. The measurement of particle densities in both the electron and μ components.

The subject of directional studies is of more immediate interest and will be discussed in Chapter 7. The application of the flash tube array to particle density measurements will be fully described in Chapter 10.

CHAPTER 7

The Application of a Flash Tube Array to Directional Studies in E.A.S.

7.1 Introduction.

The large area of collection presented by the flash tube array is a particular advantage for investigations of the μ meson component of E.A.S. and directional studies with the array will normally be directed at this component.

Investigations of the directional properties of E.A.S. should furnish information on the following topics:

1. Shower models
2. The nature of the primary C.R. at high energies
3. Anisotropies in arrival direction of the primary C.R. at high energies
4. Characteristics of shower development - through studies of the zenith angle dependence of E.A.S.

These will be considered in turn.

7.2 Investigation of Shower Models.

The existence of extreme fluctuations in the development of extensive air showers renders discrimination between shower models difficult. However, if we consider meson production in the shower models discussed, it is apparent that there are two limiting possibilities:

1. The production of mesons is distributed along a line source extending through the whole depth of the atmosphere. (The density distribution $\alpha \frac{1}{r}$ following directly as a geometric property of the line source).
2. All the mesons are produced at some small atmospheric depth. (The density distribution in this case being ascribed to a θ^{-1} angular divergence at production).

In both cases it is assumed that the resulting μ mesons, preserve the direction of the parent π mesons. This can be justified by considering the maximum transverse momentum imparted to the μ meson in π decay (~30 MeV/c) in relation to the observed mean momentum of the μ mesons (~8 BeV/c). (In the experimental observations, reasonably high energy μ mesons should be demanded in any case to reduce to a minimum errors introduced by multiple scattering in the atmosphere).

If then, measurements near the shower core are made of the angles between the μ mesons and the direction of the shower axis, these should be appreciably larger in the case of the line source than could be expected for mesons produced at high altitude. Experiments have been made by Earl (M.I.T. 1959) on the approximate angular distributions of μ mesons in E.A.S. and from the results he concludes that at production, the angles made by the

π-mesons to the shower axis are $\sim 2^{\circ}$. This estimate of 2° is possibly the maximum angle that can be expected since Earl's calculations refer to the case of a line source. It therefore becomes obvious that the angles of the μ mesons and the shower axis direction must be measured to an accuracy at least less than one degree. Accuracies of this order can be achieved with a suitably designed flash tube array.

7.3 The Nature of the Primary C.R. at High Energies

The exact nature of the primary C.R. at the higher energies is still uncertain. There is some evidence for the occurrence of an abrupt change in the proportion of nuclear active particles in E.A.S. at an energy of 10^{15} eV. (Nikolsky 1956). This could be explained by a change of the initiating primaries from protons to α, or heavier, particles. The mean interaction length of the α particle however, is considerably less than that of the proton, therefore, in general, showers produced by α(or heavier) particles will originate at smaller atmospheric depths. An approach to the problem therefore is to examine the heights of production of the μ mesons in showers of high energies. This should be possible by means of a flash tube array and is an ultimate aim of the device.

A previous experiment along similar lines has been carried out by Cranshaw and de Beer (1959) using two triggered spark counter telescopes operated in conjunction with the Culham E.A.S. array. The available results show unexpected features, in particular an exceptionally large fraction of μ mesons seems to originate in the upper layers of the atmosphere, also the structure function of the mesons would appear to vary with zenith angle.

It is apparent that a more extended investigation of these features would be most valuable.

7.4 Anisotropy of the Primary Radiation.

The question as to whether the primary cosmic rays of highest energy are in fact isotropic is important for theories of the origin of cosmic rays, as has been already discussed in Chapter 6. There are two main approaches to the problem:

1. Investigation of the variation of the counting rate of an E.A.S. detecting array as a function of solar and of sidereal time.
2. Measurement of the arrival directions of E.A.S. and the analysis of these when plotted as points on the celestial sphere.

7.4.1. Time variations E.A.S.

Many investigations have been carried out to detect

variations in the rate of arrival of E.A.S. with time - mainly using extensive arrays of G.M. counters. Experiments have been made over a wide variety of shower size and at various altitudes. Small sidereal effects, indicating some degree of anisotropy, have been reported by McCusker (1955 & 1956), Farley & Storey (1955), Daudin (1952) and Hodson (1951) observing showers from primaries of energy less than 10^{16} eV. Most of these, however, can be reconciled to variations expected from the Compton-Getting effect and are therefore not real anisotropies. Investigations by Crawshaw and Elliot (1956) and also by Cranshaw and Galbraith (1954) on showers from primaries of $\sim 10^{17}$ eV showed no significant sidereal variations. This method, of course, is sensitive only to quite broad anisotropies. However, one may conclude that there is no significant evidence for the existence of these in primaries up to 10^{17} eV.

7.4.2. Arrival directions E.A.S.

Two experiments have been carried out to determine the arrival directions of E.A.S.; one by Clark (1955) using fast timing methods on the shower front with an extended array of scintillators, and a second by Rothwell et al (1956) using cloud chambers. The main advantage of this method is that a point source can be detected - if the apparatus has sufficient angular resolution. The

measurements of Clark were made to an accuracy of $\pm 5^{o}$ and those of Rothwell to $\pm 3.2^{o}$. In both cases plots of the shower directions on a mercator projection of the celestial sphere revealed no point sources or anisotropies. The energy range of the primaries in these experiments was $> 5 \times 10^{15}$ eV.

It should be noted that the area of sky subtended by the solid angle $3^{o} \times 3^{o}$ is still extremely large and experiments having higher resolution are required. The accuracy to which incident directions can be located by a flash tube array is limited mainly by the extent to which the mesons preserve the direction of the primary particle. It is feasible that the solid angle could be reduced to $1^{o} \times 1^{o}$, a factor of 9. The chief difficulty would be the low rate of collection imposed by demanding μ mesons. However, an extended period of operation should yield useful results.

7.5 The Zenith Angle Dependence of E.A.S.

Measurements of the zenith angle dependence of E.A.S. provide a method of determining characteristics of shower development such as the shower absorption length Λ. For this purpose some assumptions are necessary:

1. It must be assumed that the angular distribution can be related to the altitude dependence simply by a Gross transform. This will be true if the

shower formation is due solely to interaction with the atmosphere. If decay processes were important the variation would be steeper since these processes would be more favoured in traversing large distances of rare atmosphere at large zenith angles than in traversing the same mass of air vertically. Previous investigations have found reasonable agreement between zenith angle dependence and altitude dependence suggesting that decay processes may in fact be neglected.

2. A further assumption which must be made is that the lateral density distribution does not change with zenith angle. While this is probably true for the electron component, it should be remarked that the experiments of Cranshaw and de Beer indicate that the μ meson structure function may change significantly with zenith angle.

Recent reports (Rossi, 1960) of investigations of the zenith angle dependence of E.A.S. at an altitude of 4100 m were of particular interest. From the extremely high rate of arrival of showers of greater than 10^7 particles, at zenith angles as large as 40 or 50°, it was concluded that at this altitude the atmospheric absorption of showers is small or perhaps even negative.

The implication is that the showers are near their maximum development. It is apparent that observation of the zenith angle dependence of E.A.S. at these altitudes is of extreme significance.

The flash tube array is eminently suited to this particular study. For investigations on the electron component, it compares favourably with the cloud chamber and scintillator chronotron now in use. For use with the μ meson component, its combination of high resolution and large collecting area makes it superior to both.

In conclusion, it is apparent that studies of the directional properties of E.A.S. can furnish particularly useful information on the aspects discussed. The design and construction of a flash tube array for such studies will now be described.

CHAPTER 8

Design and Construction of the Prototype Air Shower Array

8.1. Introduction

The applications and ultimate aims of the directional array have been discussed: these govern the design of the apparatus. The more important requirements may be summarised as:-

1. High angular resolution
2. Reasonably large collecting area ($\approx 1\ m^2$)
3. Stability of operation
4. Simple and robust construction.

These requirements will be considered in turn.

8.2. Angular Resolution

An obvious limit to the accuracy required in measuring the directions of μ-mesons in E.A.S. is set by the variations in direction of the μ-mesons at any one point due to multiple scattering in the atmosphere. The magnitude of the scattering effect can be estimated from the approximate expression

$$\langle\phi\rangle^2 = \tfrac{1}{2}\,\frac{E_s^2\, t}{p^2\beta^2}$$ (Rossi and Greisen, 1941).

Where $\langle\phi^2\rangle$ is the mean square, projected angle of scatter, t is the scattering thickness in radiation lengths and E_s is the scattering constant, given by

$$E_s = 2m_e\,(137\ \pi)^{\frac{1}{2}} = 21.2\ \text{MeV}$$

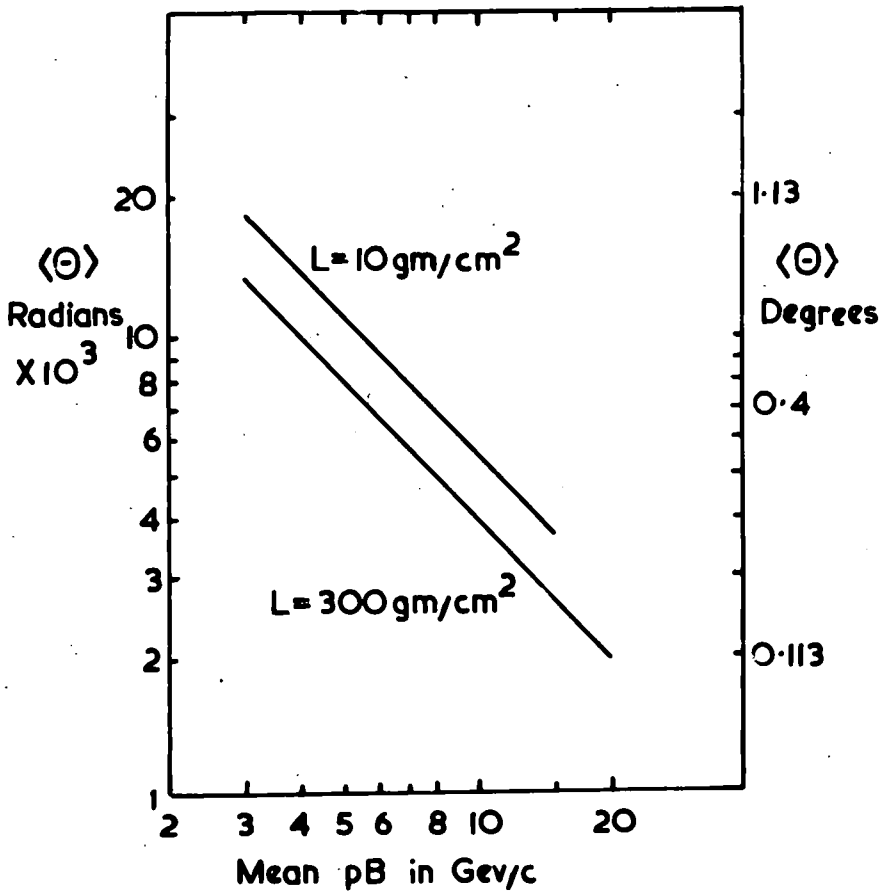

Figure 8.1. The atmospheric scattering of μ-mesons as a function of momentum. Height of production as parameter.

In the calculations the radiation length in air was taken as 43 cm^2/gm and in Fig. 8.1 the expected r.m.s. scattering angle $\langle\phi\rangle$ r.m.s. is plotted as a function of meson momentum for extreme values of atmospheric thickness, corresponding to meson production at atmospheric depths of 10 and 300 gm/cm^2. The mean momentum of μ-mesons in E.A.S. is estimated at ~8 $\frac{BeV}{c}$ (Andronikashvili, 1960) and the corresponding r.m.s. scattering angle is ~0.4^o. This figure was taken as an estimate of the angular resolution to be aimed at in the array.

The accuracy attainable in an array is determined by two factors:

1. The spatial resolution of the flash tube employed.
2. The geometrical arrangement of the flash tubes in the array.

The resolution of the flash tube is governed by two competing factors, its diameter and its efficiency. The 1.5 cm diameter tube filled at 60 cm N_e pressure presents the best compromise between the two. The characteristics of this tube are shown in Fig. 8.2. Some 900 were produced.

An approximate calculation indicated that the required accuracy in angular resolution could be achieved using four layers of tubes, the extreme layers being sep-

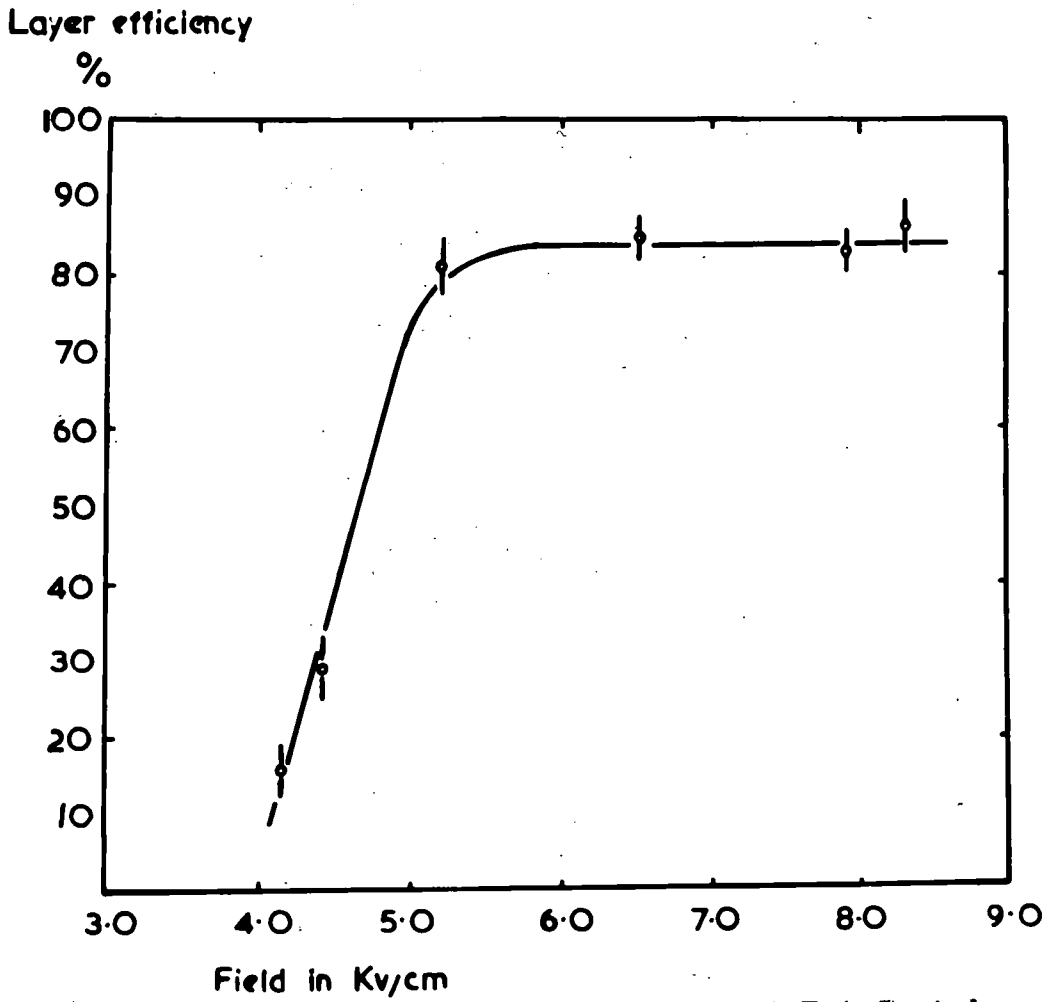

Figure 8.2. i) Field characteristics of E.A.S. tube.

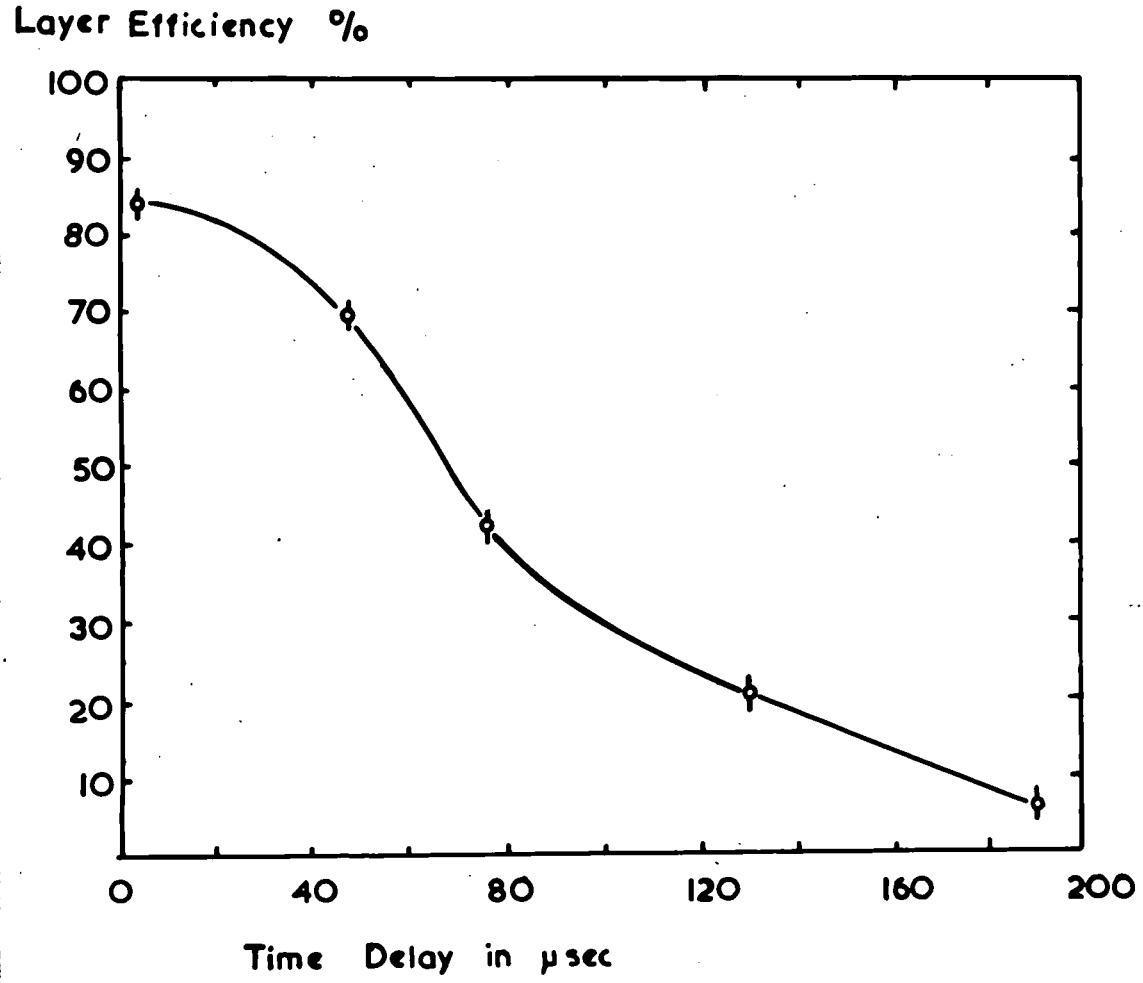

Figure 8.2. ii) Time-delay characteristics of E.A.S tube.

arated by one metre. This fact determined the main geometry of the array.

8.3 The Geometry of the Array

The final array was designed in the form of a "metre cube" since such a large collecting area (1 m^2) has useful possibilities for the measurement of particle densities. In all, 16 layers of flash tubes (each tube of sensitive length 1m) were used and alternate layers were "crossed" at right angles to permit the measurement of both spatial and projected angles. The layer arrangement of the array is illustrated in plate VIII (i) and (ii)

In principle the angle of a particle trajectory can be obtained from the tubes flashed in the extreme layers, each of which consists of two overlapping single layers thus presenting in effect a layer efficiency of 100%. The function of the intermediate layers is twofold:

1. To relate the flashes in the extreme defining layers.
2. To increase the overall angular resolution.

The separation of these layers was carefully considered: as this is increased the angular resolution is improved but the maximum density which can be accepted, whilst retaining an unambiguous relation between the flashes, is reduced. The optimum compromise between the two functions was determined graphically as 13 cm. Using a scale

Plate VIII (i) Photograph of DASI, during construction, showing the layer arrangement.

Plate VIII (ii) Photograph of west face of DASI with all tubes in position.

drawing of the array with this configuration, particle trajectories were simulated and an analysis was made to evaluate the r.m.s. accuracy of angular resolution which could be obtained. As the minimum layer efficiency anticipated was 80%, the method adopted was to draw tubes of diameter 80% of the true external diameter and assume them to have 100%.efficiency over this "sensitive" area. (This is in fact quite a close approximation to the actual operating conditions of the tube). Two sources of information on particle location are thus provided by:

a) the tubes having flashed

b) the spaces (through which the particle must have passed) between tubes which have not flashed.

Both were used in the analysis and the standard deviation of angular location was found to be 0.24^{o}.

In the actual array, some "noise" is introduced by unavoidable variations in the stacking of the tubes and in practice use is not normally made of the spaces between tubes which have not flashed. The final value of resolution obtained is therefore of the order of 0.4^{o}. (If the information given by both the flashed and unflashed tubes were used, it is estimated that the standard deviation would be 0.3^{o}).

8.4. Construction

Since the array should be suitable for adaptation to "mass production" methods, the simplest form of construction consistent with a fully efficient performance was adopted. Each layer of tubes was housed in a rectangular frame fabricated from 1" angle duraluminium. No locating grooves were considered necessary, the tubes being stacked side by side, care being taken to ensure parallelism as far as possible. The trays were then located, according to the dimensions given, in a Handy Angle framework of size 4 ft. cube. The 'crossed tubes' were located at right angles to within $\pm$ 0.12°.

The electrodes were made of aluminium foil in order to reduce electron scattering effects in the apparatus to a minimum, and were fitted using Pyrex glass insulators for the positive UHT electrodes.

8.5. The Electronic Circuitry

The electrostatic capacity of each layer of tubes was 900 pf, and the application of a sharply rising square pulse to a capacitance of this value poses a major problem. It was evident from previous work that with eight separate layers, each of this capacity, at least four pulsing units would be required. Trigatron units were therefore considered, since four such units can be efficiently triggered from a single hydrogen thyratron

(with a consequent reduction in expense). The impedance matching of a normal delay line P.F.N. to a large capacitative load is extremely difficult and experiments were necessary to find a more suitable method of producing a high quality pulse. The best result was achieved by simply discharging a large condenser into the primary of the pulse transformer. The impedance match in this case is far less critical and it was found possible to produce a pulse with a rise time of 0.3 μ sec. The pulse width (2.5 μsec) was of course shorter than that obtainable with a delay line, but a layer efficiency of 80% was still attained. It was decided to adopt this technique and the final pulsing circuit is shown in Fig. 8.3. Wire wound resistors of the low inductance type were used to form the characteristic impedance across the secondary of the pulse transformer and these were wax encapsulated to obviate atmospheric effects. The actual pulse applied to the array is shown in plates VIII (iii) and (iv).

The ancilliary electronic circuitry comprised a six channel Rossi coincidence unit,* which furnished the trigger pulse, and various circuits necessary to effect the timing sequence of illuminating clocks and fiducial lights and moving the camera film after each event. Standard power packs were used to provide HT and LT requirements together with a 24v d.c. supply and positive

* Appendix III

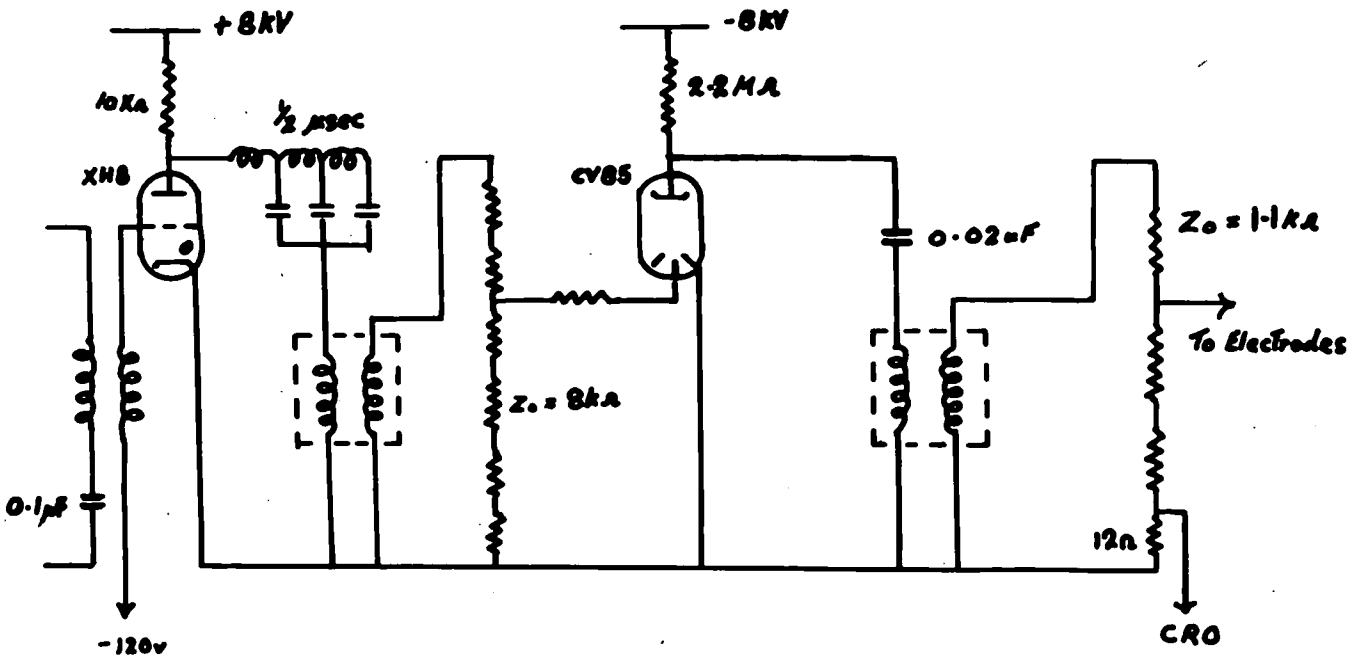

Figure 8.3. The condenser pulsing circuit.

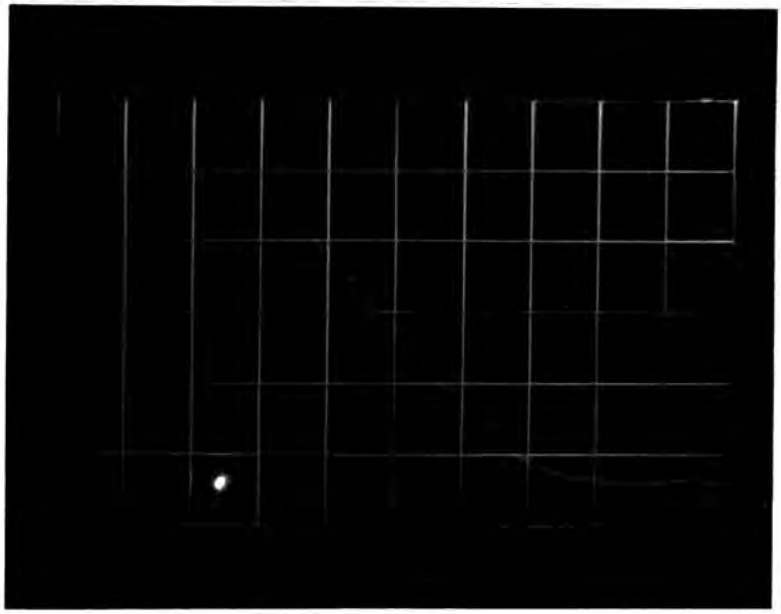

μ seconds

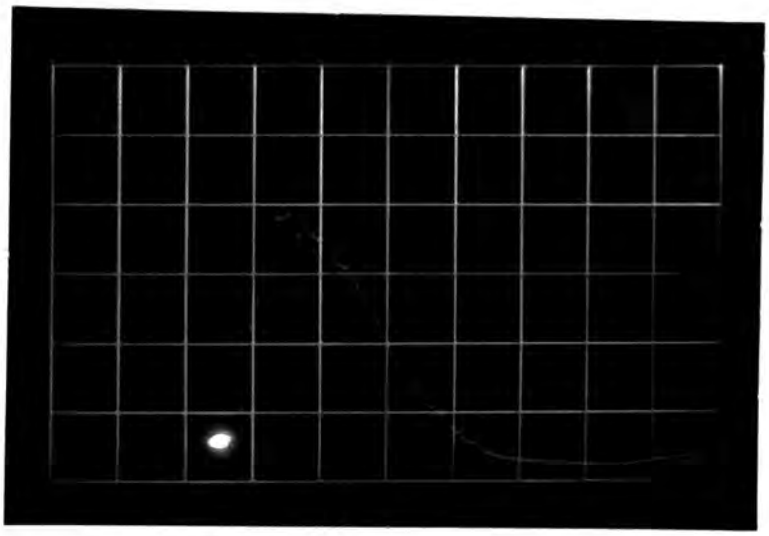

μ seconds

Plates VIII (iii) and (iv)

Oscilloscope photographs of the high voltage pulses applied to DASI.

and negative sources at 8 Kv. The entire electronic circuitry was accommodated in a single cabinet of size 5 ft x 2½ x 2½ ft.

8.6. Photographic Recording of events

Each of the two faces of the array was photographed by a separate camera (f 2.8). Clocks were therefore incorporated in both faces to synchronise events in addition to recording the times of occurrence. Fiducial lights were used to define a vertical reference axis for each event. Owing to the sharpness of the polar diagram of light emission from the long tubes it was necessary to situate the cameras at a distance of 2.6 metres from the faces of the array. (This being the minimum distance which permitted the efficient recording of flashes in tubes at the corners of the array). No distortion of the image was observed, therefore measurement of trajectory angles by direct projection could be employed. The final arrangement of apparatus was in an L-shape of side 14 ft. The equipment was given the title "Directional Air Shower Indicator", the abbreviated form 'DASI' being normally used.

8.7. Fundamental Data Pertaining to DASI

a) Scattering: Some scattering of low energy particles is inevitable in the material of the apparatus. To esti-

mate the magnitude of this effect, the "scattering thickness" of the array was calculated. Allowing for both glass and aluminium content, the thickness is x = 13.4 gm/cm^2 giving a corresponding value of

$$t = 0.4 \text{ radiation lengths}$$

The expected r.m.s. angle of scatter for electrons of various energies is shown in Table 8.1.

TABLE 8.1.

Electron Energy	30 MeV	100 MeV	1 GeV	6 GeV
r.m.s. angle of scatter	18^o	5.4^o	0.54^o	0.09^o

b) Absorption: The minimum energy required by an electron to fully traverse the apparatus is also dependant on the effective thickness. For electrons of energy >2 MeV it may be assumed that

$$E_{min} = K x$$

where K is proportional to N and Z for the absorber.

Assuming mean values of Z = 10, ρ = 2.8 for glass and using the empirical data of Katz and Penfold (1952) it is found that

$$K \simeq 2.03 \text{ MeV/gm/cm}^2$$

Therefore $E_{min} = 27.5$ MeV.

c) Critical energy: Another quantity of interest is the critical energy for electrons in the apparatus. This is the energy at which the losses due to bremmstrahlung and ionisation become equal and is found to be 60 MeV.

CHAPTER 9

A Measurement of the Zenith Angle Dependence of E.A.S.

9.1. Introduction.

The application of DASI to studies of such aspects of E.A.S. as arrival directions and the heights of production of mesons requires the use of a large and somewhat elaborate E.A.S. detecting array (and this was not available). However, basic studies such as the zenith angle dependence of E.A.S. are possible using a relatively simple form of detecting array therefore an investigation of this topic was undertaken - mainly as a means of testing the prototype unit. Measurements of the angular variation of E.A.S. were carried out on both the electron and the μ-meson components.

9.2. The Importance of the Zenith Angle Dependence

If certain assumptions are made, as described in Chapter 7, the attenuation length of E.A.S. may be derived from measurements of the zenith angle dependence.

If $S(N, x)$ is the differential spectrum of number of showers per unit area per unit time per unit solid angle having N particles at atmospheric thickness x then

$$S(N, x) \quad \alpha \exp -\left[\frac{x-x_o}{\Lambda}\right]$$

where x_o is the depth of the atmosphere in the vertical direction and Λ is the shower attenuation length.

At zenith angle θ, the atmospheric thickness x is increased to

$$x = x_o \sec \theta$$

Thus

$$S(N,\theta) \alpha \exp -\left[\frac{x_o}{\Lambda}(\sec\theta - 1)\right]$$

$$\alpha \exp -\left[\frac{x_o}{\Lambda} \cdot \frac{\theta^2}{2}\right]$$

$$\alpha \quad 1 - \frac{x_o}{\Lambda}\frac{\theta^2}{2} \qquad \ldots\ldots\ldots\ldots(i)$$

Also if it is assumed that

$$S(N,\theta) \quad \alpha \cos^n \theta$$

$$S(N,\theta) \quad \alpha \left(1 - \frac{\theta^2}{2}\right)^n$$

$$\alpha \; 1 - n\frac{\theta^2}{2} \qquad \ldots\ldots\ldots\ldots(ii)$$

Comparing (i) with (ii) it is apparent that

$$n = \frac{x_o}{\Lambda}$$

from which

$$\Lambda = \frac{x_o}{n} \qquad \ldots\ldots\ldots\ldots(iii)$$

Therefore, expressing the variation in intensity of E.A.S. with zenith angle as

$$I(\theta)\, d\omega = K \cos^n \theta \, d\omega$$

where $d\omega$ is the solid angle subtended at zenith angle θ, the attenuation length of E.A.S. can be derived from an experimental measurement of the exponent n.

9.3. The Detecting Array.

The detecting array consisted of 3 trays of G.M. counters arranged round the DASI on the circumference of a circle of radius 1.9m. Each tray contained six adjacent G.M. counters ("G60 - 20th Century") connected in parallel to provide a sensitive area of $0.126m^2$. A threefold coincidence of the detecting trays was demanded to "trigger" DASI. With regard to the detecting array three points are of interest:

1. the spectrum in particle density of the E.A.S. detected
2. the rate of detection of E.A.S.
3. the distribution in size of the showers detected.

9.3.1. The (Expected) Spectrum in Particle Density.

The chance of obtaining a threefold coincidence with a shower giving a mean density Δ over the areas, S, of the detecting trays is

$$P\Delta = (1 - \exp - S\Delta)^3$$

and the probability of obtaining a mean density Δ is given by the differential density spectrum of E.A.S. as

$$N(\Delta)d\Delta = 0.28\ \Delta^{-2.4}\ d\Delta \text{ per sec (Singer 1954)}$$

Therefore the expected spectrum in density is given by

$$R(\Delta)d\Delta = P\Delta\ .\ N(\Delta)d\Delta$$
$$= 0.28\ (1 - \exp -S\Delta)^3\ \Delta^{-2.4}\ d\Delta \quad ....(iv)$$

This is plotted in Fig. 9.1.

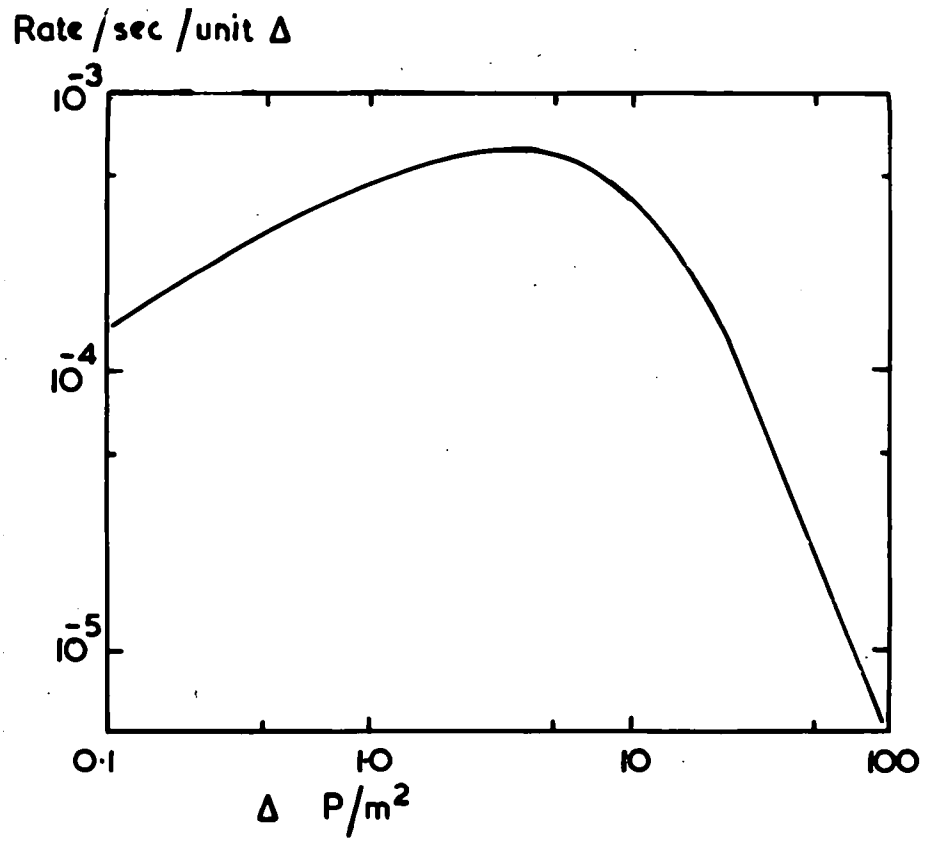

Figure 9.1. The theoretical spectrum in density of showers detected by the G.M. detecting array.

9.3.2. The Rate of Detecting E.A.S.

The expected rate of events is obtained by integrating over all Δ expression (iv) :-

$$R = 0.28\int(1-e^{-S\Delta})^3 \Delta^{-2.4}\, d\Delta. \text{ per sec.}$$

The integration was carried out and the expected rate was calculated to be 53 events/hour.

The observed rate of events was 20.2 $\pm$ 1.3/hour, a value well removed from that expected. The discrepancy was presumed due to the comparatively large separation of the detecting trays and a simple decoherence test was made. The resulting curve is shown in Fig. 9.2. It is apparent that the rate of triggering with the trays separated by a distance of the order of 3.8m is approximately 0.4 times the rate obtained with the trays in closest proximity. Applying this approximate correction, the expected rate for the conditions of the experiment is reduced to

$$53 \times 0.4 = 21/\text{hr.}$$

The close agreement is reassuring.

An experimental check was also made on the rate of spurious coincidences of the detecting trays. This is given theoretically as

$$N = 3n^3\tau^2$$

where n is the counting rate of a single tray and τ is the resolving time of the Rossi coincidence circuit, in

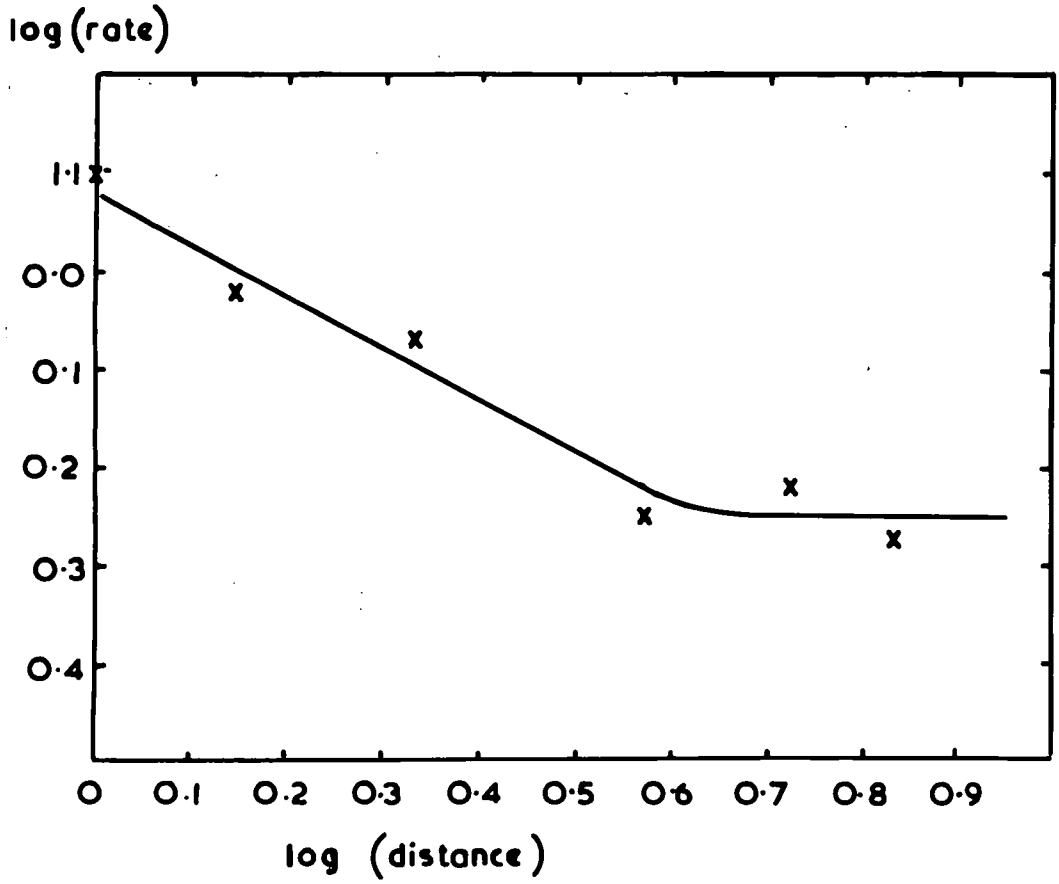

Figure 9.2. The decoherence function for the G.M. detecting array.

this case 6.5μsec. As n was found to be 70/sec, the expected number of spurious counts is

$$N = 3 \times 3.44 \times 10^{5} \times 4.25 \times 10^{-4} \text{ counts/sec.}$$

$$= \underline{0.158 \text{ counts/hour}}.$$

This was verified experimentally, the average rate of spurious counts being (0.15 $\pm$ 0.02) per hour over a test run of 24 hours. Taking the normal rate of events as 20/hr. the significance is that one spurious event will be counted in each 120 events. For the present experiment this was no disadvantage.

A further check on the functioning of the detecting array was provided when the interval distribution was compiled from the recorded times of the events. The curve is given in Fig. 9.3. From the reasonably good agreement with the expected distribution it may be concluded that the detecting array was operating correctly.

9.3.3. The Response in Shower Size.

A shower will be recorded only if it is of such size as to provide a density at the detecting tray furthest from the shower core sufficient to trigger that detector. The contribution to the counting rate from showers in the size interval N to N+dN is therefore

$$\mathbf{\Sigma}(\rho) \quad N = \pi R^{2} \, KN^{-\gamma} . \, dN \qquad \ldots\ldots\ldots(v)$$

where R is the distance of the shower core from the furthest detector and ρ is the minimum density required

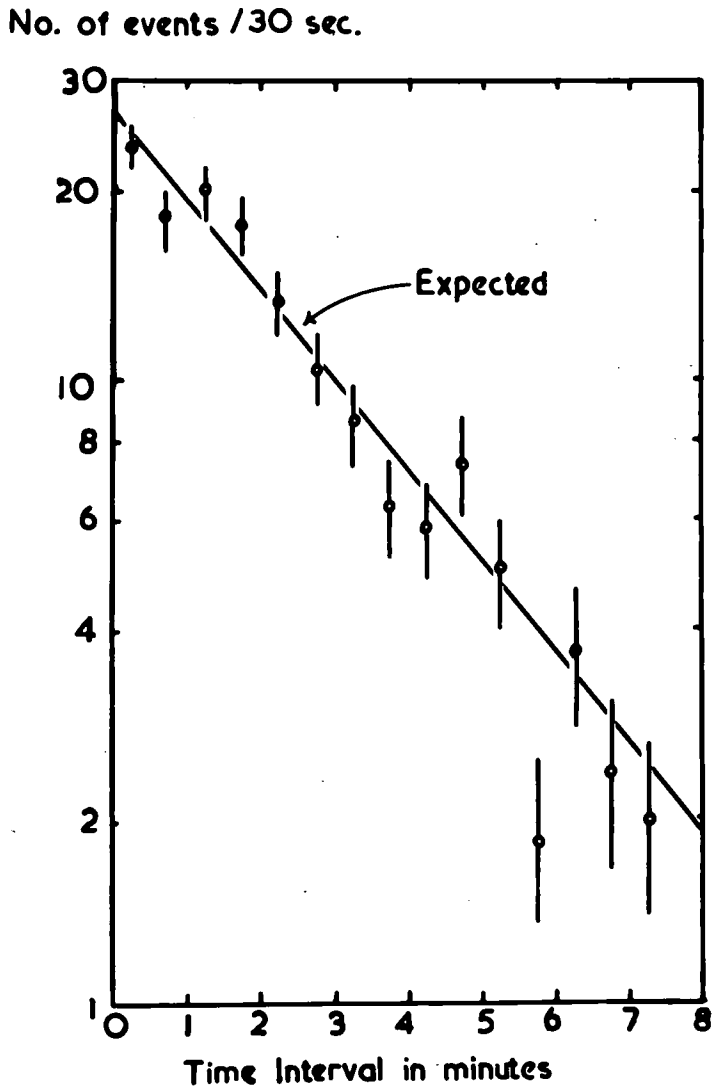

Figure 9.3. The interval distribution of events in DASI.

to trigger the detector.

The density produced at a distance R from the core of a shower of size N can be obtained from the expression

$$\rho = N\, f(r)$$

where f(r) is the structure function of the shower. The exponential structure function

$$f(r) = \frac{1}{2\pi r_o} \frac{\exp}{r} - \frac{r}{r_o}$$

will be applied, thus

$$\rho = N \frac{1}{2\pi r_o} \frac{\exp}{r} - \frac{r}{r_o}$$

from which $\rho\, r\, e^{+\frac{r}{r_o}} = \frac{N}{2\pi r_o}$

The minimum value of ρ for triggering will be taken as $\frac{1}{A}$ where A is the area of a tray, and r_o, the characteristic shower radius, will be taken as 79m. (sea level). Substituting these values

$$R \exp \frac{R}{79} = 2.52 \times 10^{-4} N.$$

which defines R for any value of N. The actual values of R corresponding to a particular shower size N can thus be found graphically. The contribution from showers of size N to N+dN is then obtained from equation (v). This is shown in Fig. 9.4, plotted as a function of NdN.

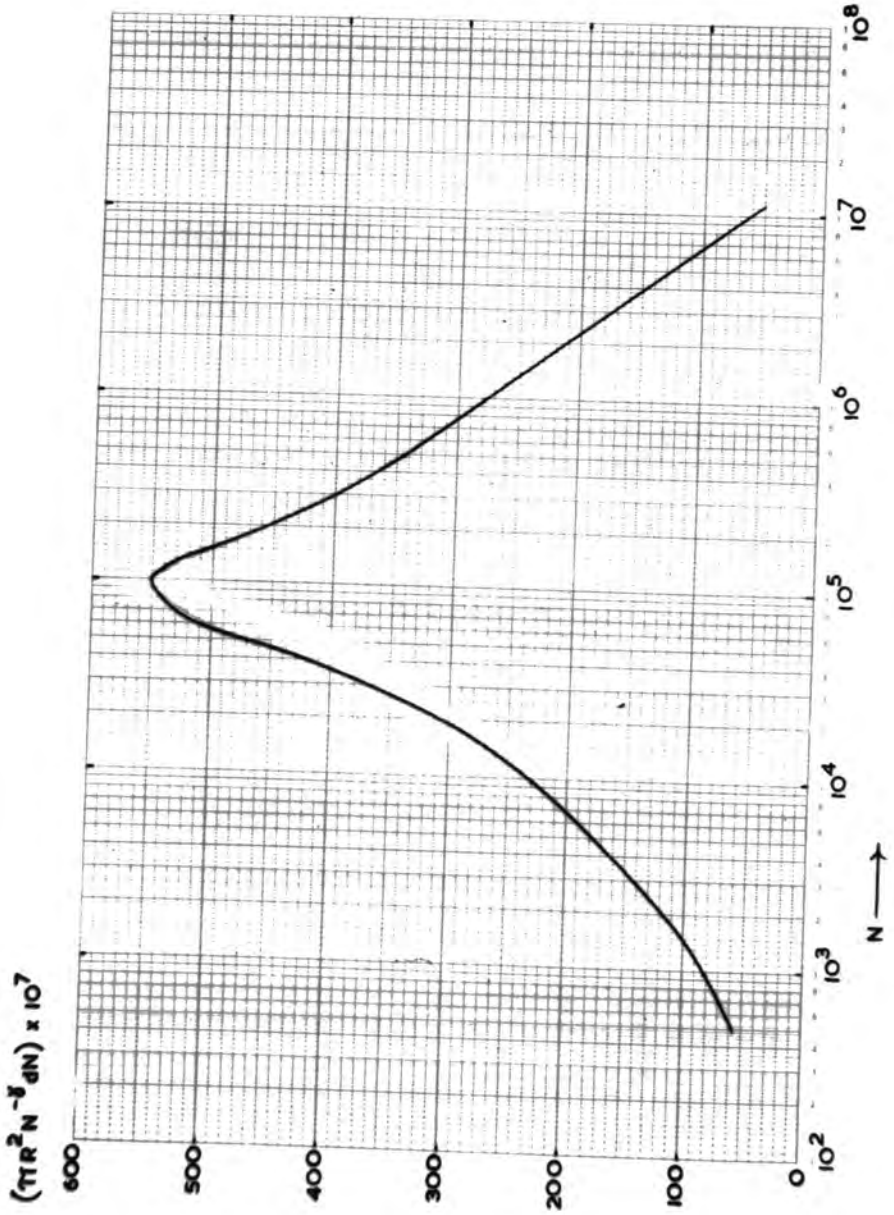
$(\pi R^2 N^{-\frac{1}{2}} dN) \times 10^7$
600
500
400
300
200
100
0
10^2
10^3
10^4
10^5
10^6
10^7
10^8
N

Figure 9.4

The most probable size of shower detected is seen to be 10^5 particles corresponding to a primary energy of 6×10^{14} eV.

9.4. A Measurement of the Angular Dependence of E.A.S. using the Electron Component.

Some 1400 showers were recorded with the DASI apparatus operated without lead screening. Photographs of typical events are shown in plates IX i-iv. All events were examined but in over 85% of the showers the particle density was too great to permit an unambiguous determination of the shower angle. This was not unexpected. An interesting effect observed was that if the number of "random" flashes was sufficiently large, the flashes exhibited "preferred" directions occurring at intervals of 10°. These instrumental "resonances" were found to correspond to the spacing between adjacent tubes in the intermediate layers. The effect must be guarded against when the examination of dense showers is necessary.

In the remaining events the density was low enough to permit an accurate determination of the directions of the showers and these events were analysed.

Plates IX (i) Typical electron event

(ii) Directional electron event.

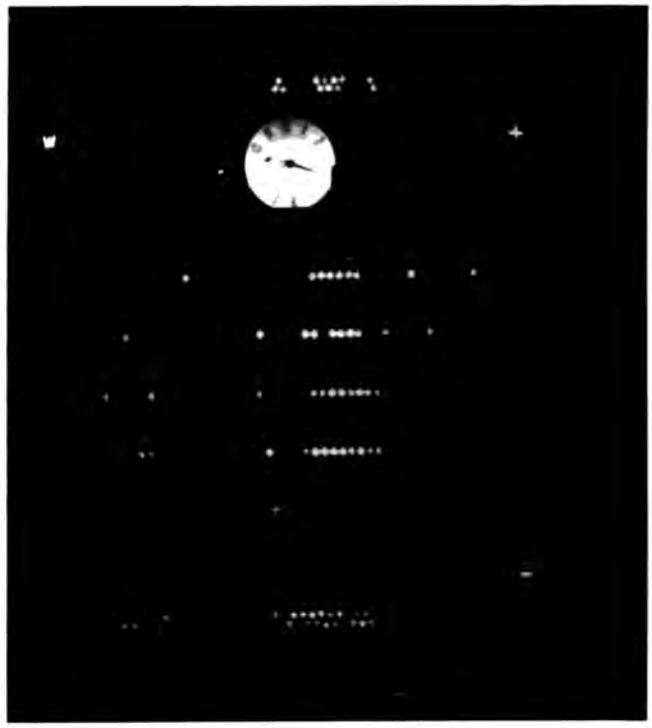

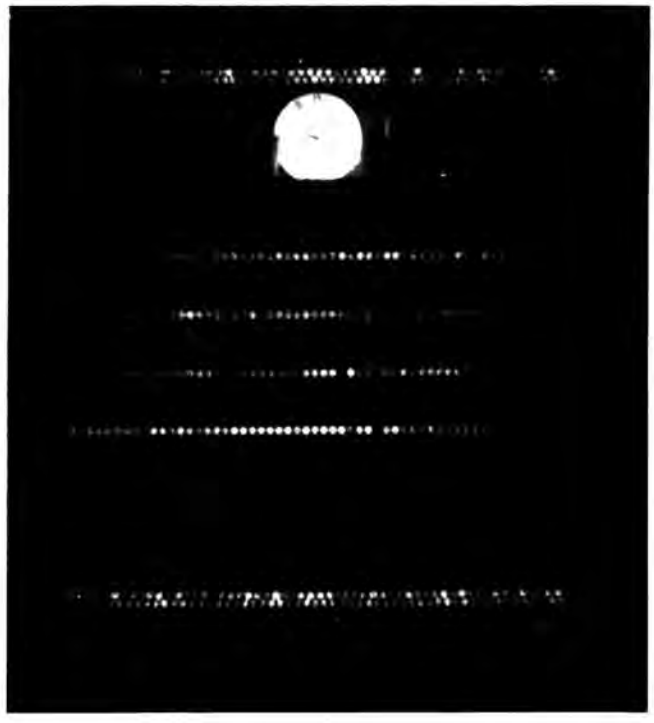

Plates IX (iii) "Core" structure in electron shower

(iv) Extremely dense electron shower

9.4.1. The Measured Distribution.

The criteria applied for the acceptance of an event were

i) Three or more tracks parallel to $<2^{\circ}$.

ii) At least four tubes flashed along each track.

iii) Density - less than 20 flashes per layer.

The mean angle of the tracks was taken as the (projected) angle of the shower.

Methods available for the measurement of directions using flash tube data have been fully discussed by Ashton et al (1958). In this study, measurement was carried out by projecting the events on to a rotatable screen which was ruled and calibrated in degrees. This method is not the most accurate but it has the advantage of providing reasonable precision at a tolerable speed. The angles of tracks could be located to an accuracy of 1° which was considered sufficiently precise for the present purpose. Appreciable scattering was observed in some tracks attributable to fairly low energy electrons.

The results were grouped in angular intervals of 5° and the distribution in projected angle of E.A.S. in DASI, as obtained from 335 ("electron") events, is shown in Fig. 9.5. The frequencies have been normalised to give a value of unity at $\beta=0$. The evaluation of the exponent in the zenith angle variation of E.A.S. will be described in § 9.6.

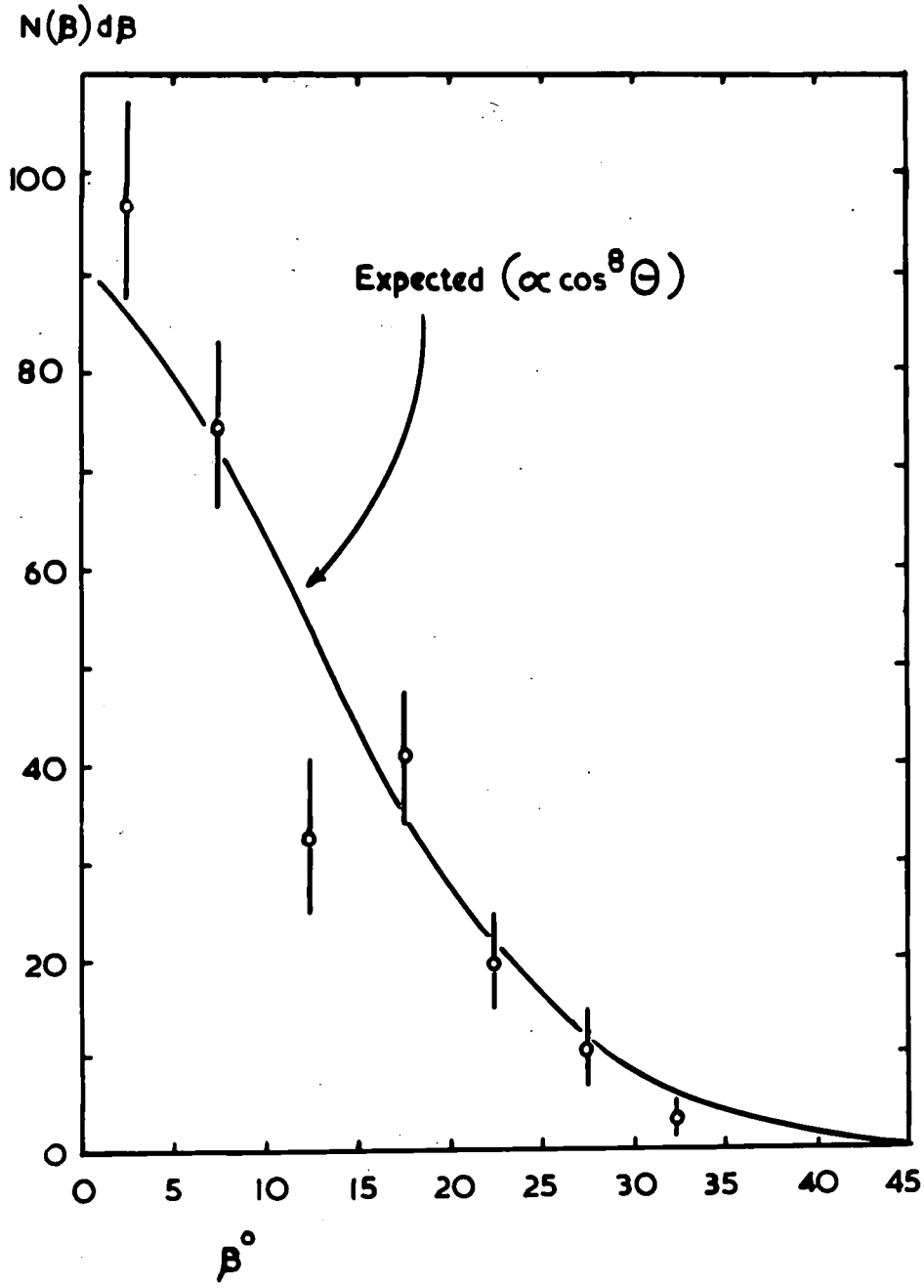

Figure 9.5. The observed distribution in projected angle of EAS from electron events in DASI.

9.4.2. The Statistical (Approximate) Methods of Determining the Angular Variation of E.A.S.

In many of the events where the shower particle density was too high to satisfy the criteria for direct measurement, a "statistical" method was applied to obtain the approximate shower direction and thence the angular dependence of E.A.S. The method is based on the relative numbers of "paired" flashes, directed respectively to left or right, which are observed in the uppermost double layer of DASI.

Firstly the assumptions must be made that:

i) All shower particles have parallel trajectories

ii) The efficiency of the flash tube is 100% over the distance η_{int} x 2r, where r is the internal radius and η_{int} is the internal efficiency of the tube.

iii) The distribution of shower particles is "random".

A section of the top double layer of tubes is shown in Fig. 9.6. Consider a particle trajectory at an angle ϕ. If tubes B and C are flashed, the "acceptance width" x is given by

$$x = (r-s) + d.\phi.$$

For A and C flashed, the "acceptance width" y is given by

$$y = (r-s) = d\phi.$$

Thus the ratio of the number (N_R) of 'right' directed

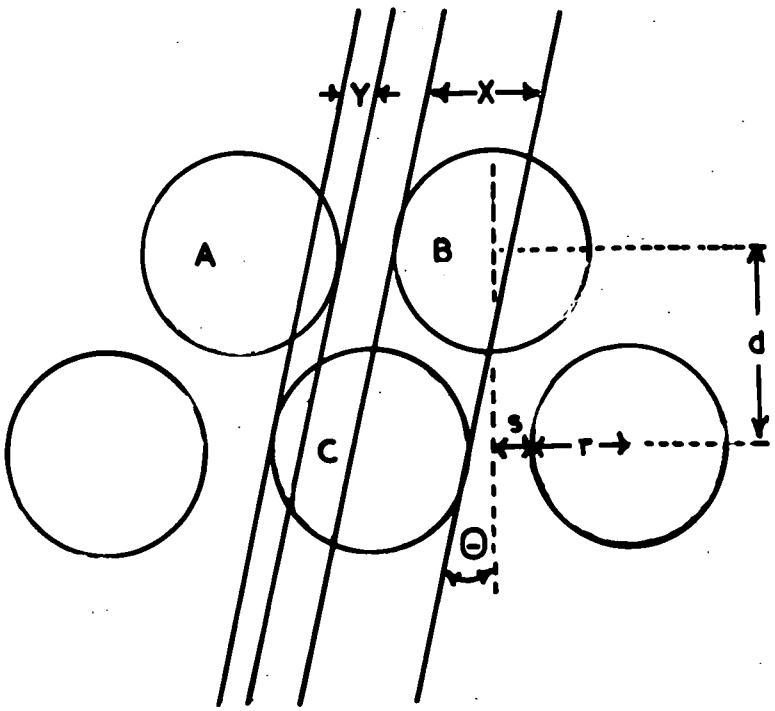

Figure 9.6. A cross section of the top layer of tubes in DASI.

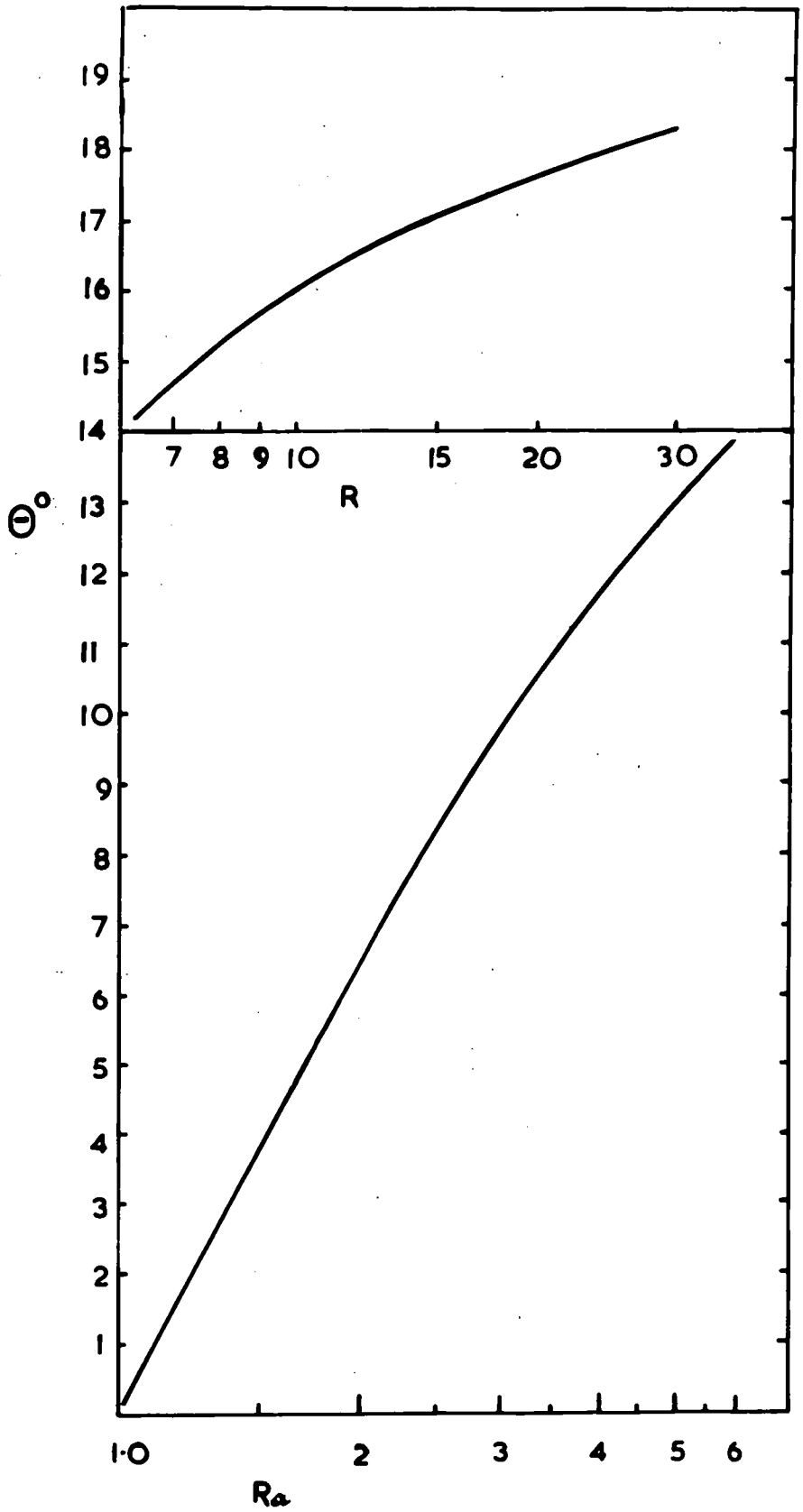

Figure 9.7. The relation between the projected angle of the shower and the figure R obtained from the statistical method of direction analysis.

pairs (i.e. B and C) to the number (N_L) of 'left' directed pairs (i.e. A and C) is

$$R_a = \frac{N_R}{N_L} = \frac{x}{y} = \frac{r-s + d\phi}{r-s - d\phi}$$

if $\frac{r-s}{d} = \alpha$ then

$$R_a = \frac{\alpha+\phi}{\alpha-\phi}$$

therefore

$$\frac{R_a+1}{R_a-1} = \frac{2}{2}\ \frac{\alpha}{\phi}$$

and $$\phi = \frac{(R_a-1)}{(R_a+1)}\alpha$$

From the dimensions of the array, $\alpha = 0.343$ radians

$$\alpha = 19.6\ \frac{(R_a-1)}{(R_a+1)} \text{ degrees } \ldots\ldots\ldots\text{(vi)}$$

The method was applied experimentally by counting the numbers N_R and N_L for each event and taking the ratio $\frac{N_R}{N_L}$ or $\frac{N_L}{N_R}$ whichever gave $R_a>1$. The corresponding value of ϕ was then obtained from a plot of equation (vi) which is shown in Fig. 9.7. It is apparent from an inspection of equation (vi) that the method can only be applied to determine shower directions at angles less than 19.6°. Showers arriving at greater angles were assigned to a single group therefore the angular distribution obtained was of integral form. Fig. 9.8 is the integral distribution in projected angle of E.A.S. obtained from 1150 events.

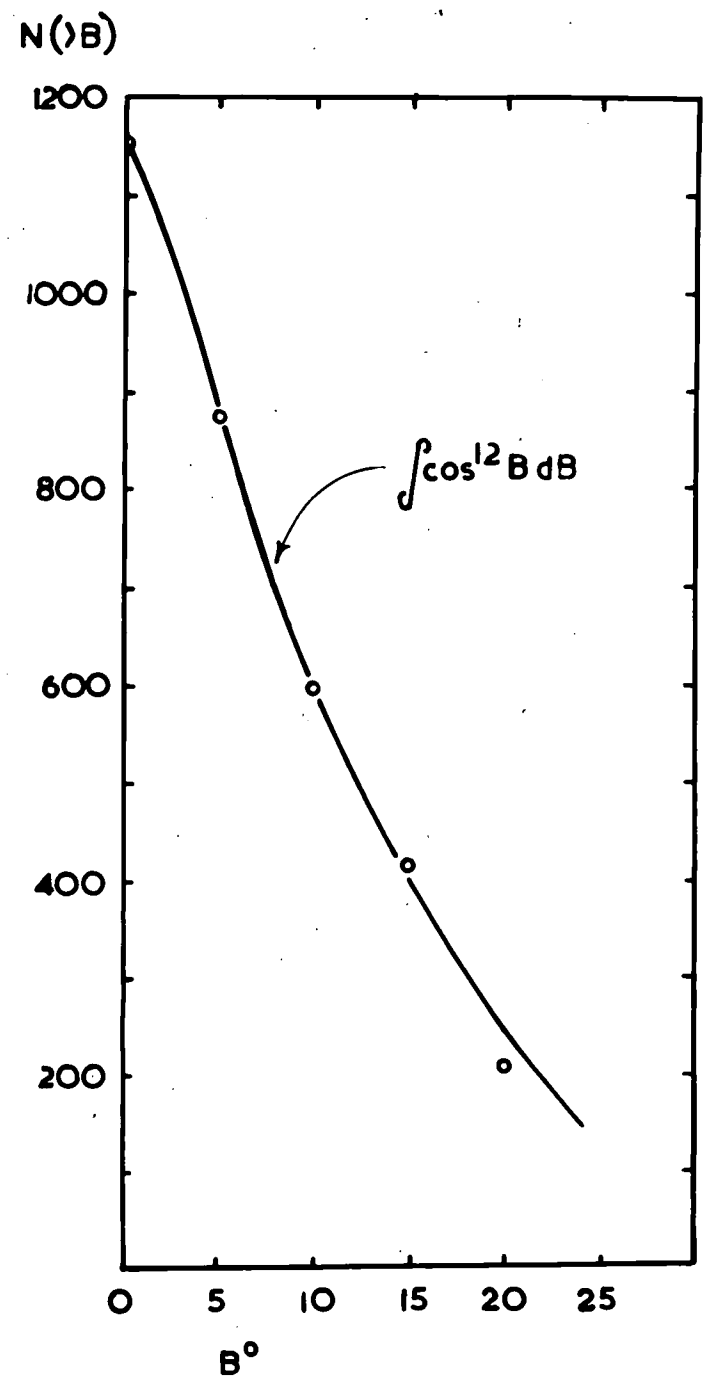

Fig. 9.8. The integral distribution in projected angle of E.A.S. from the statistical method of analysis.

To check the method a sample of 108 events was taken in which the shower directions could be obtained by both direct measurement and the statistical method. From a comparison of the two distributions, (Fig. 9.9) it would appear that there is reasonably good agreement between the two methods at angles below 15^{o}. At 20^{o}, however, the statistical method overestimates the probable value by a factor of 1.7 and this factor was used to correct the point at 20^{o} in Fig. 9.8.

The overestimate given by this method is presumed due to the angular distribution of E.A.S. which falls rapidly with increasing angle. Thus events giving a particular value of R_a are more likely to have true angles $< R_a$ and therefore to occur at correspondingly higher rates.

A further indication is that if the integral distribution is represented as

$$I(>\phi) \propto \cos^{m}\phi$$

then the statistical method will tend to give a slightly lower value of m than is obtained by direct measurement. The "expected" distribution can be determined quite rigorously and the angular dependence obtained, as will be described in §9.6.

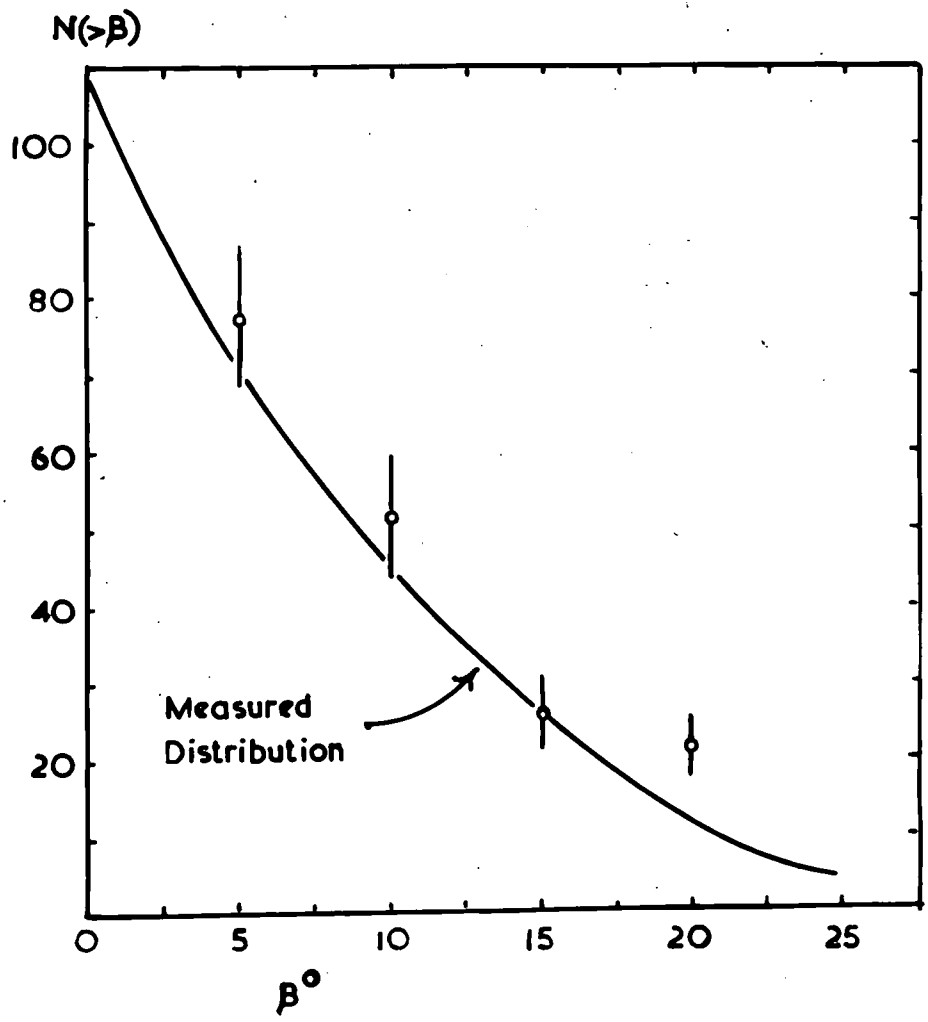

Figure 9.9. A comparison of the integral distributions in projected angle of E.A.S. obtained by direct measurement and by the statistical method.

9.5. An Investigation of the Angular Dependence of E.A.S. using the μ-meson Component.

An electron filter, two layers of lead providing a total thicknessof 16.5cm (187 gm/cm^2), was erected over the apparatus to permit a study of the angular dependence of E.A.S.by measurements on the penetrating component (mainly μ-mesons). Screening of DASI from the electron component is difficult because of the amount of lead (~12 tons) required to completely shield an apparatus of such dimensions. The arrangement employed was merely a compromise and the electron component was still much in evidence in some 70% of the total number of events. However, rigorous criteria were applied to ensure that measurements were in fact made only on the μ-component:-

i) At least two particle tracks parallel to $<2^{\circ}$

ii) Each track, in both projections, to have passed through the complete thickness of lead.

iii) At least four flashes in each track.

No changes were made in the detecting array and a further 1600 showers were recorded. Typical events are shown in plates IX (v to vi). From these some 279 useful events were obtained. An angular interval of 5° was again used and the distribution in projected angle of E.A.S. as measured using the penetrating component is given in Fig. 9.10. The frequencies have been normalised to correspond to a value in the electron distributions of

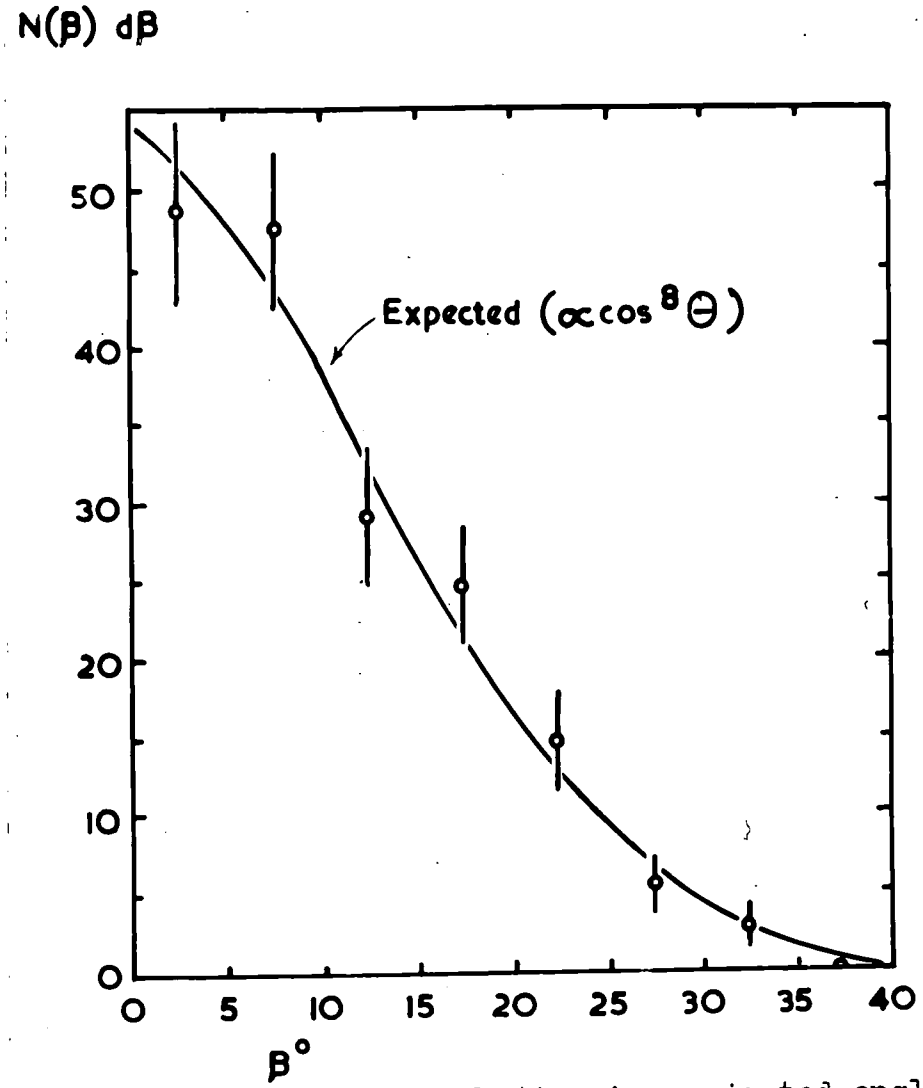

Figure 9.10. The distribution in projected angle of E.A.S. as obtained from μ-meson events in DASI. (The frequencies are normalised to correspond to a figure of 100 in the 'electron' distribution at $\beta = 0^{o}$.)

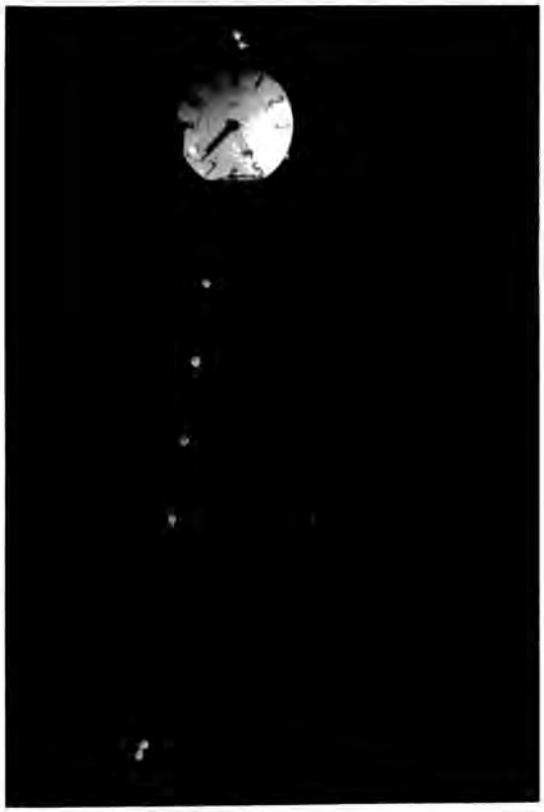

Plates IX (v) and (vi) μ-meson events under 16.5 cm Pb.

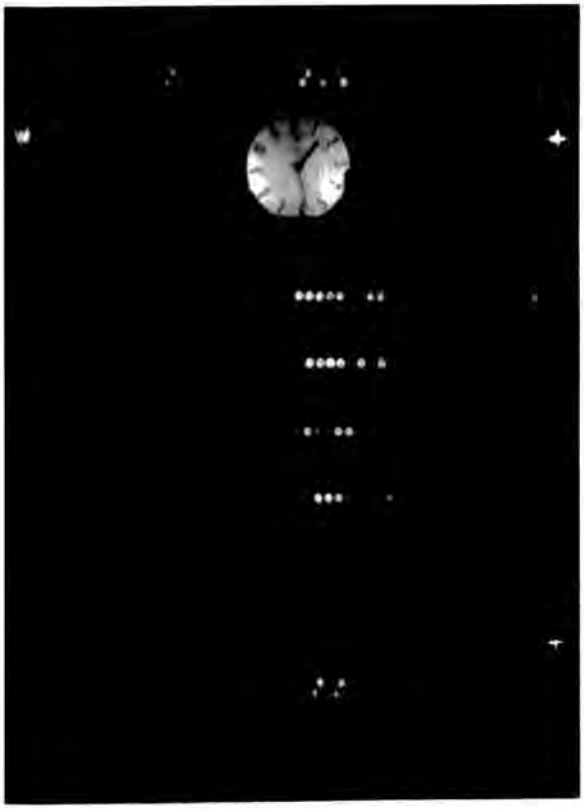

Plates IX (vii) Interesting cascade under 16.5 cm Pb

(viii) Scattered particles observed under 16.5 cm Pb

unity at $\beta=0$.

Scattering effects were much less obvious in the case of the meson component - which, together with the more stringent criteria employed for acceptance, possibly accounts for the lower "spread" of the experimental points. The angular directions could be measured to an accuracy of 1^{o} using the simple projection method.

9.6. Analysis of Experimental Data : The Exponent of the Angular Variation of E.A.S.

The aim of the analysis is to derive from the experimental data the exponent of the angular variation of E.A.S. From this the shower attenuation length may be obtained directly. When considering the measured distributions in DASI, factors which must be taken into account are

a) The collecting area of the apparatus and that of the detecting array varies with the zenith angle of the shower.

b) The distribution as measured in DASI is in projected angle.

The probability of obtaining an event at an angle θ depends firstly on the chance of detecting a shower at that angle and secondly on the probability of observing the shower in DASI. Thus the number of events at zenith angle θ is given by

$$N(\theta) = \left[I(\theta)d\omega G(\theta)g(\theta)\right]\left[A(\theta)\ f(\theta)\right] \quad \ldots\ldots\ldots(vii)$$

where

i) $I(\theta)\ d\omega$ is the intensity of E.A.S. (spatial flux per unit area perpendicular to the flux) at zenith angle θ, assumed to be of the form

$$I(\theta)\ d\omega = K_1 \cos^n\theta\ d\omega.$$

ii) $G(\theta)$ is a function to allow for the difference in area presented normally to the shower axis by the detecting array at angle θ and takes the general form

$$G(\theta) = (\cos^k\theta)^\gamma$$

The constant k depends on the shape of the detector being zero for an isotropic detector and unity for a rectangular tray. The factor γ is the exponent of the integral density spectrum of E.A.S. and reflects the variation in counting rate with change in detector area due to the slope of the density spectrum.

In this case $G(\theta) = \cos^\gamma\theta$

iii) The function $g(\theta)$, of the form $(\cos\theta)^{-\alpha}$ where α represents the slope of the decoherence curve, is normally required to allow for the change in the separation of the detecting trays with change of zenith angle. However, for the separation used in the present array $\alpha \simeq 0$ therefore $g(\theta) = 1$ and this term may be ignored.

iv) $A(\theta)$ is simply a geometric function allowing for the change in (normal) collecting area of the measuring apparatus (DASI) with zenith angle.

$$A(\theta) = A_\theta \cos\theta$$

where for analytic purposes A_θ will be taken as

$$A_\theta = A_o \cos^R \theta$$

R being a constant govered by the variation in surface area of the apparatus with angle.

Thus $$A(\theta) = A_o \cos^{R+1} \theta$$

v) The remaining function, $f(\theta)$, is to allow for any change with zenith angle of the structure function of showers, and will also be represented as a term in $\cos\theta$ i.e.

$$f(\theta) \propto \cos^r \theta$$

This is important only in the case of the μ-meson distribution. No change in the structure function of 'electron' showers with zenith angle has been observed, therefore in the case of the electron distribution $r = 0$.

Returning to expression (vii), the number of events expected at the angle θ may now be written as

$$N(\theta) = A_o K_1 \cos^n \theta \cos^\gamma \theta \cos^{R+1} \theta \cos^r \theta \cdot d\omega$$

or

$$N(\theta) = K_2 \cos^q \theta \, d\omega.$$

where $q = n + \gamma + R + 1 + r$ .....(viii)

and $K_2 = K_1 A_o$.

Next must be considered how $N(\theta)$ is distributed in projected angle:-

In Fig. 9.11, θ is the spatial angle of the shower flux and β is the measured projected angle. It may readily be shown that the spatial and projected angles are related by the expression

$$\cos\theta = \cos\alpha \cos\beta$$

and that the solid angle

$$d\omega = \cos\alpha \, d\alpha \, d\beta$$

Therefore as $N(\theta) = K_2 \cos^q \theta \, d\omega$

$$N(\beta,\alpha) = K_2 \cos^q \beta \, d\beta \cos^{q+1} \alpha \, d\alpha$$

and the flux in the angular interval between the projected angles β and $\beta+d\beta$ is obtained by summing over α as

$$N(\beta)d\beta = K_2 \cos^q \beta d\beta \int_{-\pi/2}^{\pi/2} \cos^{q+1} \alpha \, d\alpha$$

$$= K_3 \cos^q \beta d\beta \qquad \text{.....(ix)}$$

where $$K_3 = K_2 \int_{-\pi/2}^{\pi/2} \cos^{q+1} \alpha \, d\alpha.$$

9.7. Results.

Expression (ix) represents the experimentally observed distribution and the value of q is easily obtained from a logarithmic plot of the normalised experimental frequencies against $\cos\beta$. (Fig. 9.12). The slopes of the distributions were found by the method of least squares and the values obtained were

$q_e = 18.22 \pm 0.67$ for the electron distribution and

$q = 17.16 \pm 0.43$ for the μ-meson distribution.

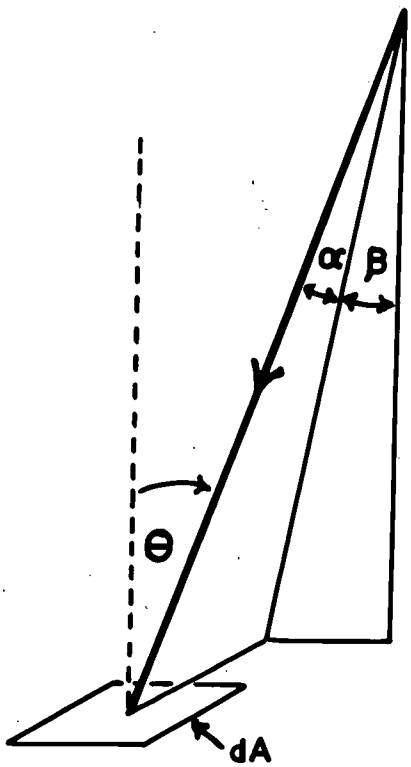

Figure 9.11. The relation between spatial angle and projected angle.

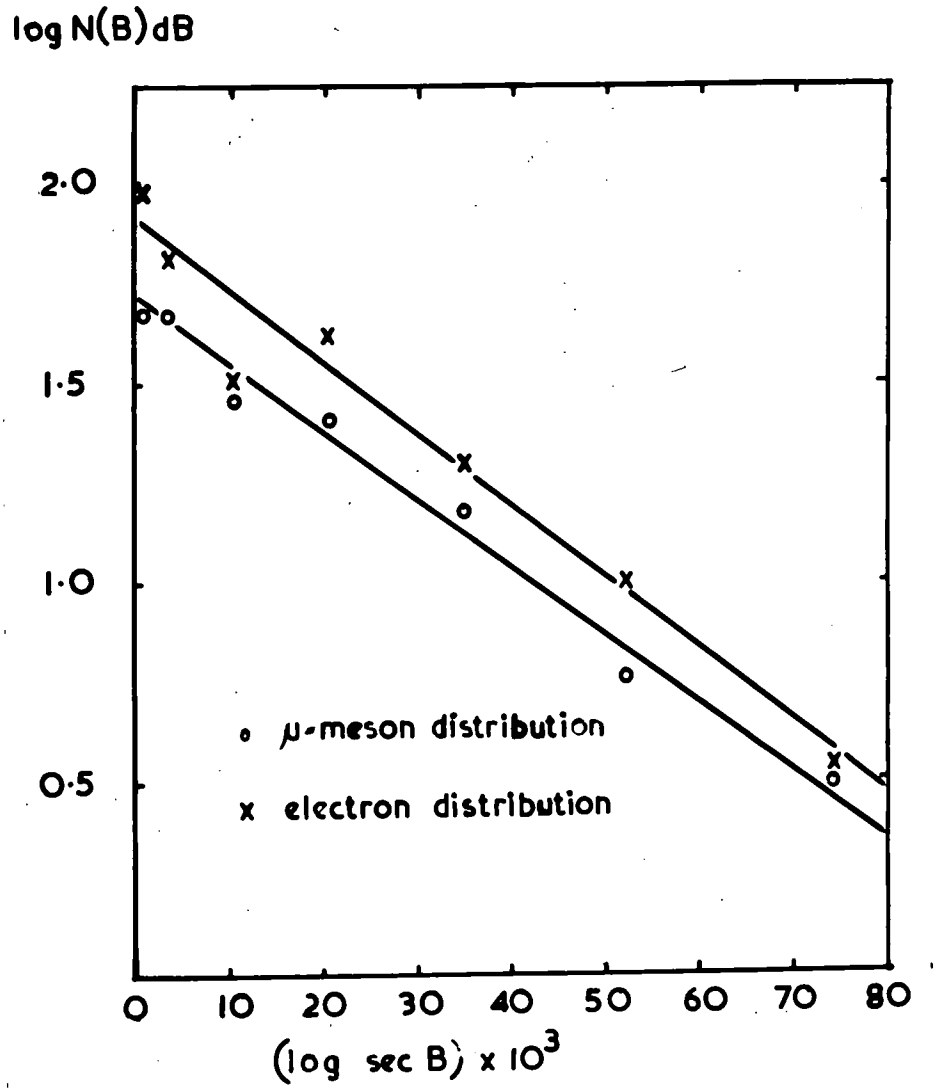

Figure 9.12. Logarithmic plot of frequencies of 'electron' and 'μ-meson' events against sec β to determine n. The full lines are least-squares fits to the points.

Expression (viii) may now be used to evaluate n if the factors γ, R and r are known. The exponent γ was determined experimentally (Chapter 10) as $\gamma = 1.61$, the factor R for a cubic detector was determined as R = 7.5 (appendix IV) and, for the case of the electron shower distribution, it may be assumed that r = 0.

9.7.1. The Electron Distribution.

Using the results from the electron distribution, and expression (viii)

$$q_e = n + 1.61 + 7.5 + 1$$

thus
$$n = q_e - 1.61 - 7.5 - 1$$
$$= 18.22 - 10.11$$
$$= 8.1.$$

The error in n depends only on the known uncertainties in q_e and in γ. Taking the experimental values ($q_e = 18.22 \pm 0.67$), and $\gamma = 1.61 \pm 0.04$, it is found that

$$n = 8.1 \pm 0.35$$

Thus the distribution in spatial angle of E.A.S. may be represented as

$$I(\theta)\, d\omega \propto \cos^{8.1 \pm 0.35}\theta \; d\omega.$$

9.7.2. The μ-meson Distribution.

The exponent n of the angular variation of E.A.S. may not be obtained directly from the μ-meson distribution since the assumption of $f(\theta) = 1$ (r = 0) is no longer valid. As the properties of the showers examined

depend only on the characteristics of the detecting array and as this was identical in both experiments, the angular variation of E.A.S. should be the same in both cases. Therefore, any significant difference between q_e and q_μ must be attributed to the factor $f(\theta)$.

In the present experiments the difference is not statistically significant but the trend is in the expected direction. From expression (viii).

$$r = q_\mu - n - R - 1 - \gamma$$

and assuming $n = 8$ then

$$r = 17.16 - 18.2$$
$$\simeq -1.0.$$

The negative exponent indicates that the μ-meson density is increasing with the zenith angle of the shower and this is in accord with the observations of previous workers. It has been reported (Earl 1958) from investigations of the lateral distributions of μ-mesons in E.A.S. that at distances between 15-200m. from the shower axis, the density of μ-mesons is greater in showers arriving at larger zenith angles. The topic, however, is too complex for other than qualitative conclusions to be drawn from the present experiment.

The results serve to indicate that the apparatus may be usefully applied to studies of the μ-meson component of E.A.S.

9.7.3. The Statistical Method.

To obtain the exponent of the angular dependence from the statistical method, the integral distribution in projected angle must be considered. This is obtained from expression (ix) as

$$N(>\beta) = \int_{\beta}^{\pi/2} N(\beta)d\beta = K_3 \int_{\beta}^{\pi/2} \cos^q \beta \, d\beta.$$

or in terms of the experimental projected angle

$$N(>\phi) = K_3 \int_{\phi}^{\pi/2} \cos^q \phi \, d\phi \qquad \text{.....(x)}$$

The distribution (x) was computed for various values of q and the best agreement with the experimental curve was obtained with q = 12. Therefore, from expression (viii)

$$q = n + \gamma + R + 1 + r$$

thus $$n = 12 - 1.6 - 1$$

$$= 9.4$$

since for the case of the top tray only

$$A_\theta \equiv A_o$$

i.e. R = 0, and r = 0 for all electron distributions. The higher value of n obtained from the statistical method is somewhat unexpected - the method should furnish a minimum value of n for the reasons previously discussed. However, the significance of this result will be considered in § 9.5.3. The uncertainty in this determination is not readily calculable because of the assumptions inherent in the method. However it was estimated that

the value of n lies within the range

$$n = 9.4 \pm 1.5$$

thus the angular variation may be expressed as

$$I(\theta)\, d\omega \propto \cos^{9.4 \pm 1.5}\theta \; d\omega .$$

9.8. Conclusions: The Attenuation Length of E.A.S.

The experimental determinations of n enable an evaluation of the attentuation length of E.A.S. using expression (iii).

$$\Lambda = \frac{x_o}{n}.$$

The value of the atmospheric thickness in the vertical direction was taken as

$$x_o = 1034 \text{ gm/cm}^2.$$

and the results obtained for Λ are as follows:

Method	Exponent of Angular variation	Attenuation Length Λ (gm/cm^2)
Direct measurement	8.1 ± 0.35	128 ± 6
Statistical method	9.4 ± 1.5	110 ± 18

The two values are not statistically inconsistent but the disparity is large enough to merit some consideration. The obvious difference between the two methods lies in the particle densities of the events examined. The particle density at any point depends on both the shower size and the distance to the shower axis. How-

ever, it is possible that the criteria of low densities necessary for directional measurements biassed the selection of events towards showers smaller than the average size examined in the statistical method. On this assumption the statistical method might be expected to give a larger value for the attenuation length: experimentally γ is found to increase with N whilst λ remains constant, therefore as

$$\Lambda = \frac{\lambda}{\gamma}$$

Λ should decrease as N increases. Unfortunately this issue is by no means decided and it is difficult to conclude from the published data whether Λ increases, decreases or remains constant in the range of shower size from $N = 10^4$ to 10^8. Further studies of this problem would be valuable.

Both results for Λ obtained in the present experiment are consistent with the recently reported values from other workers which range from

$\Lambda = 107$ gm/cm^2 (Rossi 1960)

$\Lambda = 160$ gm/cm^2 (Khristiansen 1960).

Comparisons, therefore, are not particularly helpful and it will be concluded simply that the experimental values fall within the expected range and the method is therefore sound.

It may be commented that the general significance of the larger value of Λ, as obtained for smaller showers, is that these showers originate at greater heights. However caution is necessary when drawing inferences from the average behaviour of showers and neglecting the effects of fluctuations. Also it should be stated that the generally observed experimental trend of Λ decreasing with increase in N is quite contrary to the behaviour expected from purely theoretical considerations.

CHAPTER 10.

A Measurement of the Particle Density Spectrum of E.A.S.

10.1 Introduction

The possibility of using the DASI apparatus to measure particle densities has already been mentioned. Experimentally the present trend in density measurements is towards the use of scintillators and Cerenkov counters but these, however, are essentially energy loss detectors and do not give a response uniquely dependent on the number of particles traversing them. An array of flash tubes on the other hand is sensitive only to particle number - in the same manner as the G.M. detector. A study was made, therefore, of the performance of DASI as a device for measuring particle densities.

10.2 The Density Spectrum of E.A.S.

The importance of the density spectrum of E.A.S. lies in its relation to the primary energy spectrum.

From measurements of the particle density over a sufficient number of showers, the frequency spectrum in density can be obtained. Experimentally it is found that

$$\nu(\Delta)\, d\Delta \propto \Delta^{-\gamma-1}\, d\Delta \qquad \ldots\ldots\ldots(i)$$

where $\nu(\Delta)d\Delta$ is the number of showers per unit time whose densities lie in the range Δ to $\Delta+\Delta d\Delta$ particles per unit area and γ is the exponent in the integral spectrum

$$\nu(>\Delta) \propto \Delta^{-\gamma}$$

If it is assumed that

1. the shape of the lateral structure function does not change with shower size and
2. the size spectrum can be represented by a power law with a smoothly varying exponent,

then it can be shown that the size spectrum of E.A.S. is given by

$$\eta(N)dN = A.N^{-\gamma-1}\, dN \qquad \ldots\ldots(ii)$$

where (N)dN is the number of showers per unit time whose axes cross $1m^2$ at the point of observation, and which contain a total number of particles between N and N+dN. The exponent γ is the same in both the density and the number spectrum.

If, now, it is assumed that the average number of particles at a given depth t in the atmosphere arriving from a primary of energy E_o is

$$N(t,E_o) = B\, E_o^{\delta} \qquad \ldots\ldots(iii)$$

where δ is a function of t depending on the cascade model chosen, then substituting for N in (ii)

$$\eta(N)dN = A(BE_o^{\delta})^{-\gamma-1}\, B.\ E_o^{\delta-1}\, dE_o$$

Thus $$\eta(E_o)dE_o = C\, E_o^{-\delta\gamma-1}\, \delta E_o \qquad \ldots\ldots(iv)$$

is the differential spectrum giving the number of primary particles in the energy interval E_o to $E_o + dE_o$.

Therefore the primary energy spectrum is also given by a power law with an exponent $-\delta_\gamma$

$$\eta(>E_o) \propto E_o^{-\delta\gamma} \qquad \ldots\ldots\ldots(v)$$

Thus if δ is a slowly varying function of E_o then a change in the density spectrum implies a change in the primary energy spectrum.

10.3 A Measurement of the Density Spectrum using DASI

The uppermost tray in DASI consists of four separate layers of flash tubes, two containing 55 tubes, two containing 56 tubes. By observing the number of tubes flashed in each layer, four independent estimates of the particle density can be obtained for each event. A total of 1440 showers was examined, data from the upper four layers being extracted in each case. To relate the observed number of flashes to the density of the incident particles in each event, and thus obtain the incident spectrum, two methods are available.

10.3.1. The Observed Density Spectrum - Method I (Approximate)

It may be taken that the distribution of particles in a shower which is past the maximum stage of its development, is adequately described by the Poisson distribution. Therefore, if Δ is the mean density of particles incident over the apparatus, the chance of k tubes being flashed from a total of 1 tubes follows the law:

$$P_k = {}^{k}C_1 \left[1 - \exp(-S\Delta)\right]^{k} \left[\exp - (-S\Delta)\right]^{1-k} \quad \ldots(vi)$$

where S is the sensitive area of one tube.

Assuming that the density is sensibly constant over the apparatus, expression (vi) can be maximised to give the most probable density Δ_k resulting in any number of tubes, k, being flashed. This is found to be

$$\Delta_k = \frac{1}{S} \ln \frac{1}{(1-k)} \quad \ldots\ldots\ldots(vii)$$

The sensitive area of a tube (S) depends upon the length of the electrodes (L), the internal diameter (d) and the internal efficiency (η) of the tube. For the top layer of DASI the measured values were

$$L = 101 \text{ cm}$$

$$d = 1.6 \text{ cm}$$

$$\eta = 88\%$$

thus $S = 1.42 \times 10^{-2} m^2$

Using this value of S, Δ_k was plotted as a function of k and is shown in Fig. 10.1. The particle density corresponding to a particular number of tubes having flashed may thus be read off directly. In deriving the density spectrum, account must be taken of the change in cell width of density with k. i.e.

$$\nu(\Delta) = N(k) \frac{dk}{d\Delta}$$

and the expression $\frac{dk}{d\Delta}$ is shown in Fig. 10.2 plotted as a function of Δ.

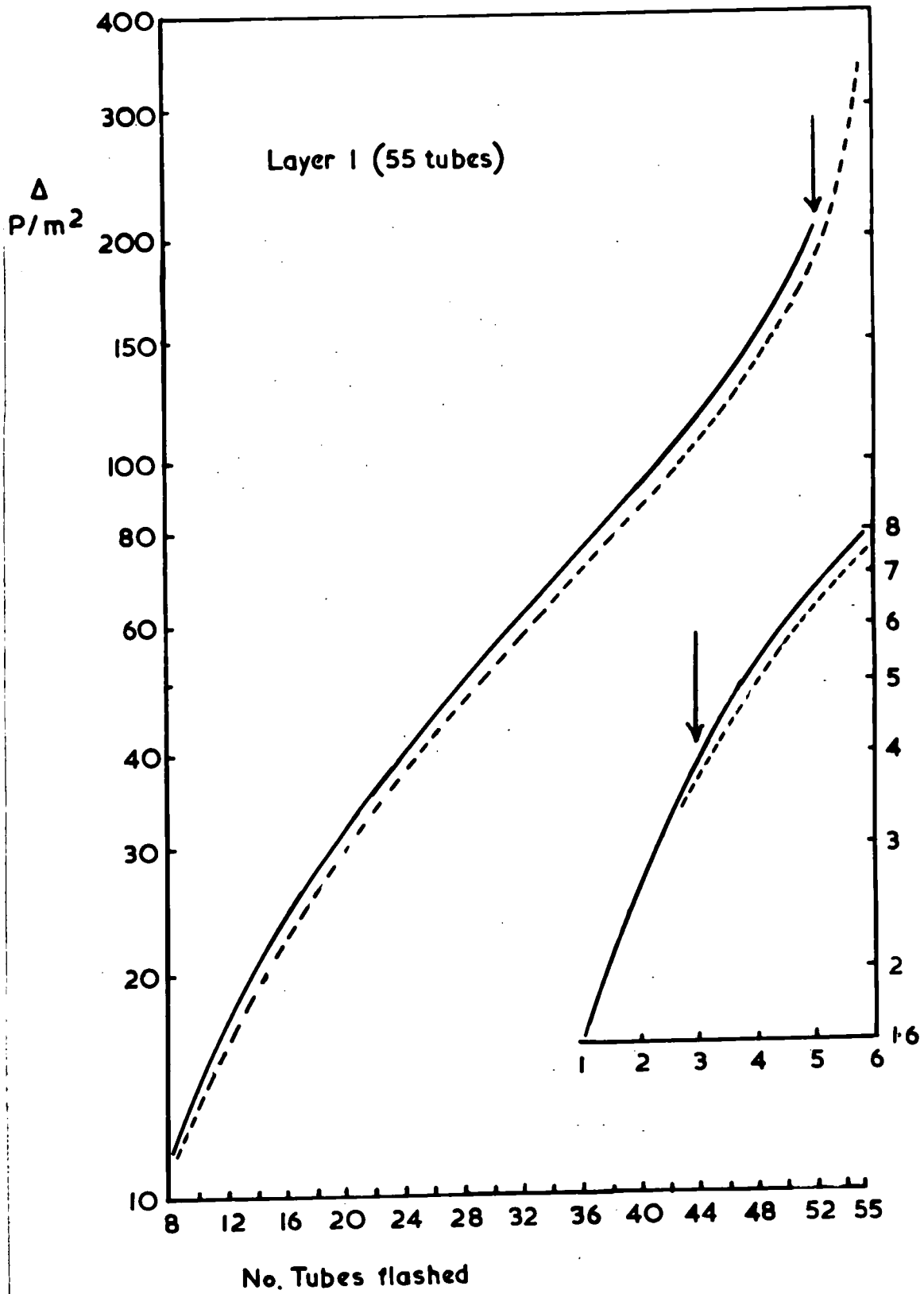

Figure 10.1. The theoretical relation between the incident particle density, Δ, and the number of tubes, k, having flashed.

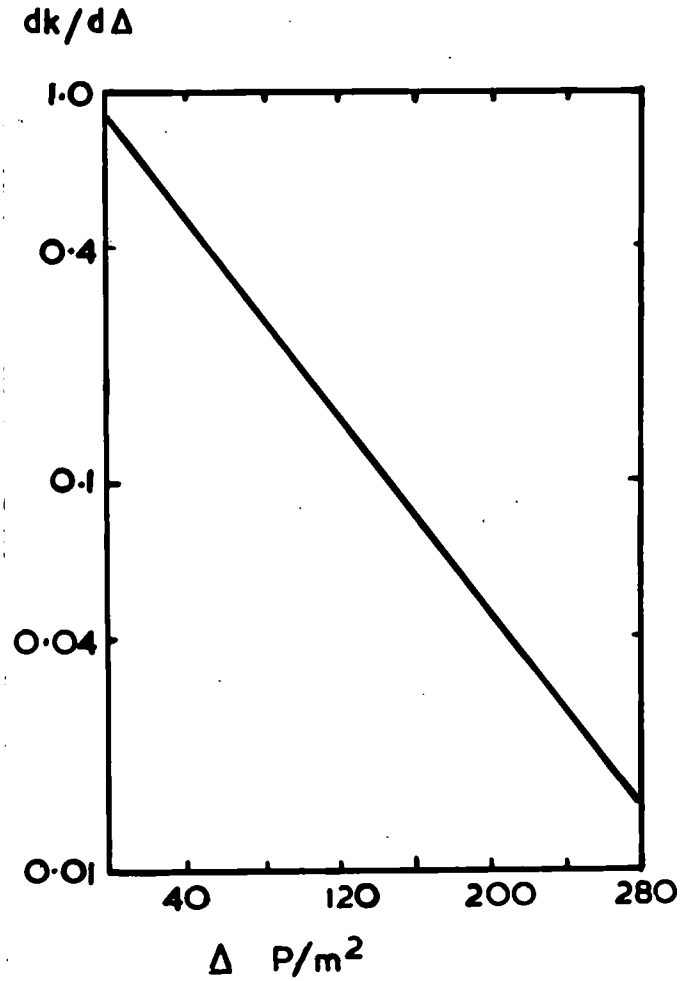

Figure 10.2. The factor $\frac{d\Delta}{dk}$ as a function of particle density.

The method is approximate, for reasons which will be mentioned, but it provides a rapid and reasonably accurate approach to the spectrum at densities limited by the conditions $1-k \rangle 3$ and $k \rangle 3$. The spectrum obtained by this method is shown in Fig. 10.3. At densities $\rangle 10$ p/m^2 the experimental spectrum can be represented by $N(\Delta)d\Delta \propto (1-e^{-S\Delta})^3 \Delta^{-2.6} d\Delta$

10.3.2. The Observed Density Spectrum Method II.

The shape of the incident spectrum has a modifying effect on the relation obtaining between the number of tubes having flashed and the most probable incident density. This effect was ignored in method I, but to obtain an accurate assessment of the spectrum, particularly at the extremes of the densities measured, the effect must be taken into account.

One approach is to assume an approximate form for the incident spectrum (the spectrum obtained by Method I may be used if necessary) and compute the distribution in numbers of tubes having flashed which would be expected from this spectrum. This may then be compared with the observed distribution and the procedure repeated, successively modifying the assumed spectrum until complete agreement between expected and observed distributions is achieved. The final form of the assumed spectrum is then

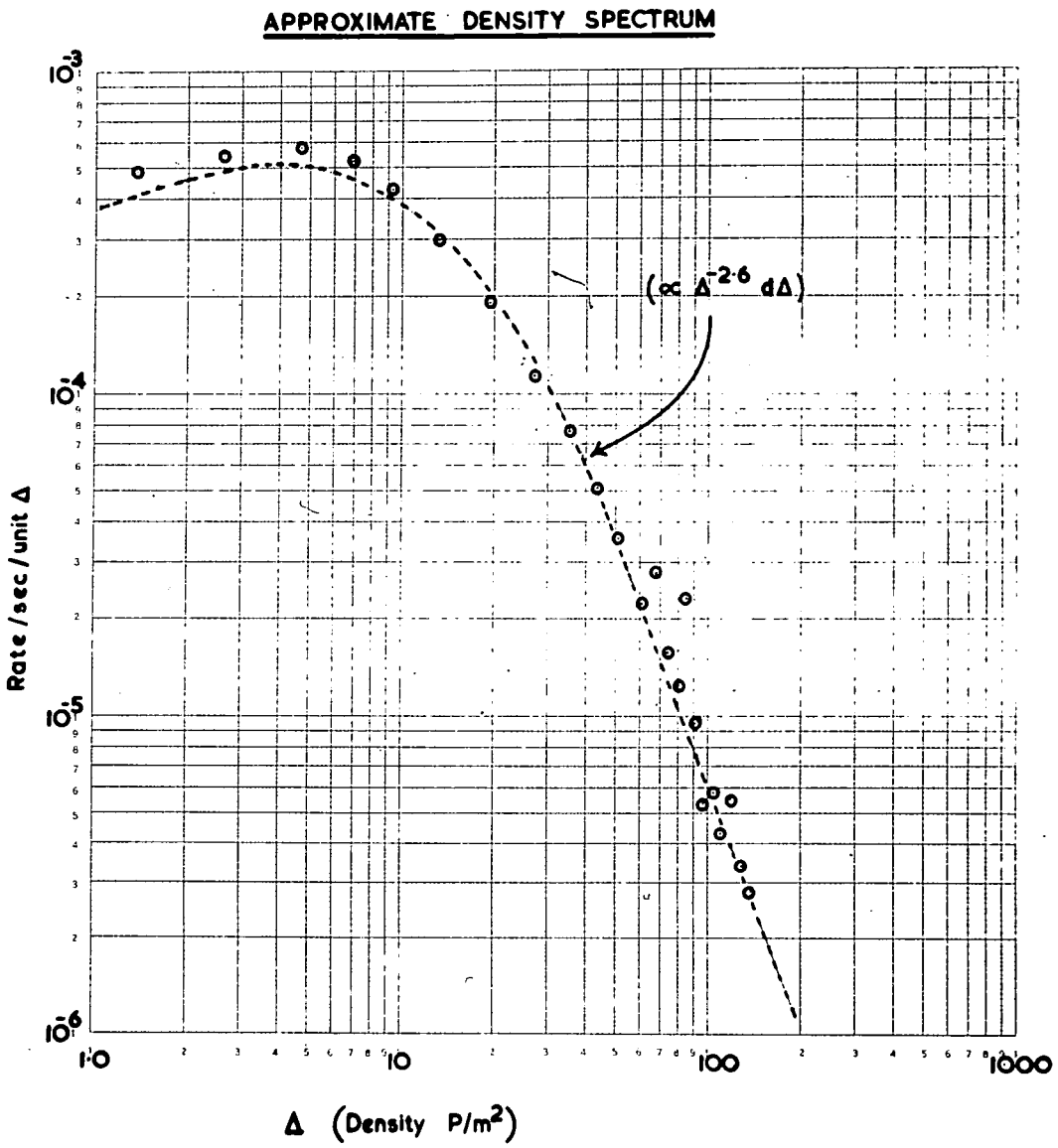
APPROXIMATE DENSITY SPECTRUM
(∝ Δ^-2·6 dΔ)
Rate /sec / unit Δ
Δ (Density P/m²)
10^-3
10^-4
10^-5
10^-6
1·0
10
100
1000

Figure 10·3

that of the true incident spectrum. This approach was adopted.

The chance (P_k) of a combination of k tubes being flashed by an incident shower of mean particle density Δ over the apparatus, is given as a function of Δ by expression (vi):-

$$P_k = {}^kC_1 \left[1 - \exp - (S\Delta)\right]^k \left[\exp(-S\Delta)\right]^{1-k}$$

Curves showing the variation of P_k with density are given in Fig. 10.4. These were computed for various values of k, in particular the extreme values k = 1, 2, 3, and k = 53, 54, 55. It may be noted that the probability of any number of tubes, k, being flashed, peaks at that value of density given by expression (vii).

When the incident spectrum is considered, the probability of observing any combination of tubes, k, being flashed by an incident shower of mean density Δ to $\Delta + d\Delta$ is given by

$$R_k d\Delta = {}^kC_1 \left[1 - \exp(-S\Delta)\right]^k \left[\exp(-S\Delta)\right]^{1-k} \nu(\Delta)\, d\Delta$$

i.e. $$R_k d\Delta = G\, {}^kC_1 \left[1 - \exp(-S\Delta)\right]^k \left[\exp(-S\Delta)\right]^{1-k} \Delta^{-\gamma-1}\, d\Delta$$

if $$\nu(\Delta)d\Delta = G.\, \Delta^{-\gamma-1}\, d\Delta$$

is the form of the assumed incident spectrum. The curves for R_k are obtained simply by multiplying those of P_k by the assumed incident spectrum ($\nu(\Delta)d\Delta = 0.28\, \Delta^{-2.4}\, d\Delta$) which is shown superimposed in Fig. 10.4. Two effects are observed:

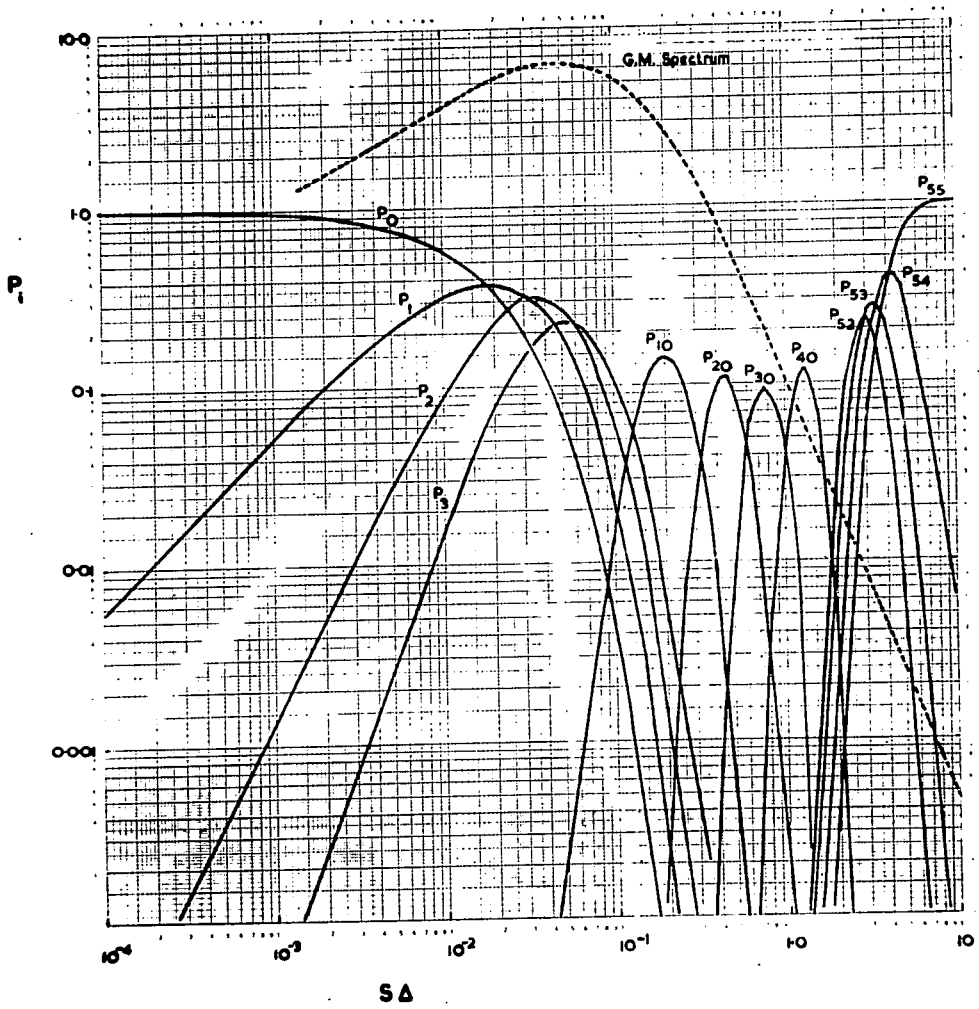
G.M. Spectrum
P_0
P_1
P_2
P_3
P_{10}
P_{20}
P_{30}
P_{40}
P_{52}
P_{53}
P_{54}
P_{55}
P_i
1·0
0·1
0·01
0·001
10^{-4}
10^{-3}
10^{-2}
10^{-1}
1·0
10
S Δ

Figure 10·4

a) the modified probability of flashing curves (R_k) peak at new values of density - shown in Fig. 10.1 by the dotted curve.

b) the areas under the curves are changed.

The second effect is the more important since the area under the R_k curve gives directly the relative contribution, N_k, expected from any combination of tubes.

i.e. $$N_k = \int_{\Delta\ min}^{\infty} R_k \, d\Delta$$

The relative contributions, N_k, are obtained by evaluating the areas under the R_k curves and the expected frequency distribution in numbers of tubes having flashed is then obtained by normalising to the total number of events. The expected and observed frequency distributions may then be compared - as shown in Fig. 10.5. To evaluate the incident spectrum, the frequency on the assumed spectrum at each value of density must be multiplied by the ratio of observed to expected frequencies, at that density, on the comparison distributions of Fig. 10.5. The spectrum so obtained is shown by the experimental points in Fig. 10.6.

The points plotted correspond to the mean frequencies obtained for groups of tubes (1, 2 or 3) chosen so as to retain as far as possible a constant cell width of density over the range of the spectrum. The errors

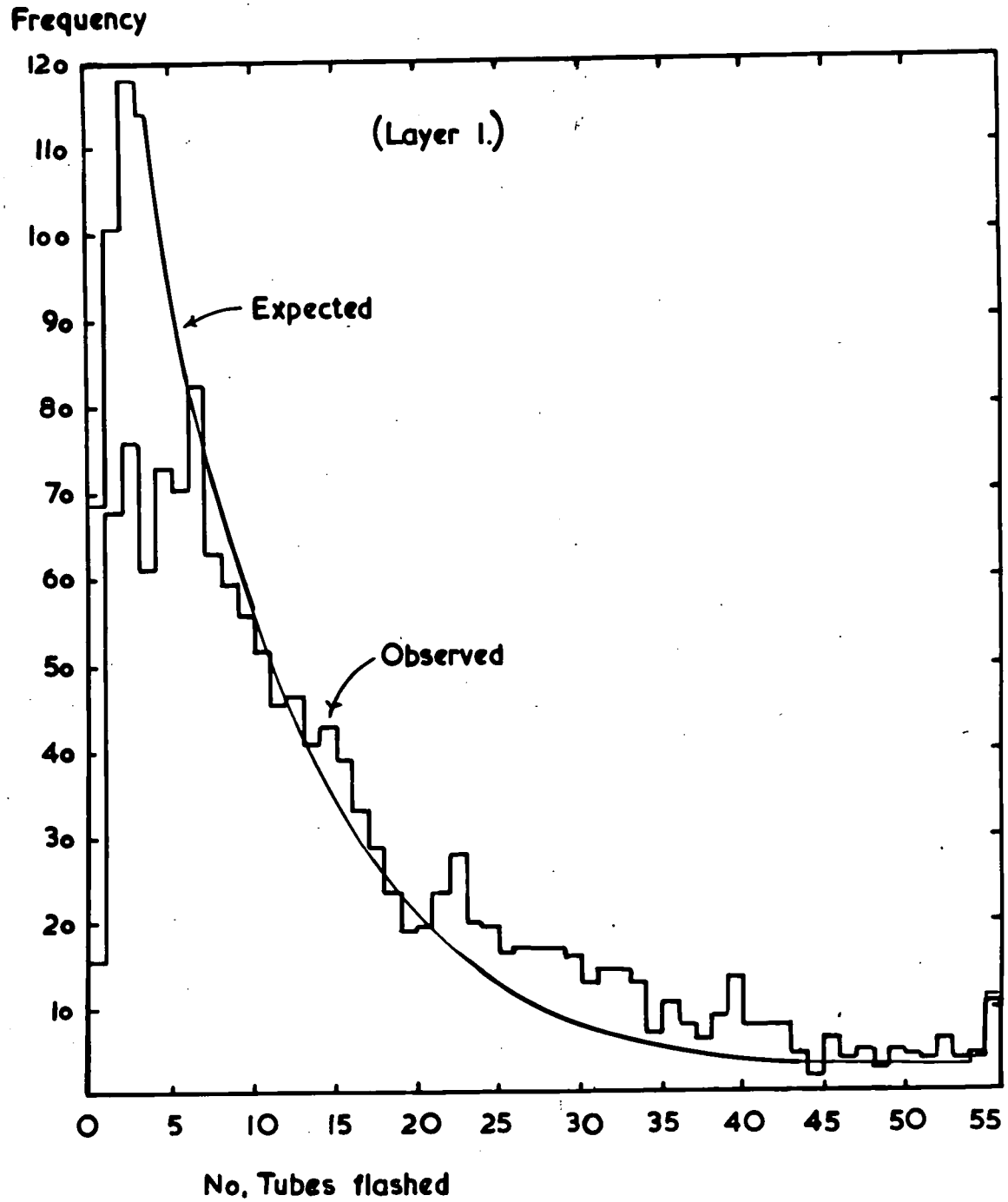

Figure 10.5. The expected and observed distribution in the frequencies of the number of tubes having flashed.

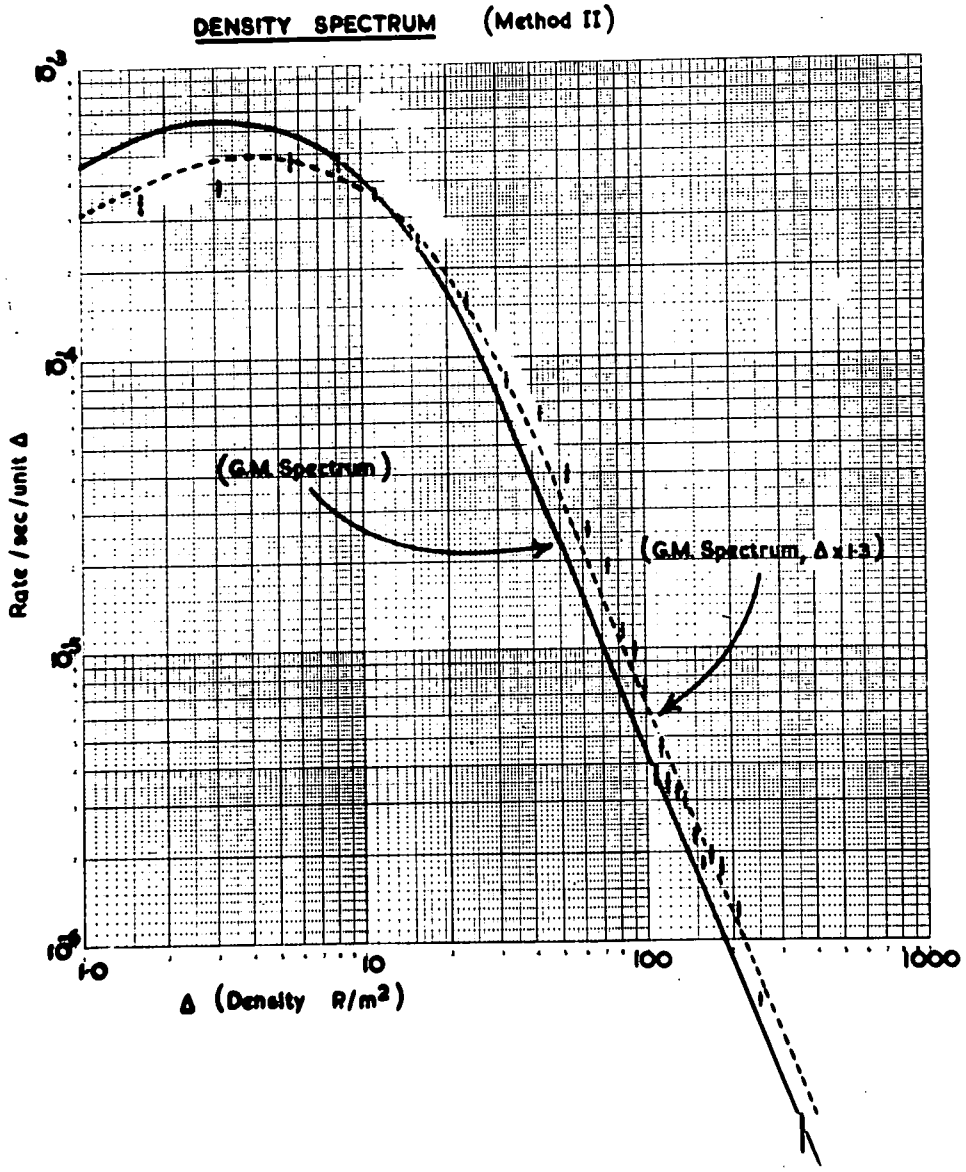
DENSITY SPECTRUM (Method II)
Rate / sec / unit Δ
(G.M. Spectrum)
(G.M. Spectrum, Δ x 1·3)
1·0
10
100
1000
Δ (Density R/m²)

Figure 10·6

on the points were evaluated assuming Poisson r.m.s. uncertainties in both the observed frequencies and the estimates of density.

The incident spectrum assumed in Figs. 10.4 and 10.6 was that calculated for the G.M. detecting array (§ 9.2) and agreement with the observed spectrum is not good. This might be expected because of the density gradient which normally exists across the detecting array. The density over DASI is therefore greater than the value calculated - which is in effect the minimum density required to trigger that detecting tray furthest from the shower core. Accordingly, a simple expedient in this case is to displace the assumed spectrum to a higher density. A change in density by a factor of 1.3 gives the dotted curve of fig. 10.6 which is in much better agreement with the experimental points. Extended computations to establish the exact incident spectrum were considered unnecessary for the present experiment.

10.4. The Exponent γ.

The most important aspect of the observed density spectrum is its slope at high densities where the 'experimental bias' of the detecting array is absent: this is simply related to the exponent γ of the E.A.S. density and number spectra. For the detecting array employed the experimental bias begins to modify the incident E.A.S. spectrum at densities <35 p/m^2. Accordingly a least squares fit was made to find the slope of the experimental points at densities >40 p/m^2. The points were suitably weighted to take account of both the statistical accuracy of the observed frequencies and the cell width of the estimated density. (The latter factor is proportional to the value of $\frac{dk}{d\Delta}$ given by Fig. 10.2). The slope of the points was determined as 2.61 ± 0.024 indicating a value of $\gamma = 1.61 \pm 0.024$.

A point of some interest is the trend towards an increase in slope at the highest densities. Unfortunately the limits of accuracy in the present experiment are not high enough to permit a quantitative estimate of this effect but it is apparent that a more prolonged

investigation might furnish data of value with regard to the variation of γ with density.

10.5. Discussion.

The density spectrum observed using DASI is in reasonable agreement with that expected from the known characteristics of the detecting array employed. The value of γ, however, is somewhat greater than the assumed value of 1.4 and possible sources of error will be discussed before the result is compared with recent values of other workers.

10.5.1. Sources of Error.

i) Systematic Error.

The only parameter which could introduce a systematic error is S, the effective area of a tube, which is dependent on the efficiency exhibited by the tube. However, for a uniform change in S over a layer of tubes it is easily seen that as

$$\frac{d\Delta}{\Delta} = -\frac{ds}{S}$$

the fractional change in S results in a constant fractional change in Δ and therefore has no effect on the slope of the spectrum. A non-uniform change, such as would be introduced by a single "bad" tube, would lead to error but this effect was eliminated by careful inspection of the tubes.

ii) Observational Error.

Observational error such as underestimating the numbers of tubes flashed at large densities, could produce a change in slope in the required direction. An underestimate by a single tube in the number of tubes flashed at the maximum density of 330 p/m^2 would lead to an error of 50 p/m^2 in the estimate of density. However in the determination of the slope the weighting strongly favours the lower densities and observational error in this region is most unlikely

iii) "Spurious" Effects.

The possible effect of spurious flashes is small because of their low rate of occurrence and their inclusion would have a marked effect only at low densities which are well removed from the region in which the slope is determined. Their influence on the shape of the spectrum at very low densities was considered and was found to be negligible.

iv) Zenith Angle Effect.

A point which must be considered is the angle of arrival of the shower particles. A simple calculation shows that a particle arriving at an angle $>28^{\circ}$ to the vertical has a high probability of flashing two tubes in the same layer and thus causing an overestimate of the

incident particle density. Fortunately, due to the rapid fall off of the intensity of E.A.S. with increasing zenith angle, the contribution from this effect is small (<1%) and may be neglected in the present experiment.

v) Density Gradient.

In the application of expression (vi) to the determination of incident particle densities it must be assumed that the density is constant over the area of the measuring apparatus. In practice there will normally exist a density gradient over the array - as has already been surmised. However, in the region of densities contributing to the measured value of γ it is considered that the cores of showers are sufficiently far removed from DASI for the density variation over the apparatus to be quite small and the gradient constant. Under these conditions the experimental estimate of density may be taken as a close approximation to the true mean density and no significant effect on γ is expected.

10.5.2. Measurements of γ by Other Workers.

From the wide range of reported values for γ it is apparent that the characteristics of this exponent are quite as complex as most parameters of E.A.S. However, certain general features are evident:-

a) The measured values of γ increase with increase in both particle density and shower size. Recent results reported by Krasilnikov et al (1960) and Kameda et al (1960) imply that the value of γ may change abruptly at shower sizes of $N = 3$ to 5×10^5.

b) The value of γ obtained in any experiment depends markedly on the dimensions of the detecting array. Experiments involving well separated counter arrays furnish values of γ in the range 1.8 to 2.0 whilst more compact arrays provide values ranging from $\gamma = 1.4$ to 1.7. This feature was presumed due to the preferential selection of showers having different structure characteristics, (and therefore different "ages") but recent investigations by Greisen (1960) cast strong doubts on this explanation and the problem must still be regarded as open.

c) If the reported values are taken seriously there would appear to be a third variation of γ - namely with time!

The most recent experiment which bears direct comparison with the present work, from the point of view of shower sizes and type of array, is that of Kukikov and

Khristiansen (1960) who report a value of

$$\gamma = 1.5 \pm 0.1$$

which is in reasonable agreement with the present result

$$(\gamma = 1.61 \pm 0.04).$$

Chudakov et al (1960), from investigations of the Cerenkov light from E.A.S. of similar size, report a value of $\gamma = 1.67 \pm 0.15$ - again in agreement with the present result, and a further value of $\gamma = 1.62 \pm 0.04$, reported by Greisen et al (1960), compares favourably since this result was obtained for showers, of somewhat larger mean size ($N = 10^6 \sim 10^7$) than those of the present experiment.

10.6. Conclusions.

It may be concluded that the exponent $\bar{\gamma}$ as obtained from the present experiment is in agreement with currently reported values from other workers and offers definite support for the value of γ lying in the lower range of 1.4 to 1.7 for showers of size $N \sim 10^{15}$.

10.6.1. The Particle Number Attenuation Length of E.A.S.

Accepting the value of $\bar{\gamma} = 1.61$ it is now possible to evaluate the attenuation length, λ, for the number of particles in E.A.S. As derived in Chapter 6

$$\lambda = \gamma\Lambda$$

where Λ is the shower (rate) attenuation length. Inserting the values of Λ obtained from the measurements

of the zenith angle dependence

$$\lambda = 1.61 \times 128$$
$$= 206 \text{ gm/cm}^2$$

and $$\lambda = 1.61 \times 110$$
$$= 177 \text{ gm/cm}^2$$

Allowing for the known uncertainties in Λ and γ the values of λ may be stated as

$$\lambda = 206 \pm 12$$

and $$\lambda = 177 \pm 29$$

thus both values are consistent. It is also apparent, from comparison with the most recently reported values, as listed in table VIII, that both figures are realistic. The large spread in reported values is again most obvious but it may be concluded that the present results are in good agreement with the values reported by Rossi, Cranshaw and Oda.

The significance of λ becomes complicated if the presence of large fluctuations in shower development is admitted. It has been pointed out by Miyake (1958) and also by Cranshaw (1960) and Zatcepin (1960) that λ can not always be understood simply as the particle attenuation length of E.A.S. and in fact the observed value of λ bears little relation to the altitude variation curve. (Fig. 6.2). However, λ is fundamentally related to the interaction characteristics of the high energy nucleon

TABLE VIII

	MIT (Rossi)	HARWELL (Cranshaw)	MOSCOW (Khristiansen)	TOKYO (Oda)	CORNELL (Greisen)
N	$10^2 - 10^8$	$10^4 - 10^8$	$10^4 - 10^8$	$10^4 - 10^8$	$10^4 - 10^8$
γ	1.5 - 1.9	1.6 - 1.9	1.6	1.8	1.6
λ	110	125 100	160	113	140
λ	175	200 190	260	200	220

cascade in the shower core and the observed values permit some testing of the theories advanced for the cascade development of E.A.S. The present value of $\lambda = 206$ gm/cm^2 is in particularly good agreement with the predictions of Olbert, Model B (1960) and thereby offers some support for this theory. The immediate implications are an inelasticity of 0.5 and an interaction length for the nucleon cascade of 70 gm/cm^2. Comparisons with other models such as that of Miyake are less conclusive.

10.6.2. The Exponent of the Primary Spectrum.

Finally, the experimental determination of γ permits an evaluation of Γ, the exponent of the primary cosmic ray spectrum. As shown in § 10.2, if the integral primary spectrum is given by

$$n(>E_o) \propto E_o^{-\Gamma}$$

then $$\Gamma = \delta\gamma$$

where γ is the exponent of the number spectrum and δ is the factor $\frac{\partial \ln N}{\partial \ln E_o}$

Thus, knowing γ, the evaluation of Γ is reduced simply to the selection of an appropriate value of δ.

δ is a complex function based on the track length integral :-

$$\int_o^\infty N(E)\, dt$$

and involves calculations on a) the multiplicity of production of π_o mesons, b) the competitive processes of energy injection from the nucleon cascade and energy loss by the creation of μ-mesons, neutrinos and low energy nucleons and also c) a calculation of the height of the shower maximum. An estimate given by Greisen (1956) for primaries of energy 10^{15}eV is

$$\delta = 1.21 \pm 0.06$$

Later calculations by Olbert furnish values of δ varying with the particular nuclear interaction theory employed:-

Date	Theory	δ
1957	Fermi	1.1
1957	Landau	1.16
1959	Olbert	1.14

Using the figure due to Greisen the primary exponent is obtained as

$$\Gamma = 1.95 \pm 0.107 \qquad \ldots.(a)$$

and using the latest value of Olbert

$$\Gamma = 1.83 \pm 0.045 \qquad \ldots.(b)$$

Both values are statistically consistent but the value (b) is probably more significant due to the use of the more recent calculations of δ.

For comparison purposes, the corresponding value of the exponent in the primary C.R. spectrum reported by Bossi (1960) is $\Gamma = 2.0 \pm 0.1$ $(E_o \sim 10^{15}\text{eV})$

which is significantly higher than the present result (b), In view of the uncertainty inherent in estimating the shower sizes detected by the present array and the obvious limitations involved in the use of the available values of δ, it is doubtful if any significance can be attached to the discrepancy. However it is interesting to note that the present result, $\Gamma = 1.83$, is in good agreement with the value ($\Gamma = 1.85$) reported by Barret et al (1953) which was obtained from underground measurements (at 1574 m.w.e.) of the μ-meson flux.

CHAPTER 11.

Discussion Future Work.

11.1. Conclusions.

The general implications of the results obtained with DASI in the present experiments have already been stated. Conclusions of particular significance were scarcely expected from the present array and none such are claimed. However, the important fact emerges that a flash tube array of the DASI type is capable of a reliable and efficient performance in investigations of the angular and density distributions of E.A.S. A critical appraisal of the present performance suggests certain modifications which will be discussed before considering future applications of the apparatus.

11.1.1. The Measurement of Angular Distributions.

The accuracy of angular resolution ($\sim 1^{o}$) which has been demonstrated is adequate for most requirements. If necessary this could be increased to the maximum of 0.4^{o} by applying a more elaborate system of analysis.

A real difficulty was encountered in providing adequate screening of the apparatus from the electron component to enable examination of the angular distribution of μ-mesons alone. Complete screening by a suffi-

cient thickness of lead (at least 25 cm) is prohibitively expensive, besides being structually difficult, and it must be concluded that successful experiments would best be made underground. However, useful experiments could be made at ground level by locating the apparatus at the periphery of the detecting array where, at reasonably large distances from the shower core, the ratio $\frac{N_\mu}{N_e}$ approaches, and perhaps even exceeds, unity. At these distances, of course, the density of particles is low and the probability of obtaining an event correspondingly small. A compromise enabling the unit to be used nearer the core is to incorporate a thin layer (~1 radiation length) of lead above the lowest tray in the apparatus and to reject electron events on the basis of multiplication produced in this layer. (This approach is to be attempted). Further modifications which are required for particular experiments will be described later.

11.1.2. The Measurement of Particle Densities.

It has been shown that particle densities of up to 300 p/m^2 can be measured with reasonable accuracy and that densities below 40 p/m^2 can be measured with precision. The examination of events would be made easier if the visibility of tubes at the corners of the array were improved and experiments directed at modifying the

predominantly forward polar emission of the light output from the tubes have been successfully carried out. Modified tubes will be used in future experiments.

Detailed investigation of the lateral density distribution of the μ-meson component of E.A.S. is of prime importance. On this account it may be noted that if the separate layers of flash-tubes in the DASI array were assembled horizontally, an area of 16 m^2 could be efficiently covered - at a cost well below that which would be involved using other available detectors. The photographic recording of events can be simplified by the use of suitable mirror systems. Alternatively, 'electrical' analysis by means of a photomultiplier is feasible but more expensive.

11.2. Future Applications.

The ultimate aims of the DASI type of array were mentioned in Chapter 7. These can now be considered in more detail.

11.2.1. The Heights of Production of Mesons.

This topic has assumed particular importance since the results of de Beer (thesis, 1960) have become known. Two explanations have been forwarded to account for the unexpectedly large number of mesons found to originate at small atmospheric depths (<100 gm/cm^2):-

i) A considerable proportion of showers is initiated by α-primaries.

or ii) There exists a new and very efficient process for producing μ-mesons.

In the range of shower sizes investigated by de Beer ($N \sim 6 \times 10^6$ to 10^8p) a predominance of heavy primaries would not be wholly unexpected. Some revision, however, of the shape of the primary spectrum might be entailed. The existance, on the other hand, of a new and fundamental process of μ-meson production would be highly significant. (Such a process has already been postulated by Khristiansen (1960) to explain results obtained in studies of the core regions of E.A.S. at sea level. It is obvious that further investigations of this topic are required and that these could be particularly rewarding.

For such investigations at least two DASI units are required and these would be operated in conjunction with an extensive array of scintillator or Cerenkov detectors. The latter would furnish details of shower size and core position in addition to providing the 'trigger' pulse.

Assuming that the measured direction of a μ-meson is the same as that with which the parent π-meson left

the shower axis, then if mesons are detected simultaneously at both units the following analysis may be applied. Let the DASI units, A and B, be located at the points (-1,0,0) and (1,0,0) in a rectangular cartesian system and the shower core, c, have the coordinates $(\bar{x}, \bar{y}, o)$. If the mesons at A and B have direction cosines (l,m,n) and (l',m',n',) then the respective heights of origin as measured along the tracks are obtained as

$$h = \frac{2\,\bar{n}'\bar{y}}{\bar{y}(n'l - nl') - (mn' - m'n)(\bar{x} - 1)}$$

and

$$h' = \frac{2\,n'\bar{y}}{\bar{y}(n'l - nl') - (mn' - m'n)(\bar{x}+1)}$$

The above expressions follow from the colinearity of h, h' and e. Unfortunately, if the core falls on the line AB the method gives no solution and only the mean height of origin can be obtained. This is a particular disadvantage since the probability of detecting mesons simultaneously in the two detectors is greatest for showers falling on the line joining the two, and for showers falling near either detector. The situation could be improved to some extent by providing a third DASI unit.

The accuracy in the determination of h.

The uncertainty involved in the determination of h is difficult to assess analytically. Fortunately an estimate is provided by the results of de Beer (loc cit) who, in a similar experiment, used two spark counter units at a separation of 500m. With an uncertainty of 20m in core location and an estimated uncertainty of 0.5^{o} in the measured angles of the μ-mesons it was found that the heights of production could be determined to an accuracy of 50 gm/cm^2 in the lower 800 gm/cm^2 of the atmosphere and to 150 gm/cm^2 at heights above this level.

The uncertainty in h increases rapidly as the position of the core approaches the line AB. In the experiment of de Beer, events, in which the core fell nearer than 100m to the line joining the two units were arbitrarily rejected and it was presumed that this imposed no bias on selection since the distance of the mesons from the shower core was found to bear no relation to their heights of origin. However the validity of this assumption is scarcely justified by the statistics of the experiment and it would be preferable to attempt some independence from this criterion by using three (or possibly more) detecting units. One criterion which must be applied concerns the energy of the μ-mesons.

The energy of the μ-mesons.

The condition that the μ-meson should preserve the direction of the original π-meson will not be fulfilled by low energy μ-mesons because of multiple scattering effects in the atmosphere (and a slight amount of magnetic deflection, which may be neglected). Inspection of Fig. 8.1 shows that for directional measurements to an accuracy of 1^{o}, the energy of the μ-mesons should be greater than 3.5 BeV. This figure however relates to the mean energy of the meson in its traversal of the atmosphere and the energy of the μ-meson at the detecting level will be in fact $\sim$2.5 BeV.

The modification of the DASI unit to provide means of discriminating against μ-mesons of energy $<$2.5 GeV poses certain problems. An obvious approach is to introduce scattering material between the layers of flash tubes and to estimate particle energies by measurement of the multiple scattering effects so induced. Following the established nuclear emulsion technique the particle tracks would be divided into cell widths, corresponding to the separation of the layers of tubes, and the change in direction of the track after passage through each cell would be observed. If the change in direction is θ_i, then θ_c, the mean value of the modulus of θ_i, is given by

$$\bar{\theta}_c = \sum_n \frac{|\theta_i|}{n} \pm 0.75 \frac{\bar{\theta}_c}{n}$$

where n is the number of cells. The corresponding momentum of the particle is given as

$$\rho\beta = \frac{K \sqrt{c}}{\theta_c}$$

where K is the scattering constant appropriate to the material and includes the usual corrections for the effect of using chords instead of tangents, projected instead of spatial angles etc. The point of importance is the maximum detectable momentum which is governed by the maximum resolution, $\bar{\alpha}$, which can be achieved in θ_i. In the case of a single layer flash tube system this will be taken as

$$\alpha \simeq 0.7 \frac{d}{c}$$

where d is the internal diameter of a tube and c is the cell width. Thus for d = 1.5cm and c=10cm.

$$\bar{\alpha} = \frac{0.7 \times 1.5 \times 57.3}{10} = 5.8^\circ$$

Assuming the scattering material is lead, it may be taken that

K = 820 degrees. MeV. $cm^{-\frac{1}{2}}$ (Private communication, J.V. Major 1960).

thus $$\rho\beta_{max} = \frac{820\sqrt{10}}{5.8} = 450 \text{ MeV/c}$$

It is apparent, therefore, that no distinction in energy can be made for μ-mesons of energy >0.45 GeV and the method may not be applied to the DASI unit in its present form. However, following a similar agrument it can be shown that the method may be successfully applied if a linear resolution of 1.8mm can be attained in each layer. If neccessary this could be achieved by replacing each layer of the present flash tubes by a double layer of 0.6cm diameter high pressure tubes (Method I).

It must be concluded, therefore, that for experiments in which energy discrimination of this order is demanded, the present DASI unit would require extensive modification, namely the inclusion of some 3000 high pressure tubes and at least 5 intermediate layers of lead - each ~10cm thick. The project is still quite feasible but construction would be much more involved than in the case of the present unit.

A compromise solution (Method II) is offered using the present DASI unit. A resolution of $\sim 1^{o}$ can still be achieved using only the three upper or three lower layers of flash tubes in DASI and the method would be to insert a single scattering layer in the central position between layers 3 and 4. The aim of this would be to "scatter out" an appreciable fraction of the low energy μ-mesons. The thickness of lead required to provide an

r.m.s. angle of scatter of 1^{o} can be obtained from the precise expression

$$\langle\phi\rangle^{2} = \frac{K^{2}}{p^{2}\beta^{2}}\, d$$

where $\langle\phi\rangle$ is the r.m.s.projected angle of scatter, d is the thickness of the scattering layer, $p\beta$ is the momentum of the particle and K is the scattering constant.

thus $$d = \frac{\langle\phi\rangle^{2} p^{2}\beta^{2}}{K^{2}}$$

and substituting the values

$$\langle\phi\rangle = 1^{o}$$

$$p\beta = 2.5 \times 10^{3} \text{ MeV/c}$$

$$K = 820^{o} \text{ MeV cm}^{-\frac{1}{2}}$$

thus $$d = \frac{6.25 \times 10^{6}}{(820)^{2}} = 9.3 \text{ cm.}$$

Therefore if a central layer ~10 cm lead were introduced into the unit, some 33% of the μ-mesons at < 2.5 GeV would be scattered through angles $>1^{o}$ (and so rejected) and using data from both projected views this fraction could be increased to ~55%. Extending the argument to cover the entire range of μ-meson energies it is estimated that using this method the total number of μ-mesons observed would include less than 20% of those having energies < 2.5 GeV.

With a larger scattering thickness this figure could be improved (to ~10%) and in experiments using a number of units it is possible that the 'spurious rate' could be further reduced by geometrical considerations. In this case the final figure for spurious events might be quite tolerable.

It may be concluded, therefore, that two or more DASI units, modified according to methods I or II, would be suitable for operation in conjunction with an extensive detecting array to provide data on the heights of production of μ-mesons. An estimate of the relative rate at which useful events would be obtained can be derived from the data of de Beer. Using spark counters of area 0.7 m^2 at a separation of 500 m, mesons were observed simultaneously at both units in 3% of the total number of showers detected. Assuming similar characteristics for the detecting array, the rate of observation for two DASI units (each of area 1 m^2) would be 6% of the rate of shower detection. With further assumptions as to the μ-meson structure it can be estimated that mesons would be observed simultaneously in three units in approximately 1.5% of the total number of showers. The ability of the DASI unit to provide measurements on more than one particle is an advantage over the spark counter because the probability of detecting

mesons simultaneously in two detectors is high for showers falling near either detector and in these cases the number of mesons incident on the near detector will normally be greater than one.

11.2.2. An Investigation of Shower Models.

As discussed in Chapter 7 the relation between the distance of a μ-meson from the shower core and the angle of the meson with respect to that of the shower axis is dependent on the mode of development of the shower - and this fact permits some distinction between the extreme shower models. The method would entail simultaneous measurements of the angles of arrival of μ-mesons at various distances from the core and in addition an accurate measurement of the direction of the core.

Accuracy of observation.

The precision required in the angular measurements is determined largely by θ_o, the r.m.s. angle of emision of the π-mesons in the interactions producing E.A.S. Theoretically this topic is still open to speculation but semi-empirical data is available. Earl (1958), as previously mentioned, proposes a value of $\theta_o = 2^o$ but this should probably be taken as a lower limit. The recent results of de Beer indicate a value of $\theta_o = 6^o$ and taking this value as our criterion, the arrival angles of the core and μ-mesons should be measured to

an accuracy of $>2^{o}$. (If the figure quoted by Earl were correct it would be necessary to measure the angles to 1^{o}.) Measurements of this precision can be made using DASI units, suitably modified, (Method II should suffice) and in view of the expected rate of observation at least three such units would be required.

Measurement of the direction of the shower axis to an accuracy of 2^{o} presents a more difficult problem. The normal method of measurement - by scintillator chronotron - is obviously inadequate and it is apparent that some form of directional core detector is required. The use of neutron counters or a lead shielded G.M. array (P set) is excluded by the necessity for precise directional indication and it must be concluded that the only suitable apparatus is a multiplate cloud chamber. The merits of this instrument for use in examinations of the core regions of E.A.S. have been demonstrated by several workers, notably by Naranan et al (1960).

Unfortunately the limited area of collection provided by a cloud chamber of reliable efficiency would severely restrict the investigation of showers of size greater than about 10^{5} particles and for this reason the possibility of modifying the DASI unit further-to serve in addition as a core detector - was seriously considered.

The essential characteristics of the core regions of E.A.S. are the very high energy flux and the presence of nuclear active particles. Several events which could be associated with these characteristics were in fact observed in experiments with a layer of 16.5 cm lead above the DASI unit. From these it is apparent that the insertion of layers of more dense material (at least 2-3 cm Pb or Cu) between the flash tube layers would restrict the lateral spread of the particle cascades produced, and probably enable a determination of the core direction. The modification of DASI units to function as directional core detectors is therefore feasible but might involve an extended development programme. However, in view of the increasing importance of studies of the core structures of E.A.S. such a project could well be justified.

It may be concluded that this experiment could be carried out using one or more multiplate cloud chambers adapted for core location and surrounded by not less than three DASI (μ-meson) units. The alternative arrangement of several well spaced (~100m) DASI units each capable of functioning as both core and μ-meson detector would provide a considerably larger area of collection and a correspondingly higher rate of events. Irrespective of the particular aims of the present experiment the inclu-

sion of such modified DASI units in an extensive array would undoubtly furnish much useful data on the core regions of E.A.S.

11.2.3. General Applications of DASI in Studies of E.A.S.

A full appreciation of the significance of information provided by studies of E.A.S. is at present limited by the uncertain state of knowledge of the basic mechanism of the E.A.S. Further studies are urgently required to provide:-

a) Clarification of the details of the longitudinal development of E.A.S. and the establishment of a unique model for shower development.

b) Reliable quantitative information on the U.H.E. nuclear interactions responsible for E.A.S. In particular, accurate data with regard to the numbers (and nature) of the secondary particles emitted and their distributions in energy and angle.

It is generally acknowledged that the most direct method of approach to the above problems is by investigation of the variation with altitude of the lateral distributions of the electron and μ-meson components. In all such experiments an exact knowledge of the zenith angle of the observed showers is imperative and for this

purpose the DASI unit is probably the most versatile and reliable apparatus yet available.

APPENDIX I

Statistical Treatment of the Flash Tube Data.

A. To find the standard deviation on the observed value of efficiency:-

Consider the case of single cosmic rays passing through one layer of tubes. If there are observed 'a' flashes and 'b' blanks then the layer efficiency, η, is by definition

$$\eta = \frac{a}{a+b}$$

Now a and b should both be distributed according to Poisson statistics so the standard deviation of a is $\sqrt{a}$ and that of b is $\sqrt{b}$. We have

$$\frac{1}{\eta} = 1 + \frac{b}{a}$$

thus $$-\frac{d\eta}{\eta^2} = \frac{adb - bda}{a^2}$$

$$= \frac{b}{a}\left[\frac{db}{b} - \frac{da}{a}\right]$$

and substituting for $\frac{b}{a}$

$$-\frac{d\eta}{\eta^2} = \left(\frac{1}{\eta} - 1\right)\left(\frac{db}{b} - \frac{da}{a}\right)$$

$$\therefore \quad -\frac{d\eta}{\eta} = (1 - \eta)\left(\frac{db}{b} - \frac{da}{a}\right)$$

As $d\eta$, db and da are small differentials in Calculus notation, the standard deviation is obtained by squaring and adding independently:-

Therefore $$\frac{\langle d\eta^2 \rangle}{\eta^2} = (1-\eta)^2\left[\frac{\langle db^2 \rangle}{b^2} + \frac{\langle da^2 \rangle}{a^2}\right]$$

and since the standard deviation of a is $\sqrt{a}$ and of b $\sqrt{b}$

$$\frac{db^2}{b^2} = \frac{1}{b} \quad \text{and} \quad \frac{da^2}{a^2} = \frac{1}{a}$$

thus $$\frac{d\eta}{\eta} = (1-\eta).\ \frac{1}{\sqrt{\eta b}}$$

or $$\frac{d\eta}{\eta} = \frac{\sqrt{1-\eta}}{\sqrt{a}}$$

Changing the notation to n flashes out of N frames:-

$$\frac{d\eta}{\eta} = \eta\frac{\sqrt{1-\eta}}{\sqrt{n}}$$

$$= \frac{\sqrt{\eta 1-\eta}}{\sqrt{N}}$$

Thus the efficiency is given as

$$\eta = \frac{n}{N} \pm \frac{\sqrt{\eta(1-\eta)}}{\sqrt{N}} \qquad \text{.....(i)}$$

B.

Experimental Verification.

An experimental check was made using random numbers to compare the observed and expected distributions in the S.D. of η for a given true value of η. The method was to consider a run of 100 pulese with a single layer of tubes. For each efficiency 'a', a hundred random digits were taken and the number of digits between 1 and 10a were counted. The standard deviation of this number from 100 a was computed and the process repeated for 80 'runs' at each efficiency.

If this 'observed' standard deviation is denoted by σ then the standard error on the standard deviation is given by $\frac{\sigma}{\sqrt{2N}}$ where N in this case is 80. The observed values of $\sigma \pm \frac{\sigma}{\sqrt{160}}$ are plotted in Fig. I(i) for comparison with the expected value (from (i)) which is shown by the dotted curve. The agreement is reassuring.

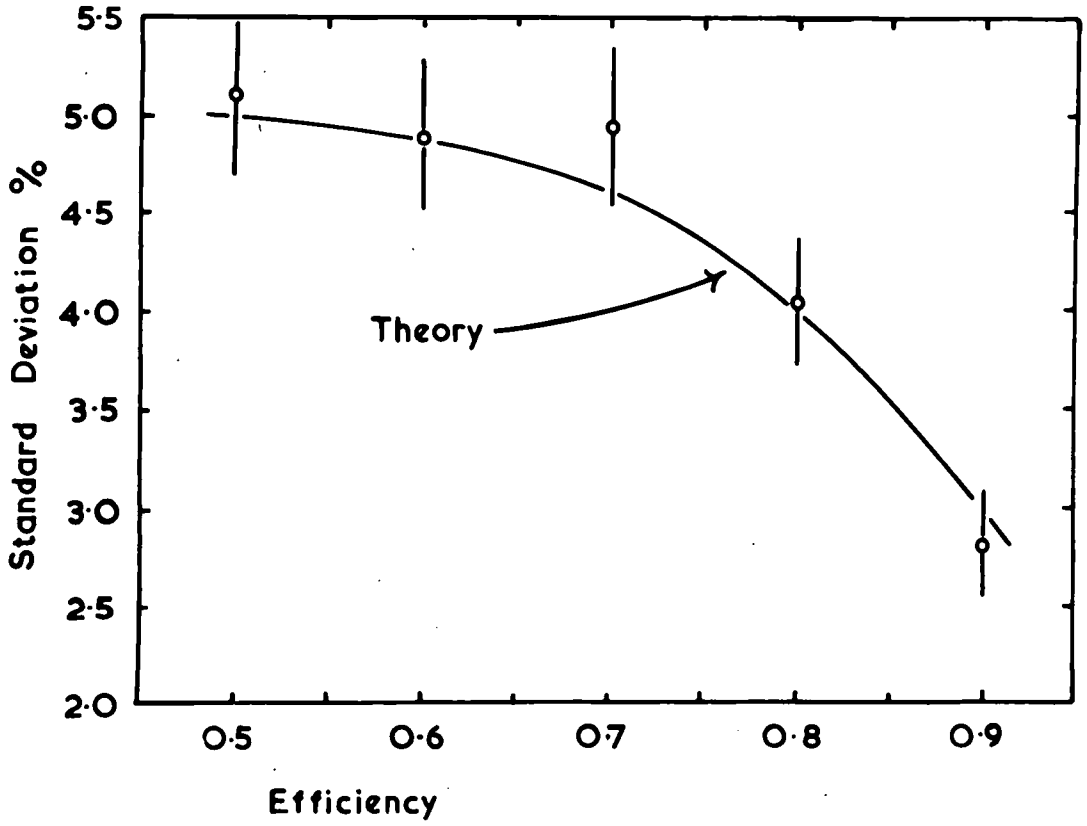
5·5
5·0
4·5
4·0
3·5
3·0
2·5
2·0
Standard Deviation %
Theory
0·5
0·6
0·7
0·8
0·9
Efficiency

Figure I·(1)

APPENDIX II

The Effective Field Inside a Flash Tube.

This problem has been considered in detail by Dr. R.A. Smith (Private communication 1959). An outline will be given of the general results obtained.

a) An approximate expression for the field inside a cylindrical dielectric shell.

For the case of an isolated dielectric shell of dielectric constant K, internal diameter a, and external diameter b, placed in a uniform electric field E parallel to the x axis:- (Fig II(a))

The complex potential, W, inside the shell is given by

$$W = \frac{4K\,E\,Z}{\left[(K+1)^2 - (K-1)^2\left(\frac{a}{b}\right)^2\right]}$$

where $Z = x + iy$. The consequence is that inside the shell, the field is uniform, parallel to the x axis and of strength

$$E_i = E.\frac{4K}{\left[(K+1)^2 - (K-1)^2\left(\frac{a}{b}\right)^2\right]}$$

Inserting experimental values, for the small tubes:-

$$a = \frac{5.5}{2}\ ,\quad b = \frac{7.5}{2}\ ,\quad K \sim 7\ ;$$

the internal field is found to be 64.5% of the applied field.

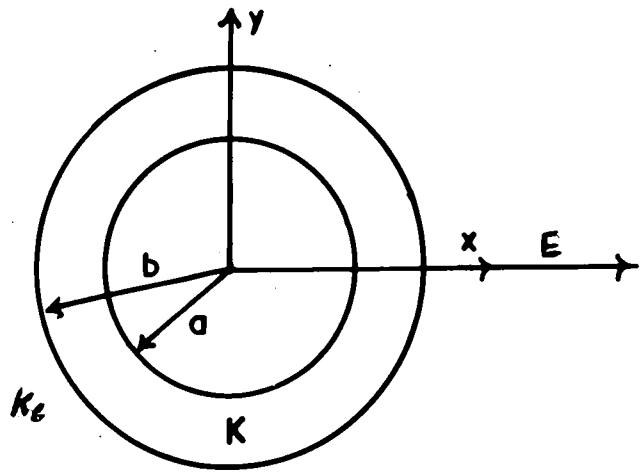

Figure II (i)

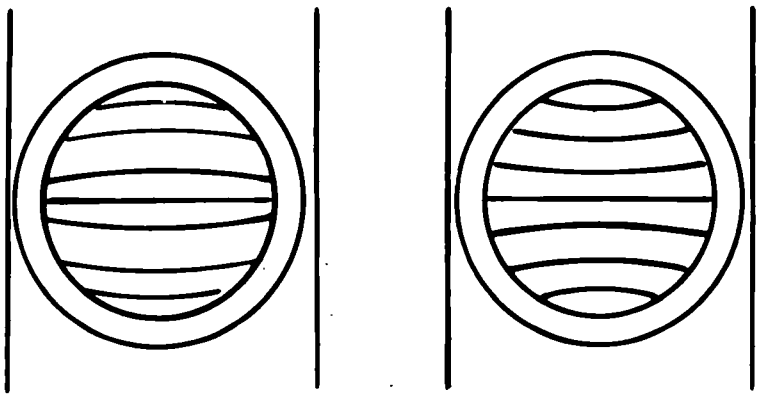

Figure II (ii)

b) <u>The internal field for the case of tubes in contact with other tubes and with the electrode system</u>.

If the correct boundary conditions are considered the problem becomes more involved. However the general result is that although the effective field is still given to a first approximation by expression (i) the internal field is no longer uniform. The extent to which the internal field departs from the uniform case depends upon the dielectric constant, K_e, of the medium surrounding the tubes and it can be shown that there is a critical value K_o of K_e, namely

$$K_o = K \left[\frac{b^2(K+1) - a^2(K-1)}{b^2(K+1) + a^2(K-1)} \right]$$

such that whenever $K_e < K_o$, the lines of force inside the tube have negative bending and whenever $K_e > K_o$ they have positive bending. (Fig. II(ii)).

In the case of paraffin wax, for which $K_e = 2$, the field inside the tube is almost uniform and this effect accounts for the superior characteristics and higher efficiencies exhibited by tubes in the "wax" stacks. (In the normal case, with air as the external dielectric, the negative bending of the lines of force will cause electrons to be accelerated towards the walls of the tube where some will be lost and the "efficiency", will therefore be lower - as is observed).

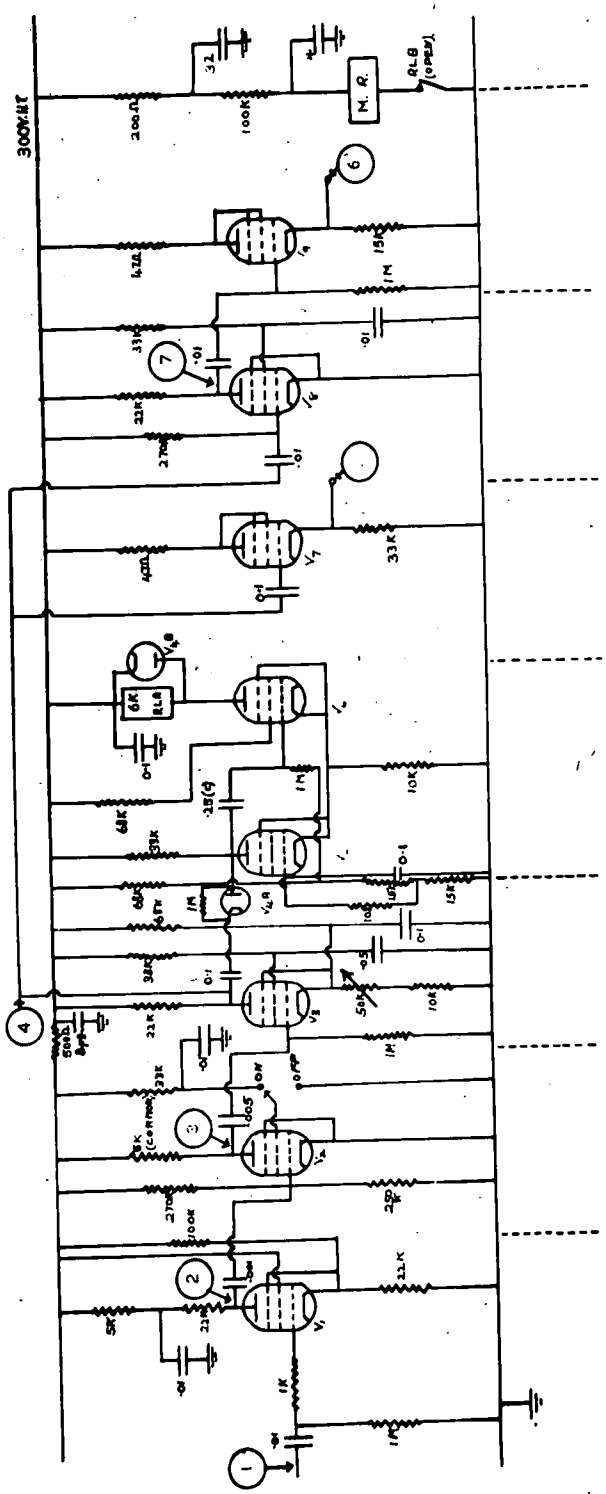

Appendix III

APPENDIX IV

The Variation with Zenith Angle of the Acceptance Area of a Cubic Detector.

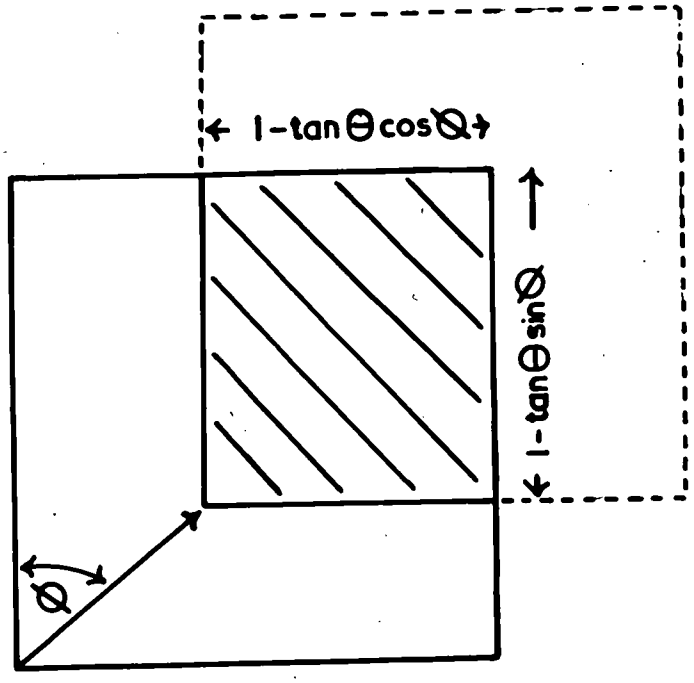

Assume the zenith angle of the particle is θ, the azimuthal angle is ϕ and the measured projected angle is β. From diagram above

a) The effective area $A_{(\beta,\phi)}$ for a given β and ϕ is

$$A_{(\beta,\phi)} = (1 - \tan\beta)(1 - \tan\beta\tan\phi)$$

Now $\cos\phi = \dfrac{\tan\beta}{\tan\theta}$

$\therefore \tan\beta = \tan\theta\cos\phi$

Thus $A_{(\theta,\phi)} = (1 - \tan\theta\cos\phi)(1 - \tan\theta\sin\phi)$

$= 1 - \tan\theta(\cos\phi + \sin\phi) + \tan^2\theta(\cos\phi\sin\phi)$ ...(i)

The mean value, A_θ, of the effective area at any zenith angle θ is found by averaging expression (i) over all ϕ i.e.

$$A_\theta = \frac{\int_0^{2\pi_2} \left[1-\tan\theta(\cos\phi + \sin\phi)+\tan^2\theta(\cos\phi \sin\phi)\right] d\phi}{\int_0^{2\pi} d\phi}$$

$$= \frac{A_o}{\pi}\left[\pi - 4\tan\theta + \tan^2\theta\right] \qquad \ldots\ldots\ldots(i)$$

Where A_o represents the area of collection at $\theta = 0$.

b) A more useful expression relating the area of collection with the particular zenith angle is of the form

$$A_\theta = A_o \cos^k\theta$$

and the exponent k is obtained quite simply by plotting log A_θ, (as obtained from expression (i)) against log cos θ. The result is shown in Fig. IV(ii) from which it is found that $k = 7.5$. Thus it may be concluded that the effective area of collection at the zenith angle θ is given by

$$A_\theta = A_o \cos^{7.5}\theta.$$

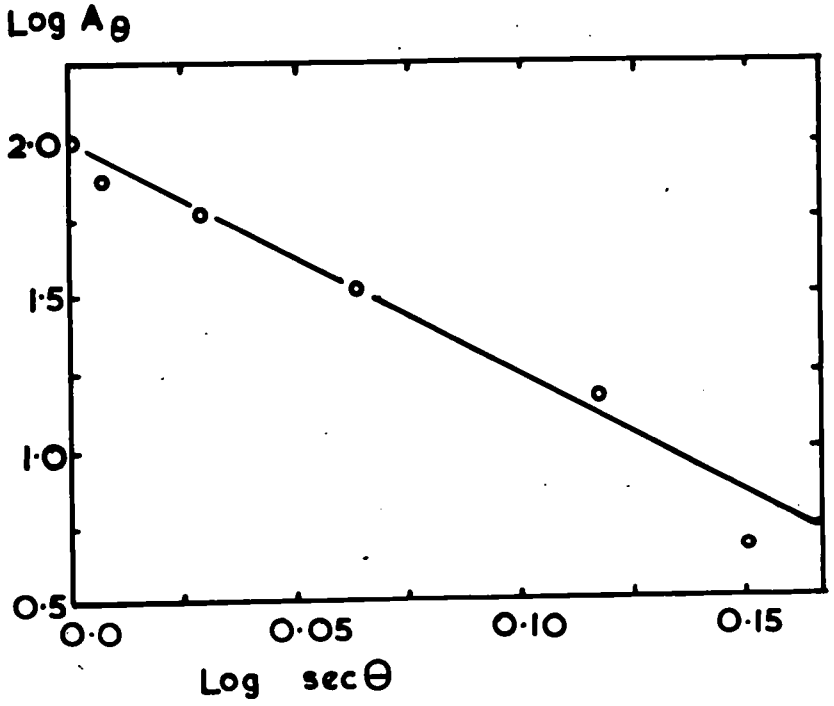

Figure IV (ii)

Acknowledgments

The author is grateful to Professor G.D. Rochester, F.R.S. for his support and continual interest in the work.

He wishes to thank Dr. A.W. Wolfendale for the guidance and constant help he has given.

Thanks are due to Drs. S. Kisdnasamy and J.L. Lloyd for many useful discussions and to Mr. P.S. Scull for his helpful cooperation. Thanks are also offered to Dr. J.V. Major for advice most generously given.

The author appreciates the ready assistance given by members of the workshop staff.

He is indebted to the Department of Scientific and Industrial Research for the provision of a research award throughout the period of the work.

REFERENCES Part I.

Ashton F., Kisdnasamy, S., and Wolfendale, A.W.	1958	Nuovo Cim. 8, 615.
Barsanti, G., Conversi, M., Focardi, S., Murtas, G.P., Rubia, C. and Torelli, G.	1956	Proceedings of CERN *Symposium* 11, 56.
Conversi, M. and Gozzini, A.	1955	Nuovo Cim. 2, 189.
Coxell, H., and Wolfendale, A.W.	1960	Proc.Phys.Soc., 75, 378
Craggs, J.D., and Meek, J.M.	1946	Proc.Roy.Soc. A 186, 241
Cranshaw, T.E., and de Beer, J.F.	1957	Nuovo Cim. 5, 1107.
Druyvestyn, M.J., and Penning, F.M.	1940	Rev.Mod.Phys. 12, 87.
Gardener, M., Kisdnasamy, S., and Wolfendale, A.W.	1957	Proc.Phys.Soc. B 70, 687
Gill, E.W., and Von Engel, A.	1949	Proc.Roy.Soc. A 197, 108
Harries, W.L., and Von Engel, A.	1954	Proc.Roy.Soc. A 222, 490
Jahnke, E., and Emde, F.,	1945	Tables of Functions (New York: Dover Pub.)

Jesse, W.P., and Sadauskis, J.	1955	Phys.Rev. 100, 1755.
Keuffle, J.W.	1948	Phys.Rev. 73, 531.
Loeb, L.B.	1948	Proc.Phys.Soc., 60, 561.
Loeb, L.B.	1952	J.Appl.Phys. 3, 341.
Lloyd, J.L.	1960	Proc.Phys.Soc., 75, 387
Meek, J.M.	1940	Phys.Rev. 57, 722.
Pidd, R.W., and Madansky, L.	1949	Phys.Rev. 75, 1175.
Raether, H.	1937	Z.Physik, 107, 91.
Raether, H.	1940	Arak.Electrotech. 20, 49.
Robinson, E.	1953	Proc.Phys.Soc. A 66, 73.
Rohatgi, V.K.	1957	J.Appl. Phys. 28, 9.
Seren, L.	1942	Phys.Rev. 62, 204.
Zeleny, J.	1942	J.Appl.Phys. 13, 444.

Part II

Andronikashvili, E.L., and Kasarov, R.E.	1960	Proc.Mosc.Conf. II p 150.
Abrosimov, A.T., Basilevskaya, G.A., Solovieva, V.I. and Khristiansen, G.B.	1960	Proc.Mosc.Conf. II p 84.
Barret, P.H., Bollinger, L.M., Cocconi, G., and Eisenberg, Y.	1952	Rev.Mod.Phys. 24, 133.
de Beer, J.F.	1960	Ph.D. Thesis (Potchefstroom)
Chudakov, A.E., Nesterov, N.M., Zatcepin, V.I. and Tukish, E.I.	1960	Proc.Mosc.Conf. p 50.
Clark, G., Clark G., Earl, J., Kraushaar, W., Linsley, J., Rossi, B., Scherb, F.	1957	Nature, Lond. 180, 353, 406.
Cranshaw, T.E., de Beer, J.F., and Parham, A.G.	1960	Proc.Mosc.Conf. II p 152.
Cranshaw, T.E., and Galbraith, W.	1954	Phil.Mag. 45, 1109
Cranshaw, T.E., and Hillas, A.M.	1960	Proc.Mosc.Conf. II p 210
Crawshaw, J.K., Elliot, H.	1956	Proc.Phys.Soc. A 69, 102.
Daudin, A., and Daudin, J.,	1952	C.R.Acad.Sci., Paris 234, 1551.

Delavaille, J., Kendziorski, F., and Greisen, K.	1960	Proc.Mosc.Conf. II p 101
Earl, J.,	1958	Ph.D. Thesis (M.I.T.)
Farley, F.J.M., and Storey, J.R.	1955	Proc.Phys.Soc. A 67, 996.
Greisen, K.	1956	Progress in Cosmic Ray Physics, Vol III Ed. J.G. Wilson. Amsterdam: North Holland.
Greisen, K.	1960	Proc.Mosc.Conf. II p 174.
Heisenberg, W.	1949	Z.Phys. 126, 569.
Hodson, A.L.	1951	Proc.Phys.Soc. A 64, 1061.
Kameda, T., Maeda, T., and Toyada, Y.	1960	Proc.Mosc.Conf. II p 58.
Katz, L. and Penfold, A.S.	1952	Rev.Mod.Phys. 24, 28.
Khristiansen, G.B., Vernov, S.N., Goryunov, N.N., Dmietriev, V.A., Ralikov, G.V., and Nechin, Yu, A.	1960	Proc.Mosc.Conf. II p 109.
Krasilnikov, D.D.	1960	Proc.Mosc.Conf. II p 115.
Kulikov, G.V., and Khristiansen, G.B.	1960	Proc.Mosc.Conf. II p 115.

Mc Cusker, C.B.A.	1955	Nuovo Cim. 11, 1340.
McCusker, C.B.A., and Wilson, B.G.	1956	Nuovo Cim. 3, 188.
Miyake, S.	1958	Progr.theor.Phys. 20, 844.
Moliere, G.	1946	Cosmic Radiation Ed. W. Heisenberg. New York: Dover.
Naraman, S., Raghavan, R., Ramanamurthy, P.V., Sreekantan, B.V., and Subramanien, A.	1959	Preprint (Sub. Nuovo Cim.).
Nikolsky, S.I., Vavilov, Y.N., Batov, U.U.	1956	Dokl.Acad.Nauk SSSR III, 71.
Nishimura, J., and Kamata, K.	1952	Progr.theor.Phys., Osaka 6, 628.
Olbert, S.	1956	Oxford Conf.Ext. Air Showers (A.E.R.E. Pub. London, H.M.S.O.)
Rossi, B., and Greisen, K.	1941	Rev.Mod.Phys. 13, 240.
Rossi, B.	1960	Proc.Mosc.Conf. II p 18.
Rothwell, P., Wade, B.O., and Goodings, A.	1956	Proc.Phys.Soc. A 69, 902.
Singer, S.F.	1951	Phys.Rev. 81, 579.

Vernov, S.N., Tulupov, V.I. 1960 Proc.Mosc.Conf. II p 158.
Khrenov, B.A., and
Khristiansen, G.B.

Zatcepin, G.T., and 1960 Proc.Mosc.Conf. II p 150.
Dedenko, L.A.

General

Allan, H.R. 1960 Colloquium E.A.S.
(Imperial College: London)

Galbraith, W. 1958 Extensive Air Showers
(London : Butterworths)